INVESTIGATION OF THE NOISE ASPECTS OF CARRIER DECK JET ENGINE OPERATION, AND EFFECTS OF NOISE SUPPRESSION ON AIRCRAFT MISSION PERFORMANCE

VOLUME I

Effects of Noise from Carrier Deck Jet Engine Operation on Hearing, Speech Interference, and Sonic Fatigue

JANUARY 31, 1964

Prepared Under Department of the Navy,
Bureau of Naval Weapons

Contract NOw 62-0887-d
Phase II

GENERAL ELECTRIC COMPANY
Flight Propulsion Division
Advanced Engine & Technology Department
Cincinnati 15, Ohio

INVESTIGATION OF THE NOISE ASPECTS OF CARRIER DECK JET ENGINE OPERATION, AND EFFECTS OF NOISE SUPPRESSION ON AIRCRAFT MISSION PERFORMANCE

VOLUME I

Effects of Noise from Carrier Deck Jet Engine Operation on Hearing, Speech Interference, and Sonic Fatigue

JANUARY 31, 1964

Prepared Under Department of the Navy,
Bureau of Naval Weapons

Contract NOw 62-0887-d
Phase II

AUTHORS:

R. J. Wells
M. W. Schulz
R. B. Tatge

GENERAL ELECTRIC COMPANY
Flight Propulsion Division
Advanced Engine & Technology Department
Cincinnati 15, Ohio

Volume I

TABLE OF CONTENTS

FOREWORD

This is the final report covering Phase II, Parametric and Systems Studies, of the work performed under the Department of the Navy, Bureau of Naval Weapons, Contract NOw 62-0887-d, in accordance with the Contractor's proposal "Jet Noise Suppression Research and System Studies", P-61-86, dated March 1961.

The objectives of Phase II of the program were to evaluate the effects of noise from aircraft carrier deck jet engine operation on hearing, speech interference, and structures, for the purpose of establishing suitable acoustical criteria for in-flight jet noise suppressors. In addition, the effects of suppressor aerodynamic performance and weight on aircraft mission performance were evaluated parametrically for several aircraft missions.

This report is presented in two volumes. Volume I is concerned with the effects of jet engine noise on hearing, speech interference, and sonic fatigue, and Volume II deals with the effects of noise suppressors on aircraft mission performance.

I. INTRODUCTION

This report is part of a study undertaken for the Navy in an attempt to better define the parameters relative to the problem of an in-flight noise suppressor for carrier based jet aircraft.

The design of such a suppressor must represent the result of compromise. The object is to balance acoustical performance of the suppressor against factors which influence aircraft performance - such as internal pressure loss, external drag loss, and weight - and also against any ill effects which noise may have on the aircraft or on carrier personnel.

Part of the overall problem, then, is to study all possible effects of the high noise levels characteristic of aircraft operations, and, where possible, to recommend criteria relative to noise levels, exposure time, etc. This divides naturally into two categories: first, the effect of noise on people, and second, the effect of noise on structure.

In the first category, the two major problems are hearing damage risk, and interference with communication. Although much has been written on both of these fields, there is need to coordinate the available information, and to present it in a form more directly applicable to the problem at hand. A similar statement might also be made relative to the effect of noise on structures.

This report is based almost entirely on literature reviews, and discussions held with research workers in the several fields. No tests were conducted as part of the project.

II. SUMMARY AND CONCLUSIONS

Information gathered from a literature search - notably the work of Ward, Glorig, et al[3-7] - relative to hearing loss vs. noise exposure is reviewed. The results of such studies are applied to the specific problem of determining criteria applicable to the hearing damage risk problem aboard aircraft carriers. Simple nomograms (Figs. 4, 8, and 9) are derived to quickly evaluate the maximum allowable exposure time to a given sequence of take-offs expressed in terms of octave-band sound level vs. time plots at the observer's ear. These charts are based upon the allowance of a computed TTS_2 (temporary threshold shift 2 minutes after exposure to the noise) of 10-13 db at 2000 cps and 20-23 db at 4000 cps. Additional nomograms allow rapid computation of TTS growth and recovery during noisy and quiet periods respectively.

TTS is considered to be of prime importance in specifying noise criteria since studies[7] indicate that a noise exposure which results in a daily temporary threshold shift of X db should, in a 10 year period, produce a permanent threshold shift of X db.

The Noise Cumulator[14,9] is discussed briefly, and an example is given of the application of such a device to TTS prediction.

Speech communication in the presence of noise is discussed briefly in terms of the well-known speech-interference-level (SIL)[16-19], and also in terms of the more fundamental 20 band AI (Articulation Index) calculation.[20,21] A simplified 6 octave-band AI calculation recently proposed by Kryter[27], is discussed in some detail. This approach has the advantage of greater accuracy than can be obtained by the use of SIL with but a minimum of added complication. Furthermore, modifications to the AI calculation may be employed to

take into account various influencing factors which are completely neglected with the usual SIL approach.

Several examples are presented which illustrate the simplified 6 band AI calculation, and also serve to indicate its superiority over normal SIL usage.

The effect of noise on structures is examined in several phases. In general, we follow the approach of Fitch[39] which considers first the determination of the acoustic environment, and the duration of important noise exposures as based on a typical mission analysis. The subject of structural design criteria is then approached via accelerated discrete frequency life testing, the results of which are interpreted using a sine-random equivalence analysis. The theory of vibration excitation due to random noise and the mechanism of structural fatigue are discussed.

Design charts developed by Belcher[40] and McGowen[41] are discussed. These charts relate sound pressure, fatigue life, resonant frequency, and dimensions of several common panel constructions.

Because of the very nature of the problem, it is not possible to specify sound criteria as fixed numbers applicable to all situations. However, the principles and information presented in this report will allow the calculation of maximum recommended exposure time to specific aircraft and flight operation with personnel at specified locations. They will also serve to specify design parameters for speech communication systems for given situations. In addition, they allow a rapid prediction of the increase in allowable personnel exposure time, improvement of speech communication, and reduction in danger of structural fatigue failures due to the use of a given exhaust silencer.

It is proposed therefore, that detailed studies be undertaken to evaluate the above aspects for all situations of major interest.

III. EFFECT OF NOISE ON PEOPLE

1. Hearing Damage Risk Criteria

Years ago, noise criteria relative to hearing damage risk were expressed simply as weighted sound levels, octave-band levels, sone values, etc. that should not be exceeded. It became apparent, however, that exposure time is an important factor which cannot be neglected. Several methods of setting criteria involving both levels and exposure time were then proposed - the one most widely adopted being the equal energy hypothesis often expressed as

$$IT = \text{constant} \qquad (1)$$

where I represents sound intensity and T represents time.[1] The Air Force Regulation 160-3 (1956) is based upon this assumption.[2]

The above equation states that if the intensity of noise (perhaps in a given frequency-band) is doubled (increased by 3 db), then only half the previous exposure time should be permitted. Similarly, if the noise is increased in intensity by a factor of 100 (20 db), then the exposure time should be reduced to 1% of the original time. With the high noise levels typical of modern jet engines, such a process gives rise to extremely short allowable exposure times - or alternatively - more required ear protection than is available from standard ear plugs and muffs.

In recent years, both studies of controlled noise exposure vs. hearing loss[3-8] and studies of hearing losses actually suffered by people exposed to jet engine noise[9,10] indicate that the equal energy hypothesis is somewhat overprotective for high level noise. This is particularly true for intermittent bursts of intense noise[3] - for which

Eq. (1) may be rewritten as

$$IRT = \text{constant} \tag{2}$$

where R is defined as the "on-fraction" of the noise.

One of the most recent papers in this field is that of Kryter.[8] However, although he gives damage risk criteria for exposure to continuous noise, his work is not directly applicable to the problem of intermittent noise - which is, of course, of concern during launch operations aboard an aircraft carrier. Fortunately, though, the work of Ward, Glorig, et al[3-7] is applicable to this problem and may be used to estimate both temporary and permanent hearing threshold shifts when one is exposed to a complex time-varying noise such as that produced by a sequence of jet aircraft take-offs from a carrier deck.

Before considering this specific problem, however, we will first summarize the basic findings of these studies. First, the general equation relating TTS_2 (temporary threshold shift two minutes after cessation of noise) to a noise exposure of duration T minutes at a sound pressure level S is apparently of the form:

$$TTS_2 = K(S - S_o)\left[\log_{10}(T/T_o)\right] + C \tag{3}$$

where K, S_o, T_o, and C are constants for a given type of noise.[4] (Two minutes is usually taken as a suitable time for measurement since hearing recovery is erratic during the first minute or so after the noise ceases.)

Second, TTS at a given frequency is primarily determined by noise in the octave-band near that frequency and in the octave-band immediately below this one. In other words, 4 KC loss is largely due to noise in the 1200-2400 and 2400-4800 cps bands, etc. The following tabulation[4] gives empirical equations for growth of TTS_2 due to octave-band noise. In these equations it is assumed that T is of the order of 5 minutes or more.

TABLE I

Exposure Band	Test Frequency	Equation for TTS_2
600-1200	1500	$0.53(S-71)\ (\log T - 0.44) - 3$
600-1200	2000	$0.41(S-68)\ (\log T + 0.15) - 8$
1200-2400	3000	$0.58(S-65)\ (\log T + 0.55) - 13.5$
1200-2400	4000	$0.61(S-70)\ (\log T + 0.33) - 9.5$
2400-4800	4000	$0.91(S-75)\ (\log T + 0.19) - 8$
2400-4800	6000	$0.51(S-68)\ (\log T + 1.80) - 22$

Although the tests were confined to octave-band levels of 120 db and below, it is not unreasonable to extrapolate the above equations to octave-band levels approaching 130 db. However, above 130 db, even very short exposures are considered serious. (Also, exposures for which the expected TTS_2 exceeds 50 db should not be permitted).

Third, if the noise is intermittent with bursts of duration between 1/4 second and 1 minute, the computed TTS_2 as given by equation (3) should be multiplied by R, the "on-fraction" of the noise.[3] Moreover, if the noise consists of several discrete levels with different on-fractions, it appears that the equation should be written:

$$TTS_2 = K \sum_{i=1}^{n} R_i(S_i - S_o) \quad \log(T/T_o) \quad + C \tag{4}$$

Fourth, after cessation of noise, recovery at all frequencies may be approximated by the relation

$$TTS_t = (TTS_2 + 9)\ (1 - 0.27\ \log_{10} \tfrac{t}{2}) - 9 \tag{5}$$

where the recovery time t is assumed to be in excess of 2 minutes.[4]

Fifth, if repeated exposures to noise are separated by periods of relative quiet with durations exceeding about 1 minute, it is necessary to employ a cumulative calculation for TTS growth and recovery.[6] The specific steps are outlined below.

1. Compute TTS_2 after first exposure.
2. Compute TTS_t after t minutes recovery.
3. Using the growth equation, calculate the value of T that would be required to obtain the TTS_t of step (2) for a TTS_2.
4. Add this "equivalent exposure time" to the actual T for the second exposure and compute TTS_2 for the total.
5. Repeat this process for the entire sequence of exposures and recoveries.

Sixth, if more than one octave-band contributes appreciably to the computed TTS_2, an approximate combination of effects may be made by adding the expected TTS values as one normally adds decibel quantities.[4] That is, with a TTS_2 of 10 db at 2000 cps due to 600-1200 cps noise and another TTS_2 of 10 db at 2000 cps due to 1200-2400 cps noise, one would expect a total TTS of 13 db at 2000 cps.

Seventh, we have the question of permanent threshold shift (PTS) versus temporary threshold shift (TTS). Studies of various industrial environments indicate that daily exposures producing X db TTS will after 10-15 years give rise to a PTS of the order of X db.[7] At 4 KC, this PTS is approximately a maximum. That is, further exposure does not increase it appreciably. For 2 KC the PTS continues to increase with further exposure.

A somewhat simplified analysis of the above type is included in the Proposed International Standard ISO 43 (Secretariat-194)314E, June 1963 for "Noise Rating with Respect to Conservation of Hearing, Speech Communication, and Annoyance". The curves and tabulations in this document are based largely on an allowable TTS_2 of 12 db at 2000 cps for a daily exposure. Kryter suggests 10 db at and below 1000 cps, 15 db at 2000 cps, and 20 db at and above 3000 cps.[8] With losses appreciably greater than

these figures, ability to understand conversation becomes severely impaired.

The proposed ISO method is not directly applicable to our problem as it does not include the R factor approach for short time variations in exposure. Moreover, a simplified computation is made only for the one frequency band which is highest with respect to a specific set of rating curves. The procedure explicitly outlined above should be somewhat more accurate in the latter regard.

In the interests of simplicity, however, it seems sufficient to consider TTS only at 2000 and 4000 cps. Actually, PTS at 4000 cps is not very important from the standpoint of understanding conversation, and at 1000 cps the TTS will almost invariably be considerably less than at 2000 cps. In a recent private communication, Dr. Glorig stated that the second equation of Table I might also be used for TTS_2 at 2000 cps due to noise in the 1200-2400 cps band. Let us consider, then, the following four equations:

TABLE II

Exposure Band	Test Frequency	Equation for TTS_2
600-1200	2000	$0.41(S-68)\ (\log T + 0.15) - 8$
1200-2400	2000	$0.41(S-68)\ (\log T + 0.15) - 8$
1200-2400	4000	$0.61(S-70)\ (\log T + 0.33) - 9.5$
2400-4800	4000	$0.91(S-75)\ (\log T + 0.19) - 8$

These equations assume the noise to be broadband in character. With pure tones (such as from compressor noise) the problem is more serious. The work of Kryter[8] indicates that in such cases the above equations should be modified by subtracting 5 db from the various values given for S_o - since the critical bandwidth for TTS appears to be of the order of 1/3 octave. Alternatively, the equations may be used as given, and 5 db

added to the values employed for S.

We will now attempt to illustrate the above approach by computing the expected TTS_2 at 2000 and 4000 cps for a man wearing ear plugs while exposed to aircraft take-off operations on a carrier deck. (Ref. 11 indicates that the noise from landing operations is less important). Fig. 1 indicates a typical idealized exposure time pattern with afterburner operation.[11,12]

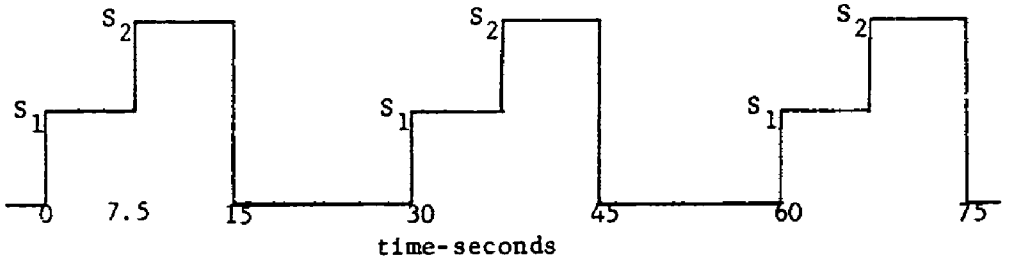

Fig. 1

Here alternate take-offs would probably be made from two catapults, so for simplicity we will assume that the man is halfway between the two, at a distance of 25 feet from the tail of each aircraft, and at the angle of maximum noise radiation. The level S_1 represents military operation, while S_2 indicates the increased levels when afterburners are started. Compressor noise is considered to be negligible with respect to exhaust noise, so the equations of Table II will be used without any 5 db corrections. It will be assumed that 20 aircraft take off, giving a total exposure time:

$$T = 0.25 + 19 \times 0.50 = 9.75 \text{ minutes}$$

Four such flights will be repeated at 2 hour intervals, and TTS computed for the entire operation. It is also assumed that all aircraft are North American A3J-1's, each using two General Electric J79 engines.

From Ref. 13, the sound levels to be expected are given in Table III for both military and A/B operation. Also tabulated is the "average" attenuation for V-51R ear plugs, as taken from Ref. 10. Subtracting these values gives the estimated exposure for the two periods. Next, the effective "on-factor" is computed, and finally the TTS_2 after the first group of planes take off. These are found to be 7.2 and 12 db at 2000 and 4000 cps, respectively - after combining the individual components as previously outlined. At the bottom of Table III, an average growth equation is given for this combined TTS_2.

Next, we consider recovery during the following 110 minutes of assumed quiet. (Other noise could, of course, effect this recovery). For t = 110, equation (5) becomes

$$TTS_{110} = 0.53\ TTS_2 - 4.2$$

As shown in Table IV, recovery is essentially complete at 2000 cps, but there is a residual TTS of 2.1 db at 4000 cps. This 2.1 db is then used with the average growth equation of Table III, to compute an equivalent exposure of 2.4 minutes. Hence, the effective T for the second group of planes is 9.8 + 2.4 = 12.2 minutes - which from the growth equation should produce 13.6 db TTS_2 at 4000 cps. This process may then be repeated for the third and fourth flights as indicated.

TABLE III

	2000 cps		4000 cps	
Octave-Band	600 1200	1200 2400	1200 2400	2400 4800
S_1	138	140	140	133
S_2	144	147	147	140
V-51R Attenuation	-18	-25	-25	-30
S_1 (with plugs)	120	115	115	103
S_2 (with plugs)	126	117	117	110

TABLE III (Cont'd)

	2000 cps		4000 cps	
$R_1(S_1-S_o)$	1/4 x 52	1/4 x 47	1/4 x 45	1/4 x 28
$R_2(S_2-S_o)$	1/4 x 58	1/4 x 49	1/4 x 47	1/4 x 35
$\sum R_i(S_i-S_o)$	27.5	24	23	15.75
$(\log T + \log T_o)$	1.14	1.14	1.32	1.18
K	0.41	0.41	0.61	0.91
TTS_2	4.9	3.3	9.0	8.9
Combined TTS_2	7.2		12	
Aver. Growth Eqn.	$13.3(\log T + 0.15) - 8$		$16.4(\log T + 0.26) - 8.5$	

TABLE IV

	2000 cps	4000 cps
1st TTS_2	7.2	12
TTS_{110}	---	2.1
Equiv. T.		2.4
Total T		12.2
2nd TTS_2	7.2	13.6
TTS_{110}	---	3.0
Equiv. T.		2.8
Total T		12.6
3rd TTS_2	7.2	13.8
TTS_{110}	---	3.1
Equiv. T		2.8
Total T		12.6
4th TTS_2	7.2	13.8

Rather than calculate $\sum R_i(S_i - S_o)$ as indicated in Table III, one might compute the numerical average of the sound levels S_1 and S_2 (since in this example they persist for equal time intervals) and use an R factor of 0.5 (since the periods of noise and relative quiet are equal). Thus, in the first column of Table III, we might compute $S_{av} = 123$, and

$$TTS_2 = 0.41 \times 0.5\ (123-68)\ 1.14 - 8$$
$$= 4.9$$

Actually, this procedure is identical in principal to the one employed above; but is easier to use. It may be readily extended to more complex sound level histories by calculating the weighted numerical average of the levels - possibly with the aid of a planimeter. (Note that we are not computing the level of the mean sound pressure, or mean-squared pressure). Thus, for the case illustrated in Fig. 2

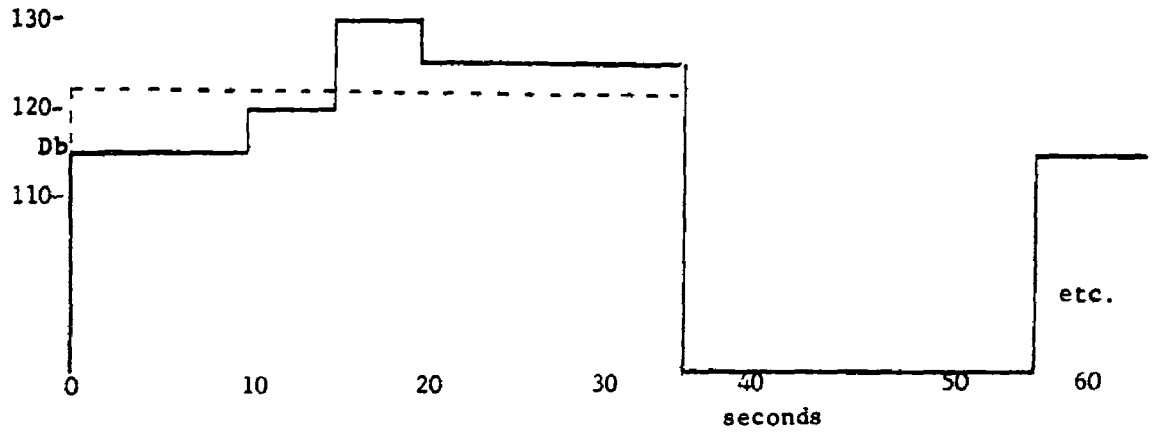

Fig. 2

the average level is

$$S_{av} = 1/7(115 + 115 + 120 + 130 + 125 + 125 + 125)$$
$$= 122 \text{ db}$$

as indicated by the dotted line, and a factor

$$R = \frac{35}{55} = 0.637$$

is applicable to the term $(S_{av} - S_o)$

When the growth equations are employed in this manner, it becomes possible to put them in the form of simple nomograms. Fig. 3 is such a nomogram applicable to both the 600-1200 cps band and the 1200-2400 cps band for estimating TTS_2 at 2000 cps. Thus, for the calculation in the first column of Table III, we draw a line between $S_{av} = 123$ and $R = 0.5$, note the intersection on the unlabeled turn line, and draw a line from this point to $T = 9.8$ intersecting the TTS_2 scale at 5 db.

Now, if as a criterion, we do not allow the TTS_2 at 2000 cps as computed from Fig. 3 to exceed 10 db for <u>either</u> the 600-1200 band or the 1200-2400 band, then the total TTS_2 at 2000 cps should not exceed 13 db. This figure is consistent with present day thinking - as previously noted. With this 10 db criterion, Fig. 3 becomes very useful for estimating allowable combinations of S_{av}, R, and T. For example, assuming $R = 0.5$ we may tabulate as follows:

<u>TABLE V</u>

S_{av}	Max. allowable T (minutes)
125	25
120	35
115	52

For $TTS_2 = 10$, Fig. 3 may be simplified to Fig. 4 which permits even quicker computations of the above type - though with unavoidable loss in perspective, with regard to the relative variation of the factors involved. (For $R = 1$, Fig. 3 reduces to a criterion for continuous noise; and though

still applicable it could obviously be simplified to a 3 line chart).

Where repeated exposures at intervals are of concern (as in the flight deck example previously discussed) we must consider TTS recovery between exposures. Fig. 5 was constructed from Eq. (5) to make such a computation easy. As a suitable criterion here, it is suggested that the time interval between such exposures be chosen with the aid of Fig. 5 so that the computed TTS_t does not exceed 1 db. In that event, exposures which produce the maximum TTS_2 of 10 db should not be repeated more frequently than once every two hours, though exposures to less intense noise could be more frequent.

If desired, Figs. 3 and 5 may be employed to determine the expected TTS after a series of repeated exposures - as in the tabulated example. If only one of the two octave-bands is of importance, the method of computation appears obvious. However, if neither band is negligible, the use of an average growth equation may be effected by using Fig. 3 in a slightly different manner. Suppose, for example, that we found $TTS_2 = 9$ db for <u>both</u> the 600-1200 band and the 1200-2400 band. We would then assume the total TTS_2 to be 12 db at 2000 cps. Now, taking the exposure time, T, as 10 minutes, we may draw a line through $T = 10$ and $TTS_2 = 12$ and determine the intersection on the unmarked turn line. (This is the effective combination of R and S_{av}, but need not be evaluated numerically.) Suppose next that we desire a 1 hour interval between repeated exposures. How does TTS build up over several such cycles? From Fig. 5, we find $TTS_t = 4$ db at 1 hour. Inserting this value on the TTS_2 scale of Fig. 3, and using the turn line point previously described, we find an equivalent exposure time of about 3.4 minutes. Hence, the effective time for the second exposure is 13.4 minutes. Using this same turn line point, we

now finds TTS_2 = 14 db. Similarly, after another cycle TTS_2 = 15 db, etc.

Figs. 6 and 7 are nomograms giving the same type of TTS_2 calculation for loss at 4000 cps due to 1200-2400 cps noise and 2400-4800 cps noise, respectively. Here, in line with Kryter's reasoning[8], we suggest an allowable maximum of 20 db as computed for either band. If only jet exhaust noise were of concern, it is probable that the criterion of Fig. 3 would govern the problem. However, compressor whine may also be of importance, and may easily be sufficient to require the use of Figs. 6 and 7. (As noted previously, 5 db should be added to S_{av} for the case of pure tones.) Since recovery seems to be independent of frequency, Fig. 5 may still be used at 4000 cps. Also, as before, it is possible to effectively use an average growth equation if both octave bands are of importance. For such a calculation, one may use either Fig. 6 or Fig. 7 with Fig. 5 - the difference in the final result being negligible.

Figs. 8 and 9 correspond to Fig. 4, except that these are drawn for a limiting TTS_2 of 20 db at 4000 cps due to noise in the 1200-2400 and 2400-4800 bands.

In summary, to use this approach in its simplest form as a criterion to determine the maximum allowable exposure time to a series of take-offs as described previously, one need only determine plots similar to Fig. 2 (evaluating both S_{av} and R) for each of the 3 bands 600-1200, 1200-2400, and 2400-4800 cps. Then Fig. 4 should be used with <u>both</u> the 600-1200 and 1200-2400 cps bands, Fig. 8 with the 1200-2400 band only, and Fig. 9 with the 2400-4800 band, with 5 db additions to S_{av} for any strong pure tones. The minimum value for T obtained among these 4 computations represents the maximum allowable exposure. If desired, of course, more detailed information on expected TTS growth and recovery can be obtained from the other charts as described above.

In most cases, personnel will be wearing some form of ear protection; and it is necessary to subtract the attenuation to be expected of such devices in determining the values for S_{av} to be used with these charts. For convenience, Table VI lists typical values for such attenuation as obtained from Ref. 2. It is recognized, of course, that the actual reduction achieved for an earplug depends to a great extent on the fit. For this reason, an ear muff, or combination of muff and plug, is often preferred.

TABLE VI

Average Octave-Band Noise Level Reduction in Ear Canal Achieved by Use of Personal Protective Equipment

Type of Equipment	Bands (cps) 600 1200	1200 2400	2400 4800
Headset Earphone Covers	13	20	30
Standard Ear Plug or Ear Muff alone	18	25	30
Standard Ear Plug and Ear Muff together	28	37	40

2. The Noise Cumulator

Several years ago, Cox[9,14] developed an instrument known as the Noise Cumulator for the specific purpose of studying noise exposures aboard aircraft carriers. In the design of this instrument the assumption was made that the total amount of time a person is exposed to noise of a given level and spectrum determines the seriousness of his exposure independent of the time sequence of quiet and noisy periods. Using the actual noise signal (or a tape recording of it) the cumulator was built to tell the total time, during any period of interest, for which the

level in any specific frequency range exceeded each of seven pre-determined sound level thresholds. These thresholds are normally spaced 5 db apart, generally covering an ample dynamic range with reasonable definition.

As previously discussed, more recent studies[3,4] show that the seriousness of a noise exposure is not completely independent of the time sequence of quiet and noisy periods - since TTS recovery occurs during quiet periods. However, if the changes in noise level are fairly rapid - as is characteristic of aircraft take-offs from carrier decks - recovery during quiet periods becomes less important, and the information supplied by the cumulator is sufficient for a calculation of TTS_2 in a manner similar to that previously outlined.

In order to demonstrate the applicability of this instrument to prediction of TTS_2, we have made use of Noise Cumulator data taken aboard U.S.S. Saratoga (CVA-60) at the Blast-Shield Operator's Station, Catapult No. 1.[15] The authors of the CVA-60 study identify this as the noisiest position which they monitored.

Three frequency ranges were studied: full band-width, 300-1200 cps, and 1200-20,000 cps. Data was recorded on eight magnetic tapes ("sub-samples"), each approximately 50 minutes long. Five of these were defined as "loud", i.e., the overall levels exceeded 130 db more than 2% of the time. Our analysis is based on these sub-samples, under the assumption that these samples represent continuously noisy conditions without appreciable quiet periods for recovery.

Figure 10 shows the percentage of time that the sound level spent in each 5 db increment for each of the frequency ranges monitored. It is immediately clear that most of the high-level sound energy was in the 1.2-20 KC range; this is shown by the similarity of the full-bandwidth and the

1.2-20 KC plots. The distribution curve for 300-1200 cps peaked some 15 to 20 db lower.

This would not be expected if the noise measured was due chiefly to jet engine exhausts. The predominance of high frequency energy may be due to compressor noise from aircraft awaiting takeoff, and to noise from the catapult itself.

As discussed previously, TTS_2 at 4000 cps is chiefly influenced by noise in the 1200-2400 cps and the 2400-4800 cps octave bands. TTS_2 at 2000 cps is governed by the 600-1200 and 1200-2400 cps bands. The CVA-60 data does not give this information, but we can make some assumptions which will allow us to estimate how the measured energy should be divided up. The fact that this involves some educated guessing points out the desirability of using filters tailored to the three octaves influencing TTS at the two frequencies of most interest.

Let us assume that the 1.2-20 KC band noise is mainly due to engine compressor noise. As such, it may be expected to have approximately equal energy in the 1200-2400 and 2400-4800 cps bands, the energy content being a function of engine type and speed. Energy at higher frequencies will be negligible compared to these bands.

We further assume that the noise in the 300-1200 cps band is due to turbojet engine exhausts (at different power settings), plus miscellaneous sources such as tractors and the public address system. We can assume that the levels in the 300-600 and 600-1200 cps octaves which make up this band are about the same.

With these assumptions we can say that the 600-1200 cps octave level is 3 db below the 300-1200 cps band level, and that the 1200-2400 and 2400-4800 cps levels are each 3 db below the 1.2-20 KC band level. Taking the average level in each 5 db increment as being at about the middle of that range, we can now calculate TTS for a subject wearing V-51R ear plugs, having attenuations of 18 db in the 600-1200 cps band, 25 db at 1200-2400 cps and 30 db at 2400-4800 cps. We make use of the growth equations in Table II with 5 db corrections for pure tones in the 1200-2400 and 2400-4800 cps bands.

Figure 11 details the procedure in calculating TTS_2 at 4 KC due to the 1200-2400 cps band, namely 22.6 db for 50 minutes of exposure during noisy periods. A similar calculation employing the 2400-4800 cps octave gives a TTS_2 of 20.1 db, the total TTS_2 at 4 KC being the sum of these, or 24.6 db. The TTS_2 at 2000 cps, calculated in a similar manner, totals 9.3 db. These values of TTS_2 corroborate the conclusion of reference 15 as to the desirability of using both insert and muff-type hearing protection simultaneously.

Fig. 3

Use for 600-1200 and 1200-2400 cps octave-bands

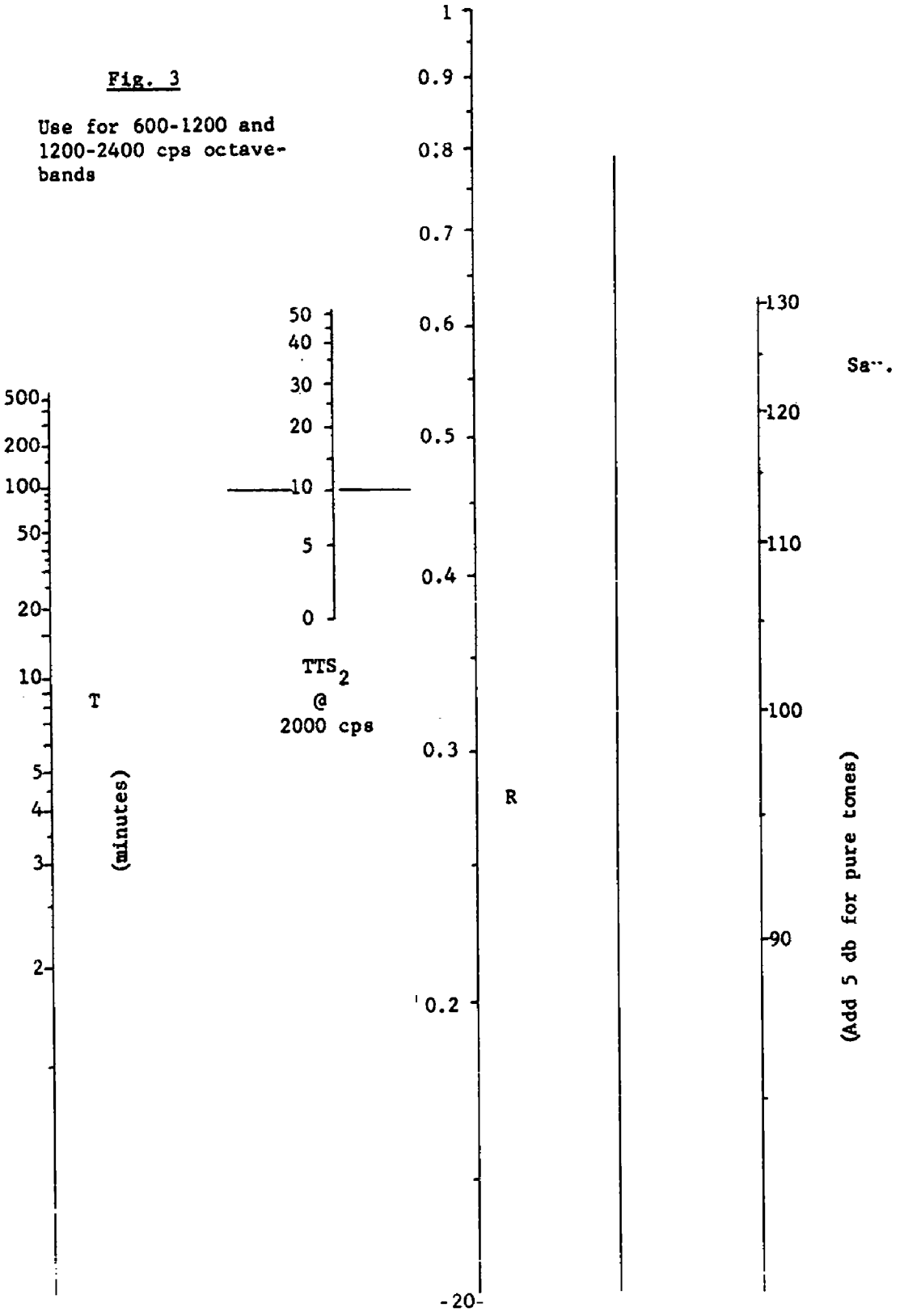

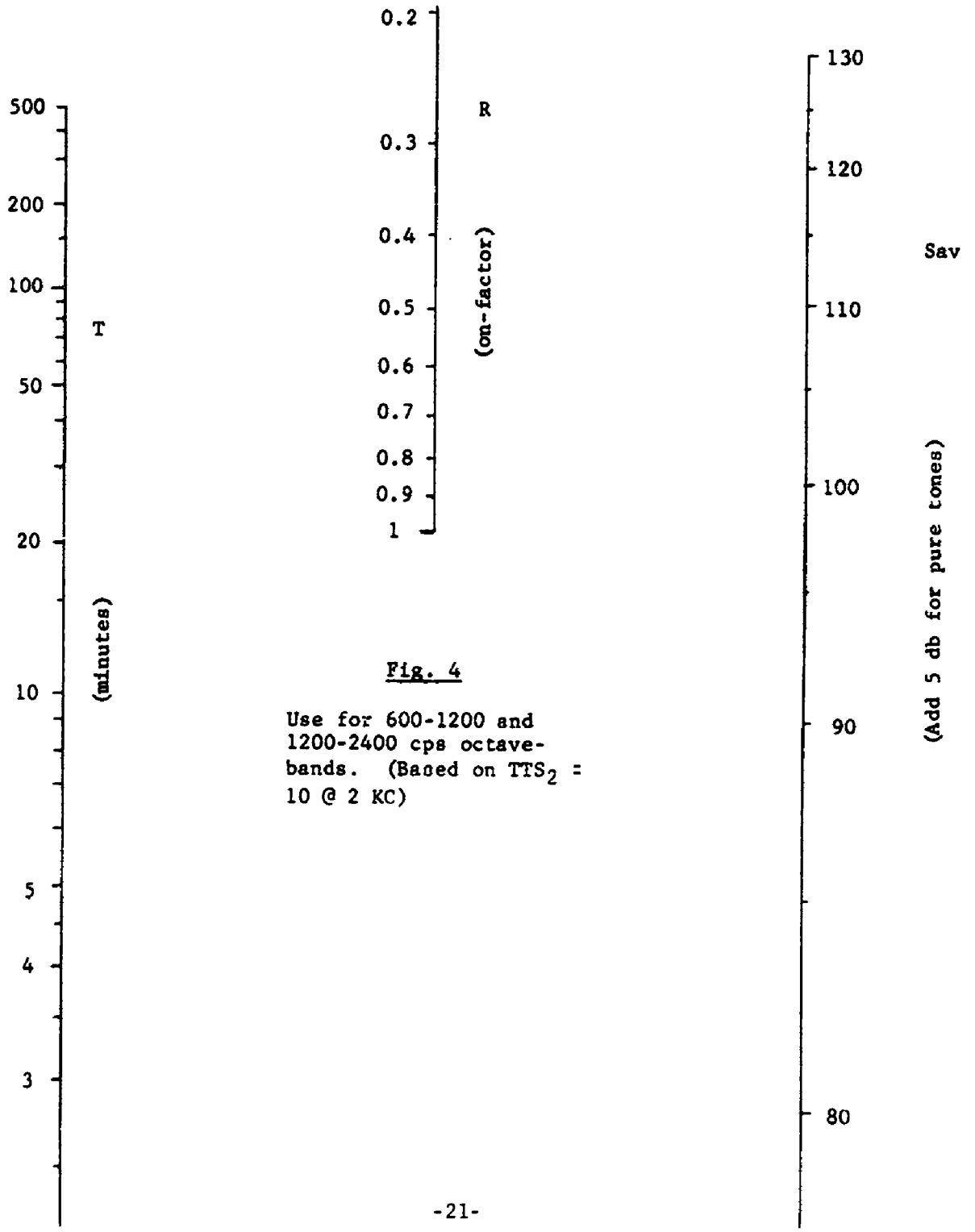

Fig. 4

Use for 600-1200 and 1200-2400 cps octave-bands. (Based on TTS_2 = 10 @ 2 KC)

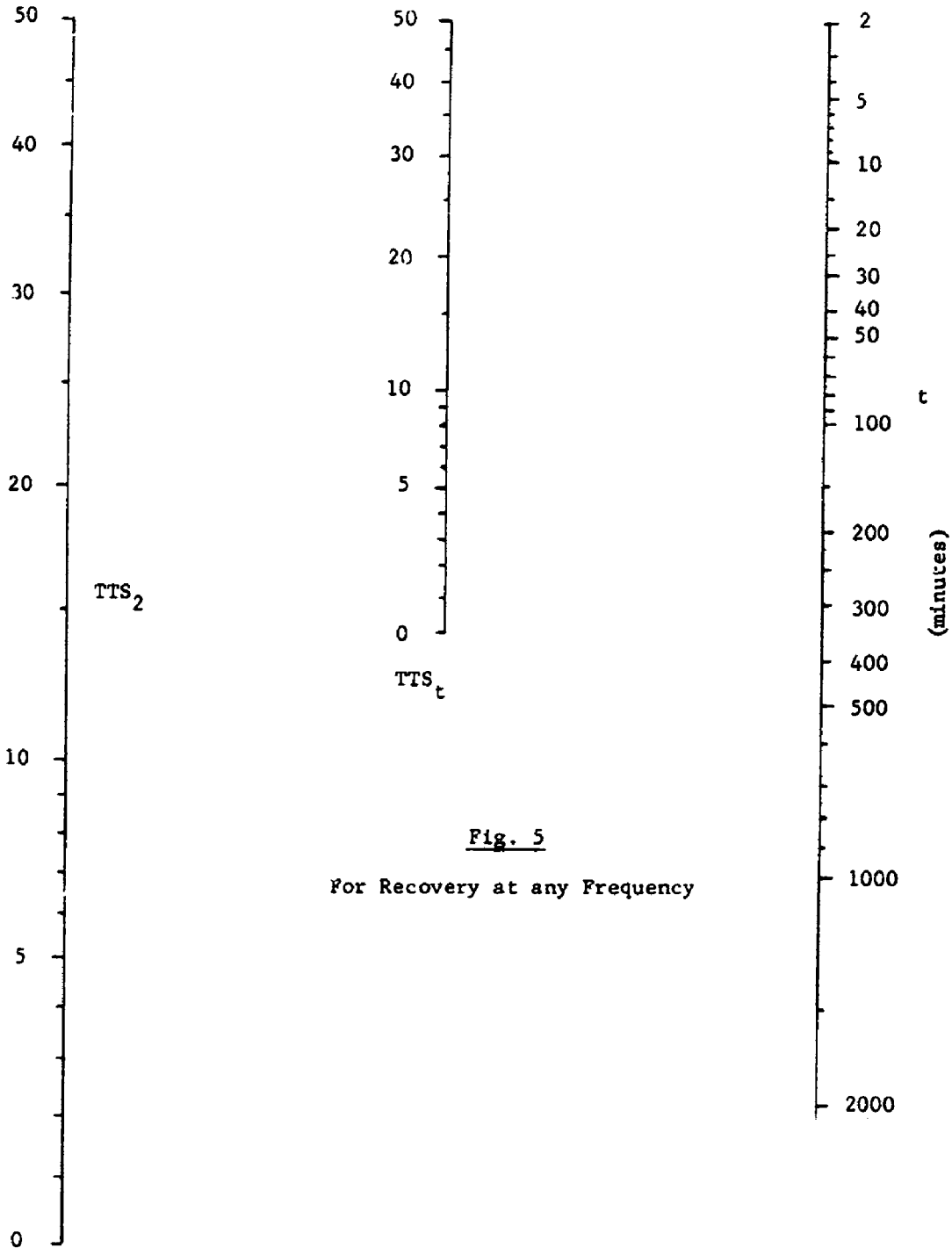

Fig. 5

For Recovery at any Frequency

Fig. 6

Use for 1200-2400 cps
octave-band only

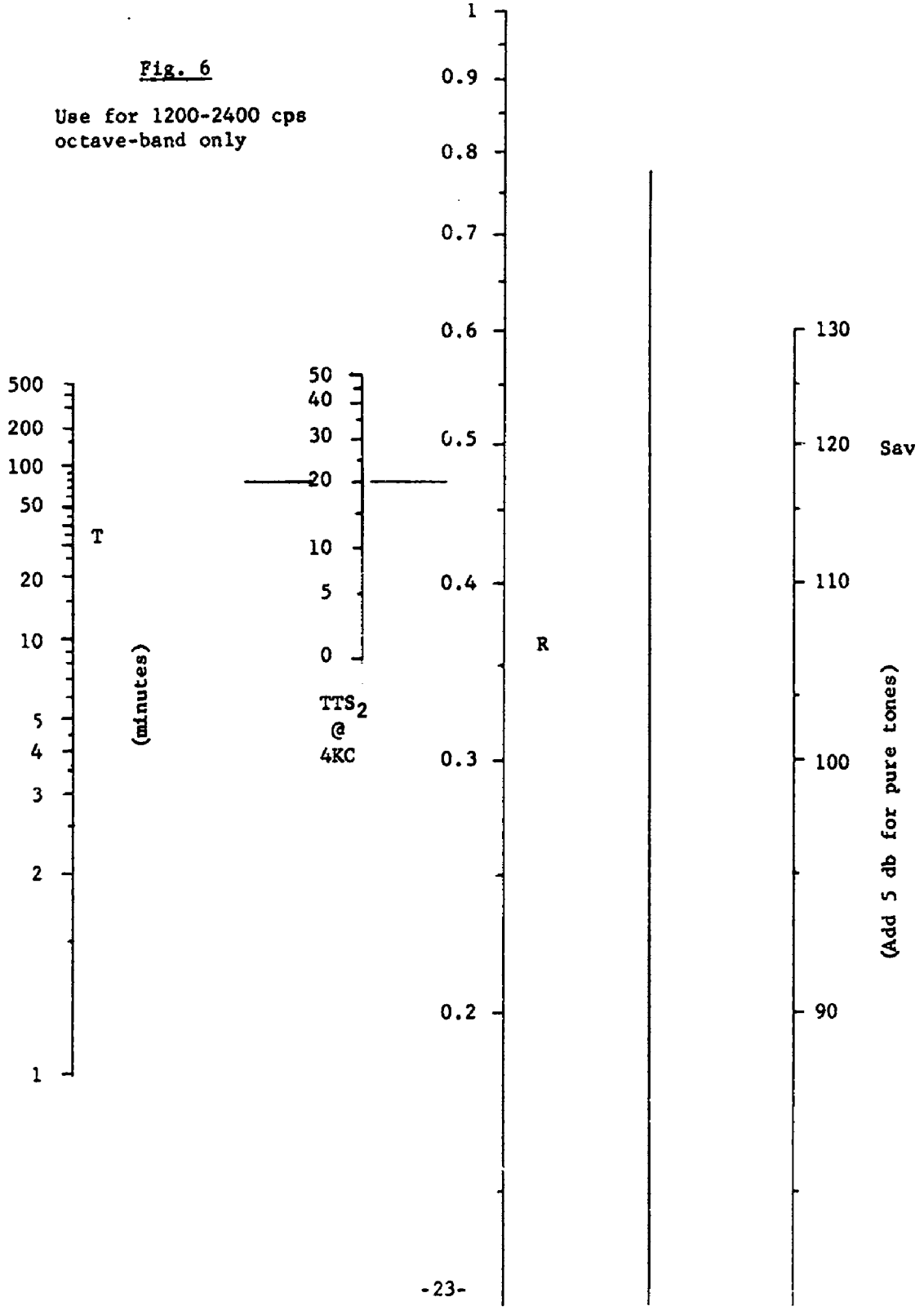

Fig. 7

Use for 2400-4800 cps
octave-band only

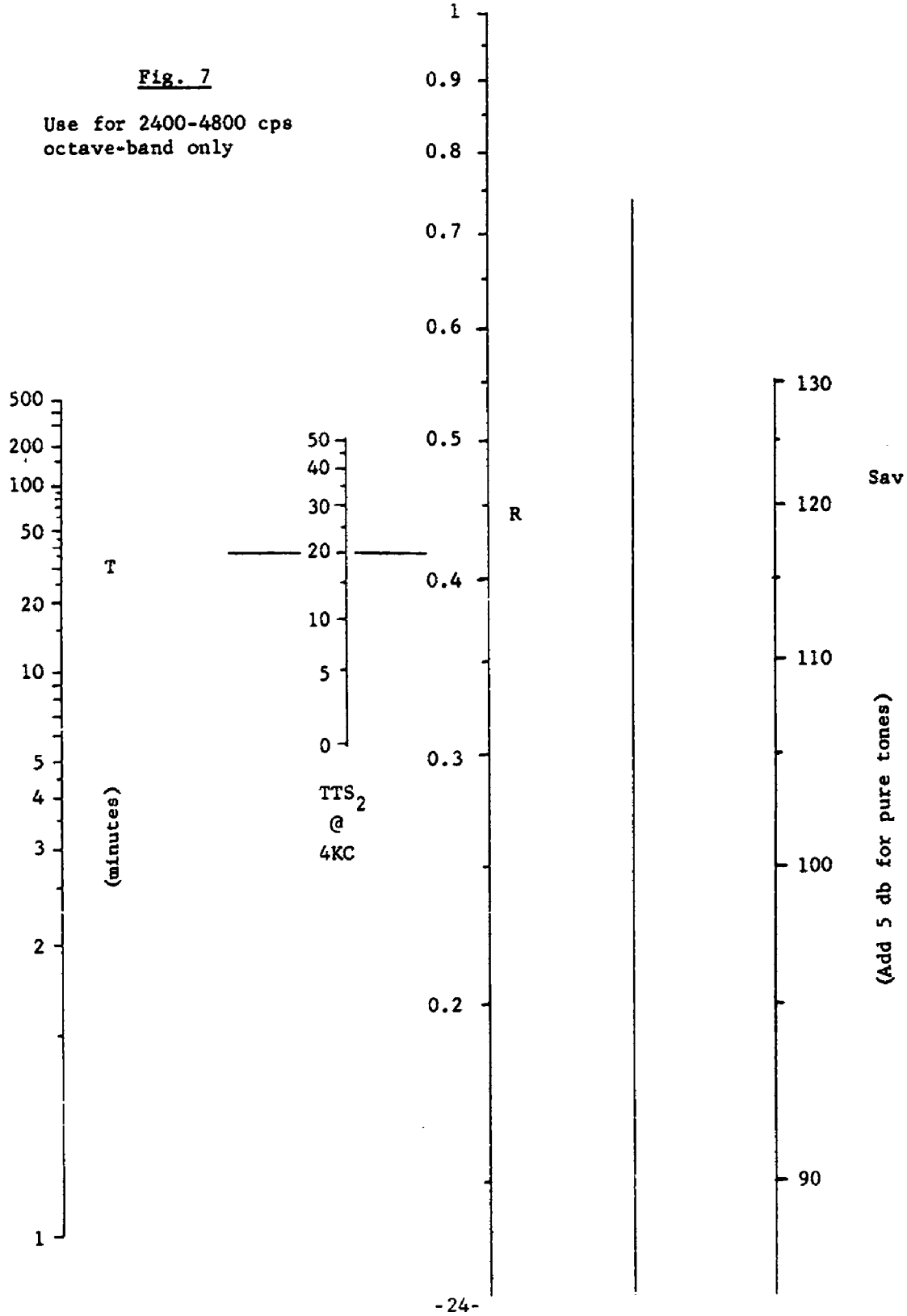

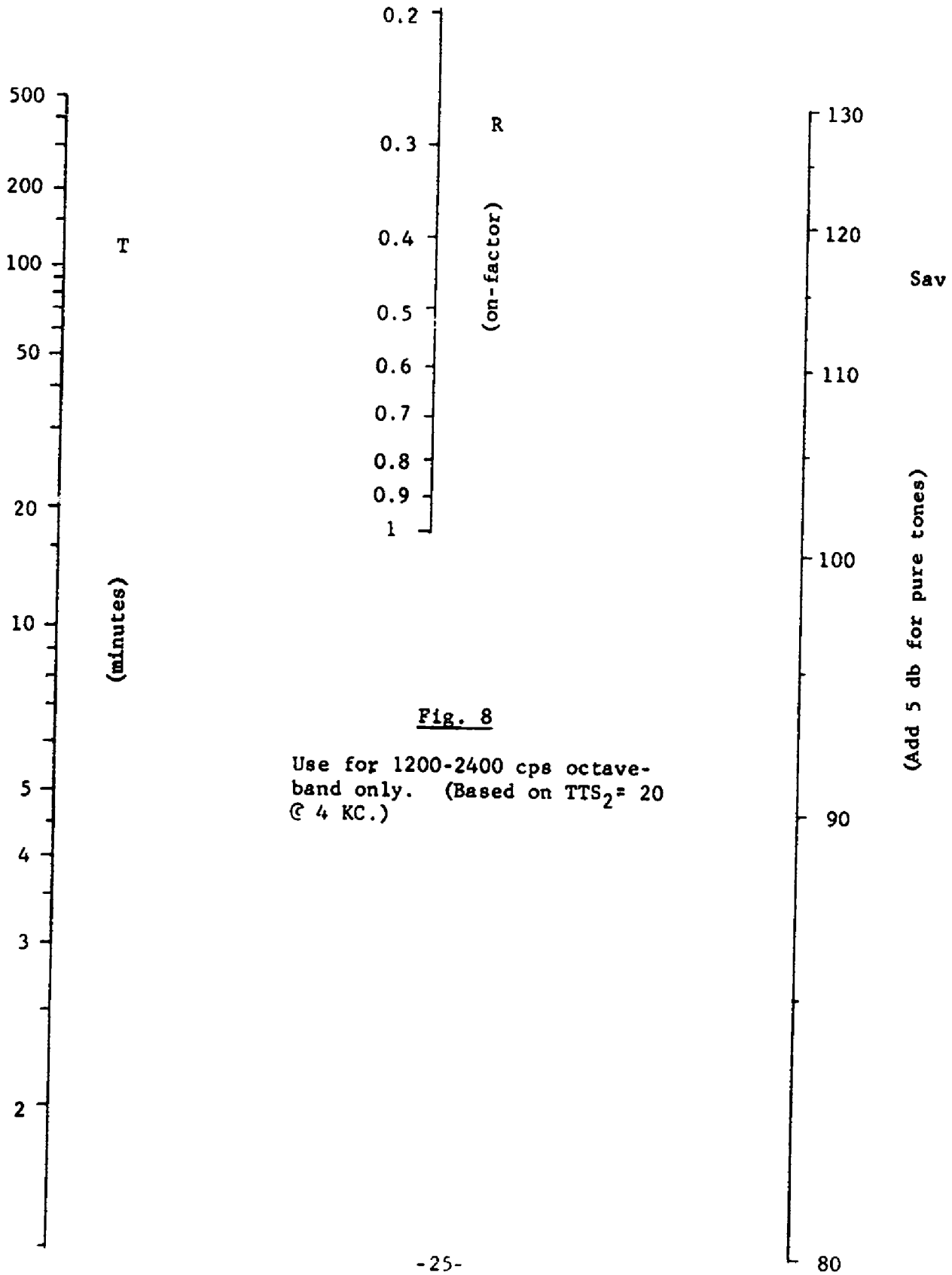

Fig. 8

Use for 1200-2400 cps octave-band only. (Based on TTS_2= 20 @ 4 KC.)

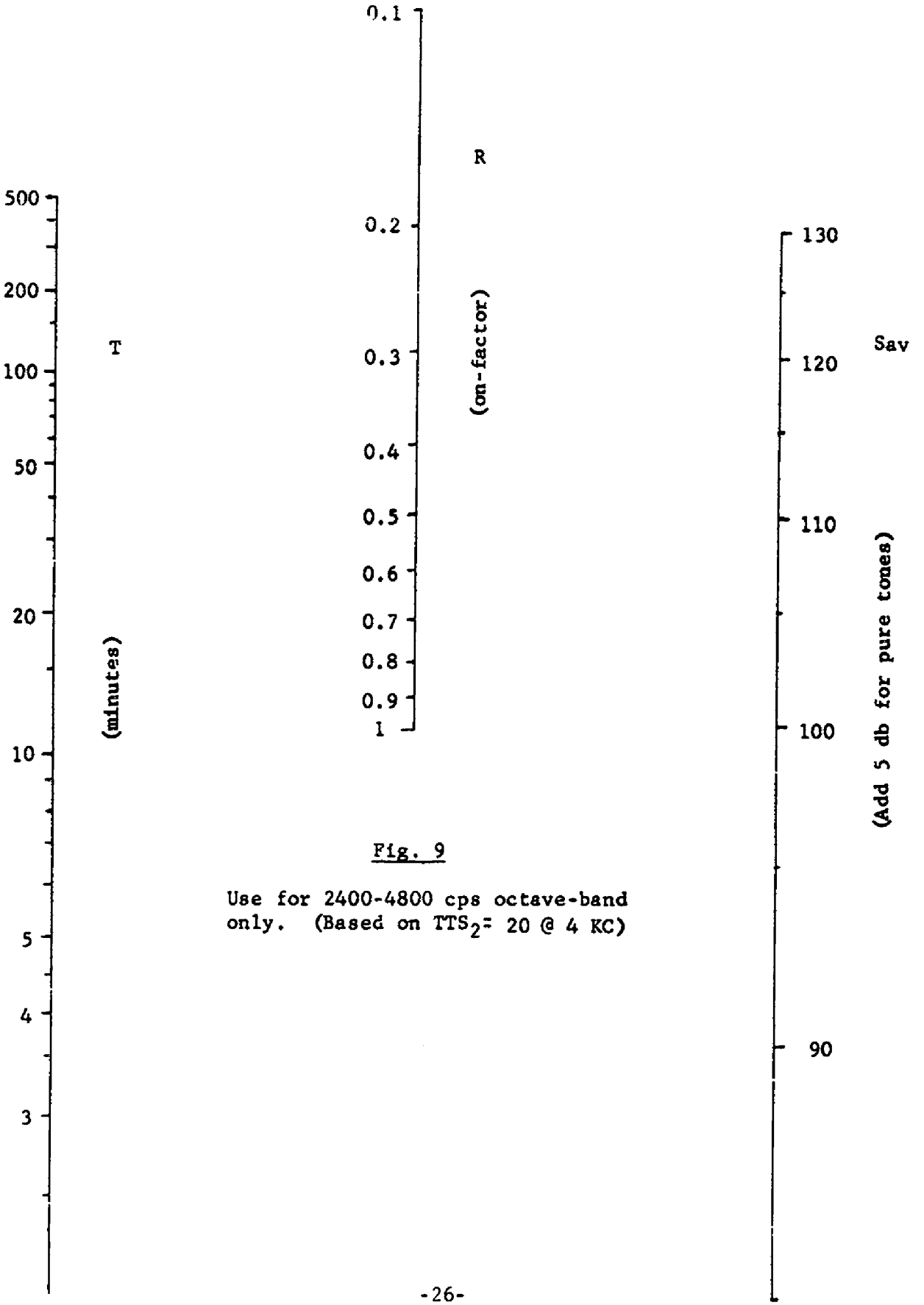

Fig. 9

Use for 2400-4800 cps octave-band only. (Based on TTS_2= 20 @ 4 KC)

Fig. 10

TIME DISTRIBUTION OF SOUND LEVELS

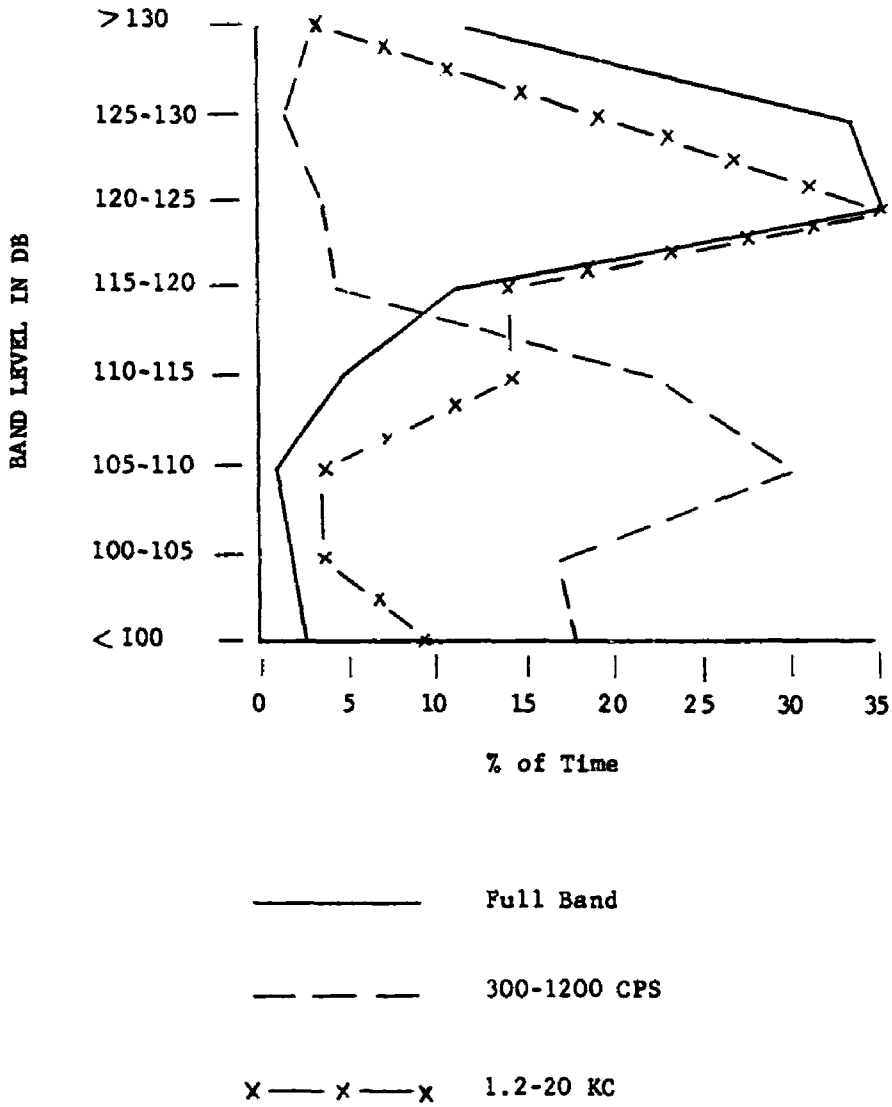

Fig. 11

TTS_2 AT 4 KC DUE TO 1200-2400 CPS OCTAVE BAND

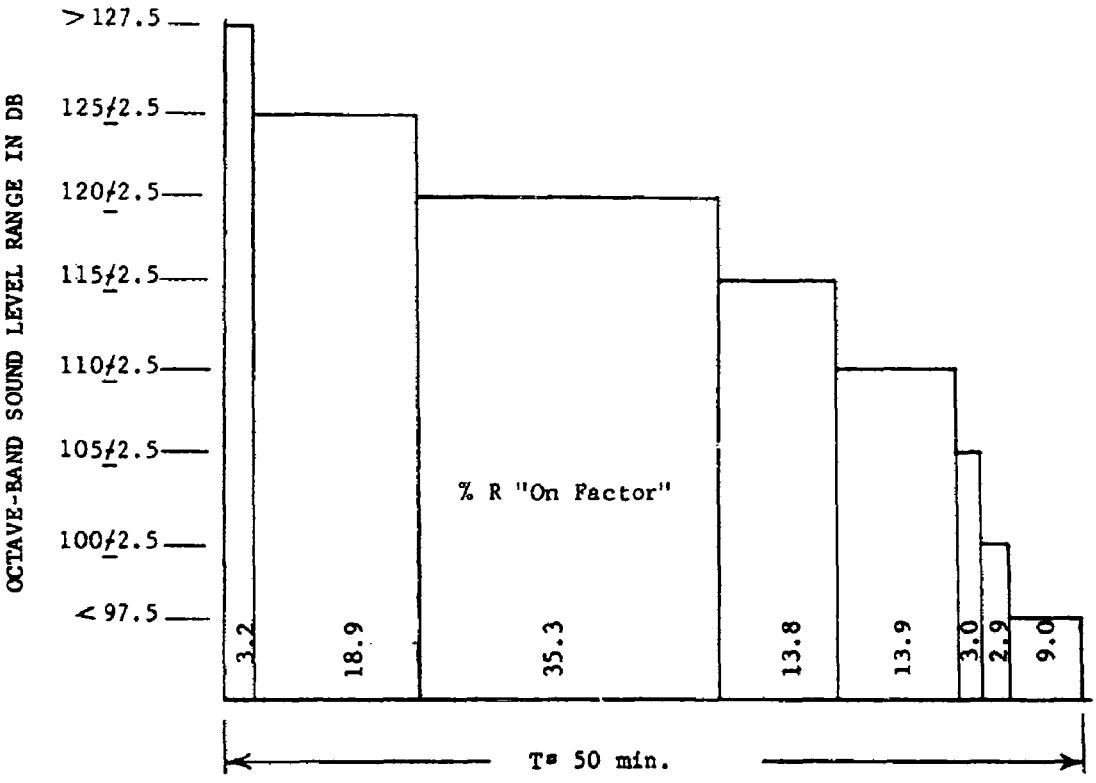

Deduct 25 db for attenuation of V-51R ear defenders:

$R_1(S_1-S_0) = .032 \left[(130-25)-65\right] = 1.28$

$R_2(S_2-S_0) = .189 \left[(125-25)-65\right] = 6.62$

$R_3(S_3-S_0) = .353 \left[(120-25)-65\right] = 10.59$

$R_4(S_4-S_0) = .138 \left[(115-25)-65\right] = 3.45$

$R_5(S_5-S_0) = .139 \left[(110-25)-65\right] = 2.78$

$R_6(S_6-S_0) = .030 \left[(105-25)-65\right] = .45$

$R_7(S_7-S_0) = .029 \left[(100-25)-65\right] = .29$

$R_8(S_8-S_0) = .090 \left[(95-25)-65\right] = .45$

$25.91 = \sum R_i(S_i-S_o)$

$TTS_2 = \left[.61 \times 25.91 \ (\log 50 \div .33) - 9.5\right] = 22.6$ db

3. Speech Communication in the Presence of Noise

In order to estimate the effects of noise on speech communication, the level and spectrum of the noise are often described in terms of a speech-interference-level.[16-19] By definition, the speech-interference-level is the arithmetic average sound level (at the point of interest) of several specified octave-bands. Tabulations are then given of the maximum distance for reliable conversation as a function of speech-interference-level (SIL) and voice level-the latter being specified simply as normal, raised, etc. There is some disagreement, however, as to which octave bands should be employed in calculating SIL. For example, Beranek[16,17] uses the 3 bands 600-1200, 1200-2400, and 2400-4800 cps; Strasberg[18] suggests the 4 bands 300-600, 600-1200, 1200-2400, and 2400-4800 cps; while recent studies of Klumpp and Webster[19] seem to correlate better with the 3 bands 300-600, 600-1200, 1200-2400 cps. Also, slight modifications of the SIL criteria should be made for the several calculation methods.

Actually, the concept of speech-interference-level is based upon a simplification of a method originally advanced by French and Steinberg[20-22] for the calculation of Articulation Index (AI) from the speech-to-noise ratio in 20 frequency bands. These bands are intended to be of equal importance from the standpoint of their contribution to speech intelligibility. Recent tests[23-25] confirm that the AI calculation is indeed a good method of predicting speech intelligibility.

Since AI calculation is adequate, the very fact that disagreement has arisen over which octaves should be employed in the simplified SIL approach indicates that we are attempting to oversimplify the problem.

This is undoubtedly due partially to the fact that the octaves employed do not contain all of the original 20 bands; nor do the various octave-bands contain equal numbers of the 20 bands of equal importance. Another factor which is usually not considered at all is the fact that SIL criteria as normally used correspond to an AI of approximately 0.40-which although sufficient for sentence intelligibility is not always enough for high intelligibility for isolated words. (There is one paper in the literature which does attempt to extend an SIL calculation to other values of AI.[26]) In addition, no SIL approach to speech intelligibility has been proposed that takes into consideration many other factors such as reverberation, frequency and amplitude distortion of speech by a PA system, intermittent noise, spread of masking, vocal effort, ear overload, etc.-all of which may be brought into the picture when AI calculation is employed. Hence, from a technical standpoint, it seems that the use of AI should be favored over SIL. Of course, the primary reason why SIL has gained favor is its basic simplicity.

A recent paper by Kryter[27,24] seems to provide an answer to this dilemma. He proposes the use of the six octave bands 150-300 cps thru 4800-9600 cps with a weighting factor for each band that depends upon how many of the original 20 bands fall within the octave. Taking these factors as n/600 (when n is the number of speech bands wherein the octave) we may quite readily compute AI for a given speech-to-noise ratio by adding the contributions of the 6 octaves. Table VII lists these weighting factors and shows the basic method of AI calculation. In such calculations, the maximum effective speech-to-noise ratio is taken as 30 db, while ratios of 0 db or less contribute nothing.

Table VII

Octave band	150	300	600	1200	2400	4800
Cps	300	600	1200	2400	4800	9600
1. Weighting Factor	.0013	.0042	.0067	.0105	.0089	0017
2. Speech Peak Level	77	80	75	70	64	58
3. Noise Level	69	67	62	53	51	48
4. S/N ratio, db (#2-#3)	8	13	13	17	13	20
5. AI contribution (#1 x #4)	.0104	.0546	.0871	.1786	.1156	.0340

6. AI = sum of line #5 = 0.48

From Figure 12, this corresponds to about 97% sentence intelligibility [27, 28, 20]. Figure 12 also shows average intelligibility scores for various lists of words and syllables. Such calculations agree well with the more involved 20 band procedures.[24]

Thus, a knowledge of the speech-to-noise ratio in 6 octaves provides a better picture of speech intelligibility than can be obtained from SIL alone. Actually, the calculation is not much more difficult; noise levels are needed in 3 or 4 of these 6 octaves in order to compute SIL, and tests have shown that a generalized speech spectrum is sufficient. It is only necessary to determine the overall speech level-which, of course, varies with voice level, distance, and use of PA system, if any. Table VIII gives typical levels for speech peaks (male voices) when the long term rms overall speech level is 65 db.[27,29,20] This is approximately a normal speech level at a distance of 1 meter. In practice, the long term rms level can be estimated by subtracting 3 db from the arithmetic average of the peak readings of a sound level meter set for slow response on the "C" scale.[27] Actual speech peaks are normally about 12 db above

the long term rms level-or 9 db above the readings of such a meter. If a sound level meter is not available, one may make a rough estimate of speech level from the fact that a "raised voice" is about 6 db louder than a "normal" voice, and a "very loud" voice about 6 db louder than a "raised" voice. Such assumptions are exactly those used in the simplified SIL approach.[17] Obviously, of course, speech level will decrease with increased distance-6 db per doubling of distance in a free field and somewhat less than that in a normal room. (The SIL approach simply uses the 6 db per doubling figure.)

Table VIII

Octave Band	150	300	600	1200	2400	4800
Cps	300	600	1200	2400	4800	9600
Typical Speech Peak Levels (65 db rms overall)	71	74	69	64	58	52

When PA systems are used, the long term average rms speech level must be measured at the location of interest. Table VIII may then be used to determine the speech spectrum. For example, if the average rms level were found to be 87 db, the speech spectrum would be estimated by adding 87-65= 22 db to the levels of Table VIII.

The previous discussion is based on the assumption that the talker and listener cannot see each other, that reverberation time is zero, that the noise is steady-state, that the communications link is distortionless, etc. In practice, all such requirements are not likely to be fulfilled in a given situation. Kryter has discussed proposed modifiers to the basic technique to permit extension to these situations. These

will be briefly discussed. All of these factors are normally neglected in the SIL approach.

Figure 13 shows the basic work-sheet for calculation of AI by octave bands, including the spectrum for normal male speech.[27] If the speech is electronically amplified, there is a maximum tolerable sound level which should not be exceeded since it overloads the hearing mechanism and does not contribute to intelligibility. If the speech link does not have flat frequency response, the effective speech spectrum should be adjusted accordingly. Another factor which should be considered for loudspeaker presentation is indicated in Table IX. This is a correction for degradation in speech intelligibility at high levels in a partially reverberent room.[27,30] It should not be applied outdoors.

Table IX

Overall rms speech level	Amount to be subtracted from speech level	Resulting Effective speech level
85 db	0 db	85 db
90	2	88
95	4	91
100	7	93
105	11	94
110	15	95
115	19	96
120	23	97
125	27	98
130	30	100

Thus, little is to be gained by increasing indoor speech levels above

about 100 db.

Speech communications systems sometimes employ peak clipping to decrease the peak-to-rms ratio, thereby improving AI.[31] Figure 14 shows the effective increase in speech level to be added to the speech spectrum normally used with Fig. 13 - as a function of the amount of clipping.[31,27] Twenty-four db of clipping is equivalent to 12 db greater speech level.

If the talker is not speaking in a reasonably normal voice, a further adjustment of the AI is necessary.[32] If a very low or very loud tone is used, the effective speech level - to be used in conjunction with Fig. 13 - must be lower than the true speech level since vocal quality will differ from normal speech. Figure 15 shows this relationship.[32,27]

Studies also show that very high background noise levels provide more speech masking for a given speech-to-noise ratio than low background noises with the same spectrum.[33] This introduces a correction to the background noise for each frequency band which is determined by the excess of the background noise above the threshold of audibility in that band. Table X and Figure 13 both show the average threshold of audibility, while Table XI lists the correction to be applied to the noise spectrum.[33,27]

Table X

Octave-band	150	300	600	1200	2400	4800
Ops	300	600	1200	2400	4800	9600
Threshold of audibility	26	17	12	9	3	13

Table XI

Band Level minus Threshold Level	Correction to be added to Noise Level for this Band
80 db	0 db
85	1
90	2
95	3
100	4
105	5
110	6
115	7
120	8
125	9
130	10
135	11
140	12
145	13
150	14

If the noise is predominately of a narrow bandwidth character, still another correction should be applied for upward and downward spread of masking beyond the actual bandwidth of the noise per se.[34, 35, 27] However, for broadband noises - as are characteristic of jet aircraft, etc. - such corrections are much less important[22] and so will not be considered in detail in this report.

If the background noise is interrupted, the calculated AI is

adjusted by means of Figs. 16 and 17.[36,28,27] As would be expected, interruption of the noise increases AI; the amount of increase is strongly influenced by interruption rate. Aircraft take-off from a carrier deck is normally at too low a frequency to increase AI appreciably. Apparently a 10 cps interruption rate is optimum to permit the listener to hear enough of each word unmasked to piece together the whole. At very high interruption rates the noise acts like a continuous noise of somewhat lower level.

Reverberation acts to decrease AI as shown by Fig. 18.[37,27] On a carrier flight-deck the reverberation time would be zero, but would not be negligible in an enclosed area.

In the same way that a deaf person can lip-read, visual cues give an improvement in AI when the listener can see the talker. As would be expected, the poorer the AI without visual cues, the more they help, as in Fig. 19.[38,27]

The four examples given below illustrate the calculation and use of AI for hypothetical situations. They should also serve to show the superiority of an AI calculation over the normal SIL procedures.

Example 1: The noise levels at a particular point of interest due to a relatively distant group of aircraft (perhaps at idle power) is as tabulated in line 1 of Table XII. A nearby loudspeaker, operating from a PA amplifier etc., delivers an average speech level - as read by the peaks of the slow response of a sound level meter on the C weighting network - of 123 db. The PA system has a flat frequency response (including microphone) except at high frequencies - it being 2 db down in the 2400-4800 cps range and 5 db down for 4800-9600 cps.

As previously discussed, the long term average rms speech level may be estimated by subtracting 3 db from the sound level meter readings obtained as described above. The result is 120 db. Table VIII gives a typical peak speech spectrum for a 65 db rms level. Hence, we need only add 120-65 = 55 db to these figures to obtain the peak speech spectrum for a flat PA system. The result is given in line 2 of Table XII. Applying the minor high frequency less corrections for the PA system, we obtain line 3 of this tabulation. (If such a procedure is sufficient to change the overall level appreciably, all numbers should be increased or decreased by the constant amount required to maintain overall level.)

Table XII

	Octave Bands	150	300	600	1200	2400	4800
	Cps	300	600	1200	2400	4800	9600
1.	Meas. Noise Level	103	109	111	113	106	100
2.	Speech Peaks (uncorrected for PA system)	126	129	124	119	113	107
3.	Speech Peaks (corrected for PA system)	126	129	124	119	111	102
4.	Audibility Threshold	26	17	12	9	3	13
5.	Line 1 - Line 4	77	92	99	104	103	87
6.	Correction to Noise	-	2	4	5	5	-
7.	Corr. Noise Spectrum	103	111	115	118	111	100
8.	Line 3 - Line 7	23	18	9	1	0	2
9.	Weighting Factor	.0013	.0042	.0067	.0105	.0089	.0017
10.	Contributions to AI	.030	.076	.060	.011	-	.003
11.	AI = sum of Line 10 = 0.18						

Since Line 3 does not exceed the maximum tolerable levels for unclipped speech - as shown on Figure 13 - no further speech corrections are required.

Line 4 gives the audibility threshold as in Table X, and the indicated corrections for high level masking (line 6) are obtained from Table XI.

Subtracting line 7 from line 3, we obtain the effective speech-to-noise ratio for each band. These must be multiplied by the weighting factors (line 9) from Table VII to give the contributions of the individual octave bands to the AI. The total AI is the sum of these contributions, or 0.18.

From Fig. 12, this would be expected to provide only about 75% sentence intelligibility, and very poor intelligibility for individual words.

Example 2: The noise level is the same as for example 1. However, 12 db speech clipping is employed in the PA system with 12 db post-clipping gain to achieve the previous peak amplitudes.

Referring to Fig. 14, the effective speech peaks have been increased 9 db due to clipping and post-clipping gain. Hence, the speech levels are as indicated in the first line of Table XIII - being obtained by adding 9 db to the corresponding figures of line 3, Table XII. In the 600-1200 band, these effective speech peak levels exceed the maximum tolerable levels of Fig. 13 for 12 db clipping by a small amount. Hence, the speech peaks are corrected as indicated in line 2.

Table XIII

	Octave Bands	150	300	600	1200	2400	4800
	Cps	300	600	1200	2400	4800	9600
1.	Effective Peaks	135	138	133	128	120	111
2.	Eff. Speech Peaks corrected for maximum level	135	138	132	128	120	111
3.	Corr. Noise Spectrum	103	111	115	118	111	100
4.	Line 2 - Line 3	32	27	17	10	9	11
5.	Eff. Speech-to-noise	30	27	17	10	9	11
6.	Weighting Factor	.0013	.0042	.0067	.0105	.0089	.0017
7.	Contribution to AI	.039	.113	.114	.105	.080	.019

8. AI = sum of Line 7 = 0.47

Line 3 shows the corrected noise spectrum, as taken from line 7 of Table XII. The calculation than proceeds as before, except that in the 150-300 cps band it is necessary to make use of the fact that the effective speech-to-noise ratio should be limited to 30 db.

The AI is now computed as 0.47, which from Table 12 corresponds to 97% sentence intelligibility and 94% word intelligibility for the 250 word list. Thus, a worthwhile improvement has been obtained by speech clipping.

Example 3: Assume the locale to be a conference room at some distance from flight deck operations. Assume the noise levels are as given in line 1 of Table XIV, and that the room has a reverberation time of about 1 second (at 500 cps) Further assume that no PA system is being used, but that the speaker is talking in a rather loud voice. For example, take the long term rms speech level as 80 db at 1 meter-though

only 70 db at a typical location of interest. (The sound level meter readings on C - slow would be about 3 db higher for peaks) It may also be assumed that the audience is watching the speaker, and hence is aided somewhat by visual cues.

From Fig. 15 it is seen that high vocal effort is limiting the speech intelligibility slightly, and that to correct for this a 2 db subtraction should be made from the actual speech levels. Hence, the effective speech level at a typical position of interest is 70 - 2 = 68 db. Then from VIII, the speech peak spectrum is as indicated in line 2 of Table XIV.

Table XIV

	Octave Bands	150	300	600	1200	2400	4800
	Cps	300	600	1200	2400	4800	9600
1.	Noise Spectrum	67	57	52	49	43	40
2.	Corrected Speech Peaks	74	77	72	67	61	55
3.	Line 2 - Line 1	7	20	20	18	18	15
4.	Weighting Factor	.0013	.0042	.0067	.0105	.0089	.0017
5.	Contribution to AI	.009	.084	.134	.189	.160	.026

6. AI = sum of Line 5 = 0.60
7. AI corrected for 1 sec reverberation time = 0.50
8. Effective AI with visual cues = 0.63

Since neither noise nor speech levels are excessive, no further corrections are necessary, and the calculation proceeds in a normal fashion as outlined in Table XIV, thru line 6.

Now, however, a correction is applied for the 1 second assumed

reverberation time. From Fig. 18, this is expected to reduce AI by 0.1. Fig. 19 indicates that this reduction is more than compensated for by the effect of visual cues - the final result being AI = 0.63.

Example 4: Assume the same room as in example 3, except that the noise spectrum has been raised 25 db and a flat response PA system used to increase the speech level 25 db without clipping - thus maintaining the same speech-to-noise ratio.

The speech level is now 70 + 25 = 95 db rms. Hence, from Table IX the effective level (in a room) is but 91 db. The speech peak spectrum is, therefore, 91 - 65 = 26 db above that of Table VIII. This is shown in line 1 of Table XV. Line 2 shows the noise spectrum as described above. Since neither speech nor noise is excessive (See Fig. 13 and Tables X and XI) the calculation now proceeds in a normal manner as indicated in Table XV. The results indicate only a slight drop in intelligibility from example 3 to example 4. However, if in example 3 the speaker had been talking with a normal vocal effort, the decrease in AI due to raising both speech and noise by equal amounts would have been somewhat greater.

Table XV

	Octave band	150	300	600	1200	2400	4800
	Cps	300	600	1200	2400	4800	9600
1.	Effective Speech Peaks	97	100	95	90	84	78
2.	Noise Spectrum	92	82	77	74	68	65
3.	Line 1 - Line 2	5	18	18	16	16	13
4.	Weighting Factor	.0013	.0042	.0067	.0105	.0089	.0017

Table XV con't

5. Contributions to AI	.007	.076	.121	.168	.142	.022

6. AI = sum of line 5 = 0.54

7. AI corrected for 1 sec. reverberation time = 0.44

8. Effective AI with visual cues = 0.60

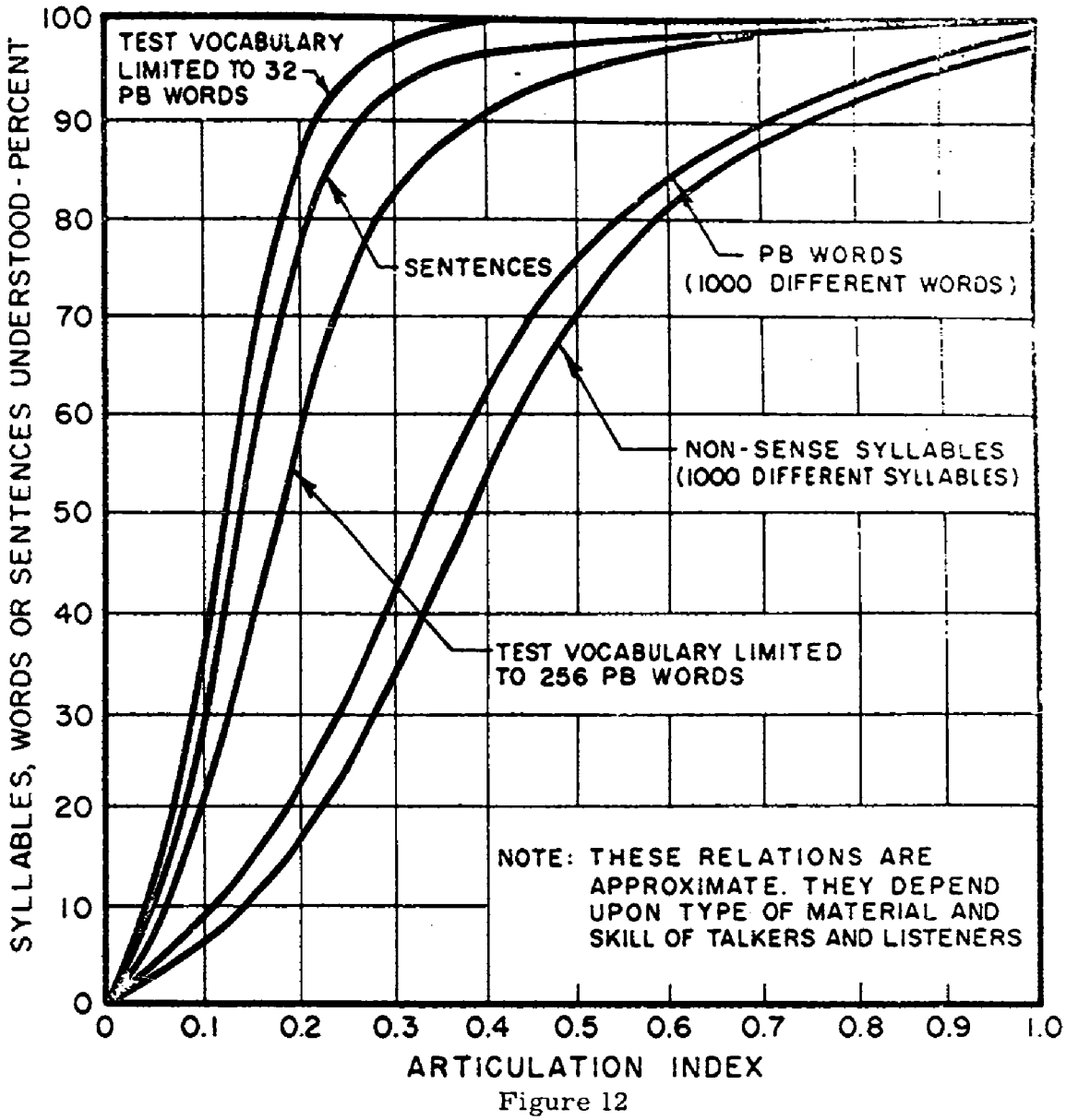
SYLLABLES, WORDS OR SENTENCES UNDERSTOOD - PERCENT
100
90
80
70
60
50
40
30
20
10
0
0
0.1
0.2
0.3
0.4
0.5
0.6
0.7
0.8
0.9
1.0
ARTICULATION INDEX
TEST VOCABULARY LIMITED TO 32 PB WORDS
SENTENCES
PB WORDS (1000 DIFFERENT WORDS)
NON-SENSE SYLLABLES (1000 DIFFERENT SYLLABLES)
TEST VOCABULARY LIMITED TO 256 PB WORDS
NOTE: THESE RELATIONS ARE APPROXIMATE. THEY DEPEND UPON TYPE OF MATERIAL AND SKILL OF TALKERS AND LISTENERS
Figure 12

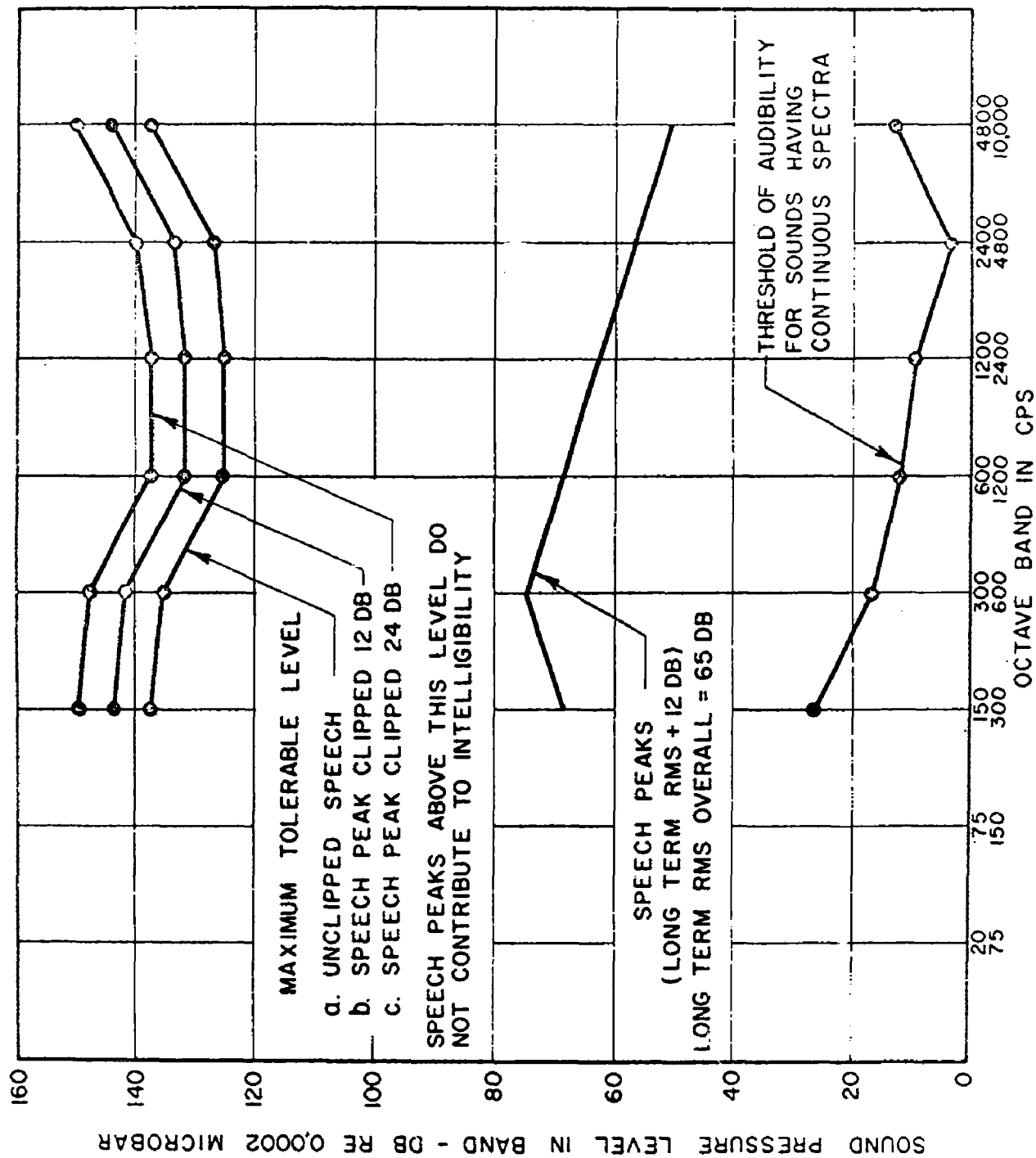
SOUND PRESSURE LEVEL IN BAND - DB RE 0.0002 MICROBAR
160
140
120
100
80
60
40
20
0
MAXIMUM TOLERABLE LEVEL
a. UNCLIPPED SPEECH
b. SPEECH PEAK CLIPPED 12 DB
c. SPEECH PEAK CLIPPED 24 DB
SPEECH PEAKS ABOVE THIS LEVEL DO NOT CONTRIBUTE TO INTELLIGIBILITY
SPEECH PEAKS
(LONG TERM RMS + 12 DB)
LONG TERM RMS OVERALL = 65 DB
THRESHOLD OF AUDIBILITY FOR SOUNDS HAVING CONTINUOUS SPECTRA
20
75
150
300
600
1200
2400
4800
10,000
OCTAVE BAND IN CPS

FIGURE 13

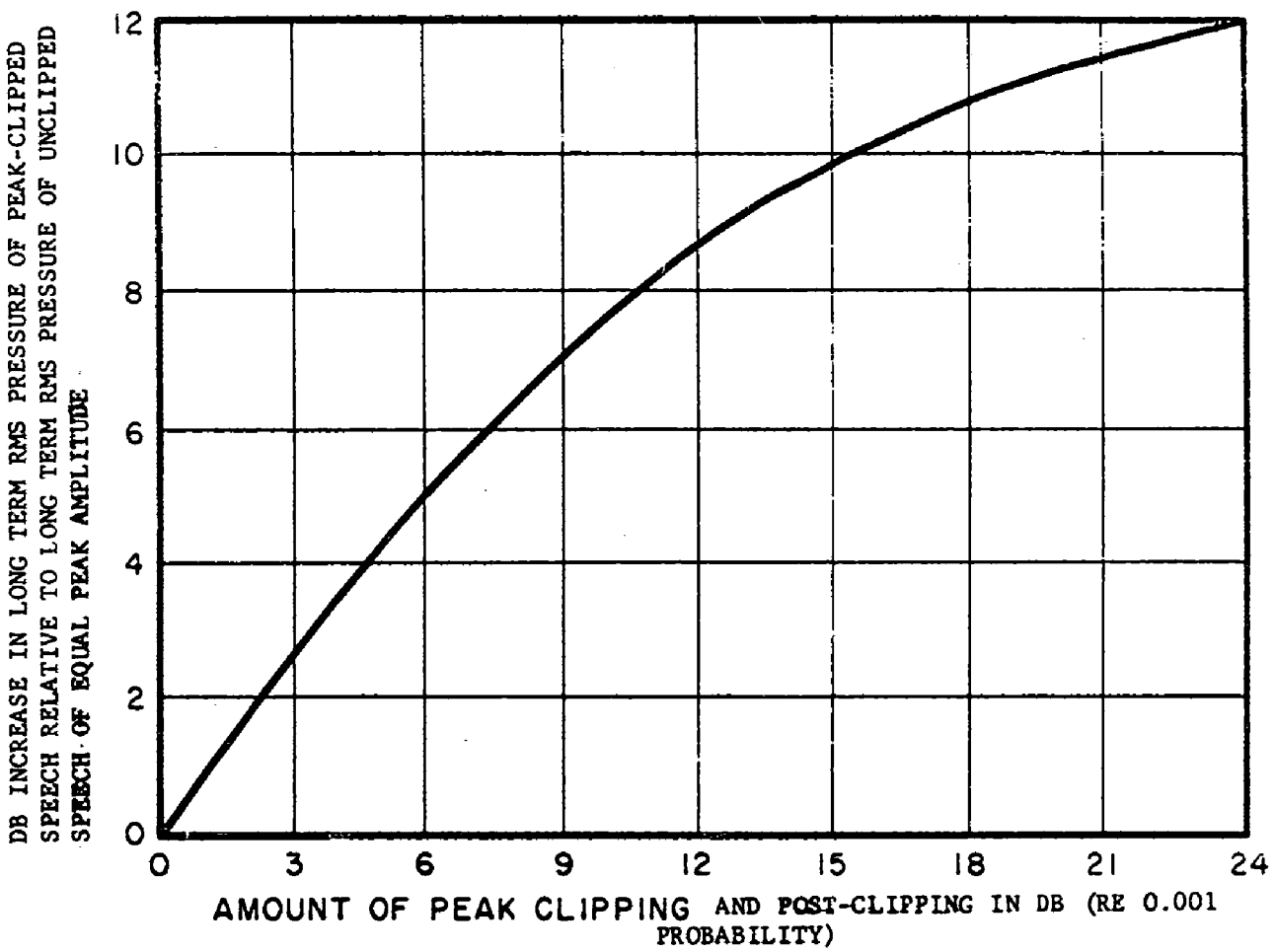
DB INCREASE IN LONG TERM RMS PRESSURE OF PEAK-CLIPPED SPEECH RELATIVE TO LONG TERM RMS PRESSURE OF UNCLIPPED SPEECH OF EQUAL PEAK AMPLITUDE
0
2
4
6
8
10
12
0
3
6
9
12
15
18
21
24
AMOUNT OF PEAK CLIPPING AND POST-CLIPPING IN DB (RE 0.001 PROBABILITY)

FIGURE 14

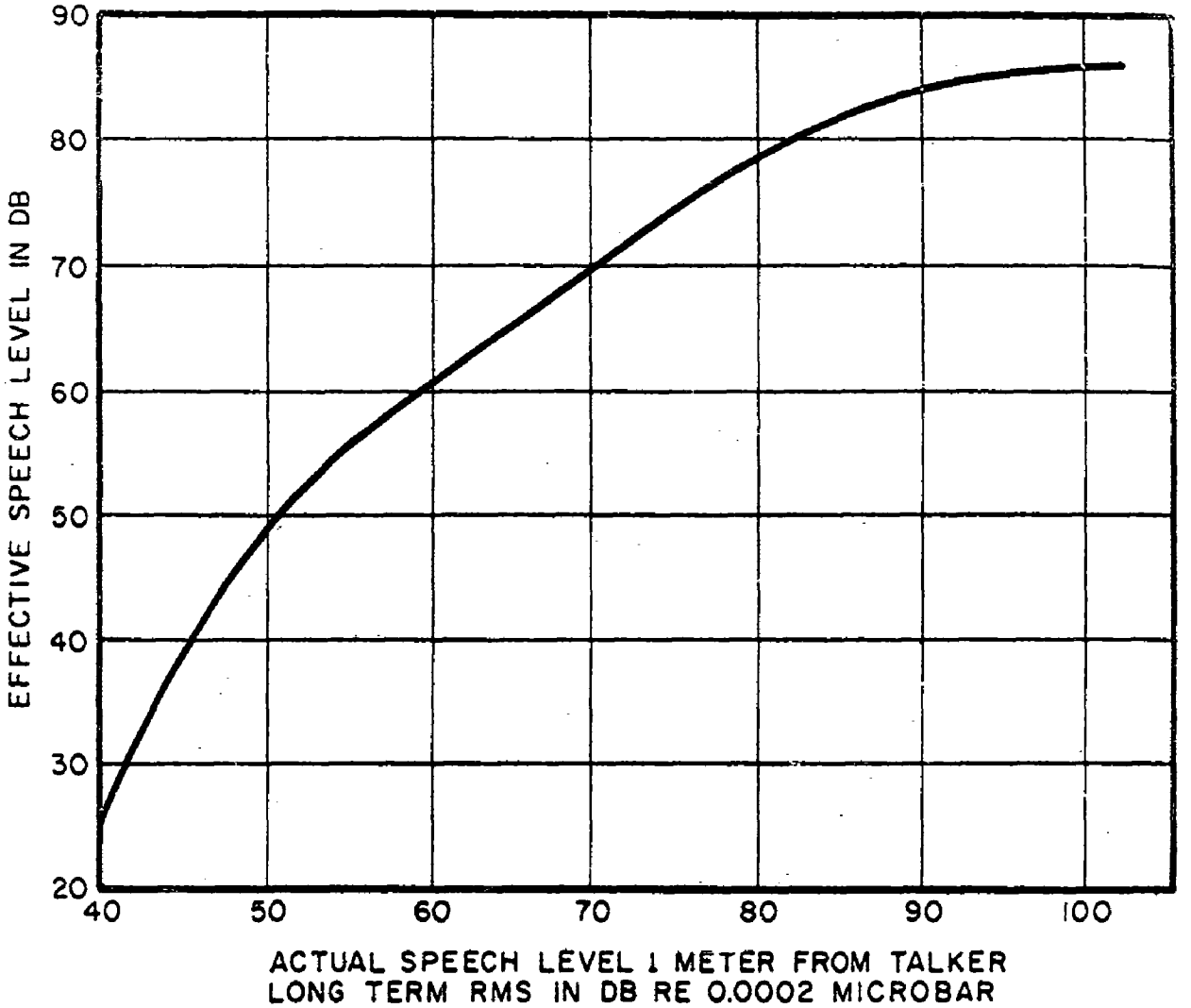
EFFECTIVE SPEECH LEVEL IN DB
90
80
70
60
50
40
30
20
40
50
60
70
80
90
100
ACTUAL SPEECH LEVEL 1 METER FROM TALKER
LONG TERM RMS IN DB RE 0.0002 MICROBAR

FIGURE 15

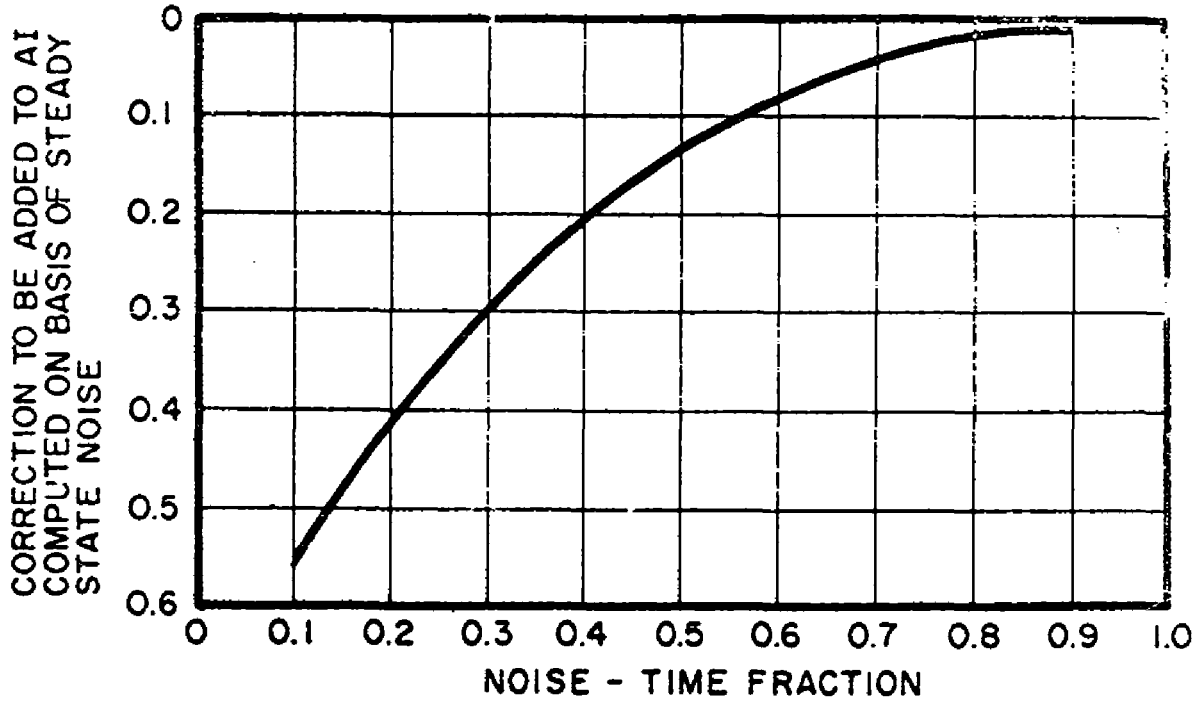

FIGURE 16 THE ORDINATE SHOWS A CORRECTION TO BE APPLIED TO THE ARTICULATION INDEX COMPUTED ON THE ASSUMPTION THAT A MASKING NOISE IS STEADY STATE FOR VARIOUS NOISE-TIME FRACTIONS. (4) THE CORRECTED AI CAN NOT EXCEED ONE (1.0)

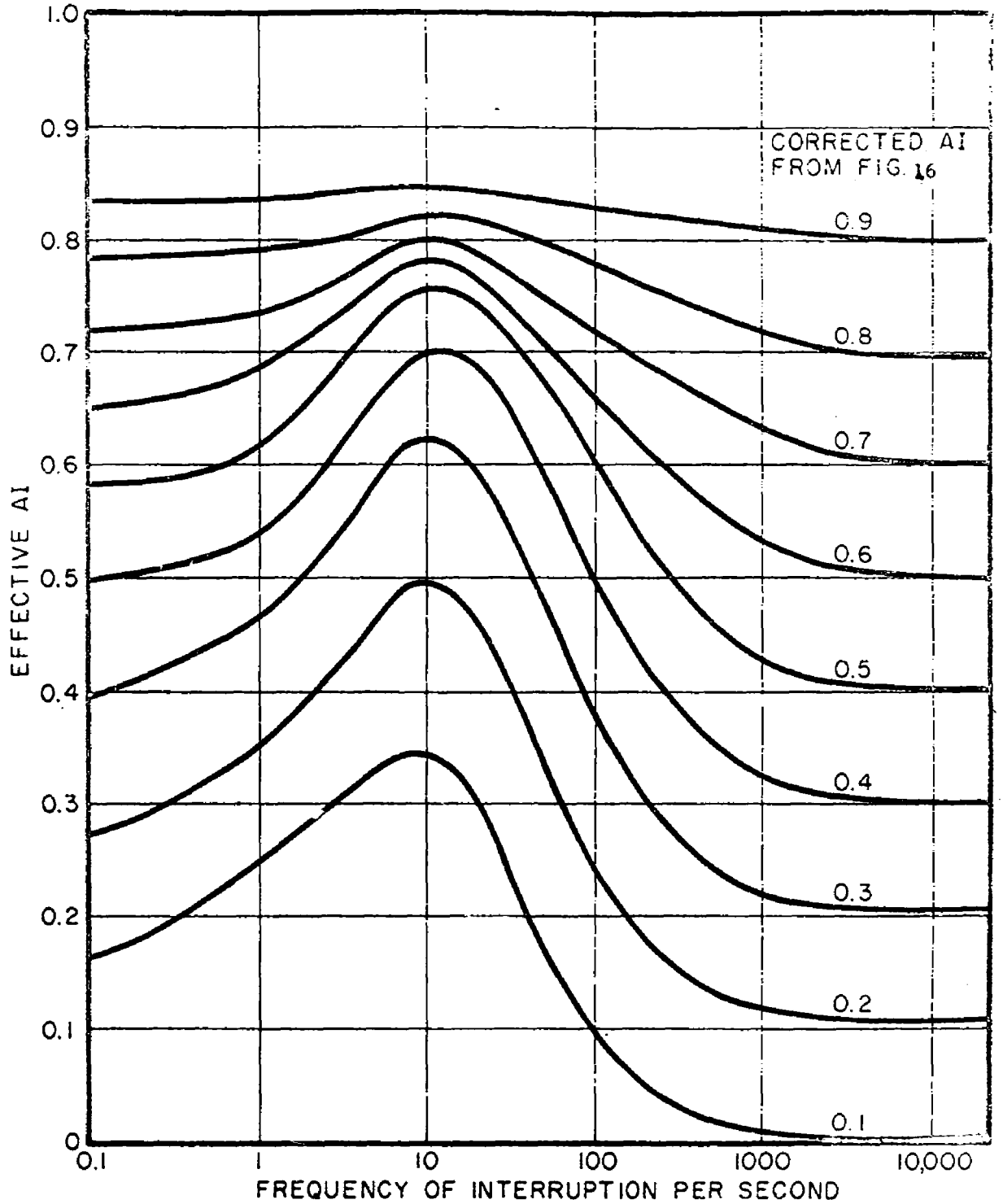
1.0
0.9
0.8
0.7
0.6
0.5
0.4
0.3
0.2
0.1
0
EFFECTIVE AI
CORRECTED AI
FROM FIG. 16
0.9
0.8
0.7
0.6
0.5
0.4
0.3
0.2
0.1
0.1
1
10
100
1000
10,000
FREQUENCY OF INTERRUPTION PER SECOND

FIGURE 17

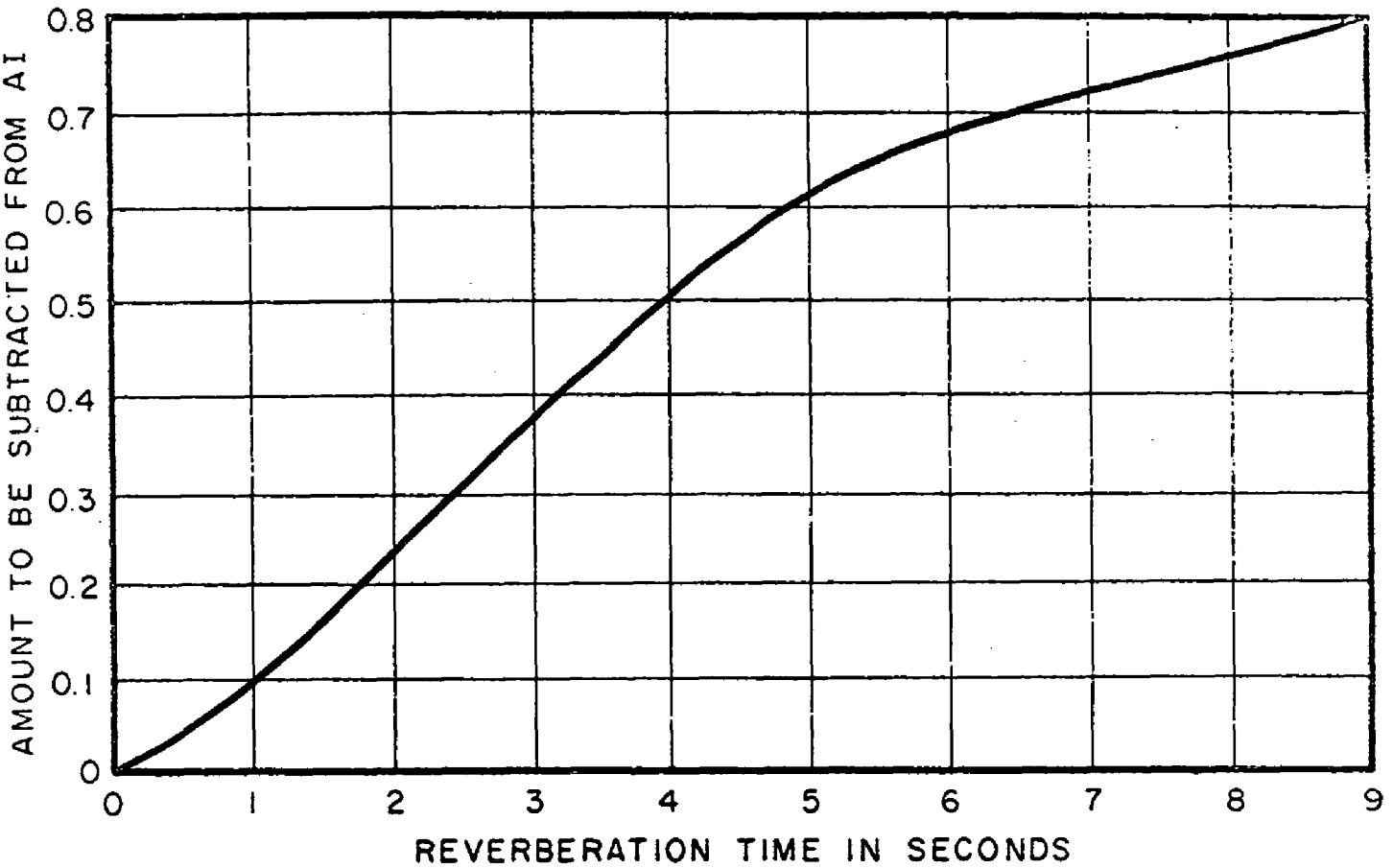
AMOUNT TO BE SUBTRACTED FROM AI
0.8
0.7
0.6
0.5
0.4
0.3
0.2
0.1
0
0
1
2
3
4
5
6
7
8
9
REVERBERATION TIME IN SECONDS

FIGURE 18

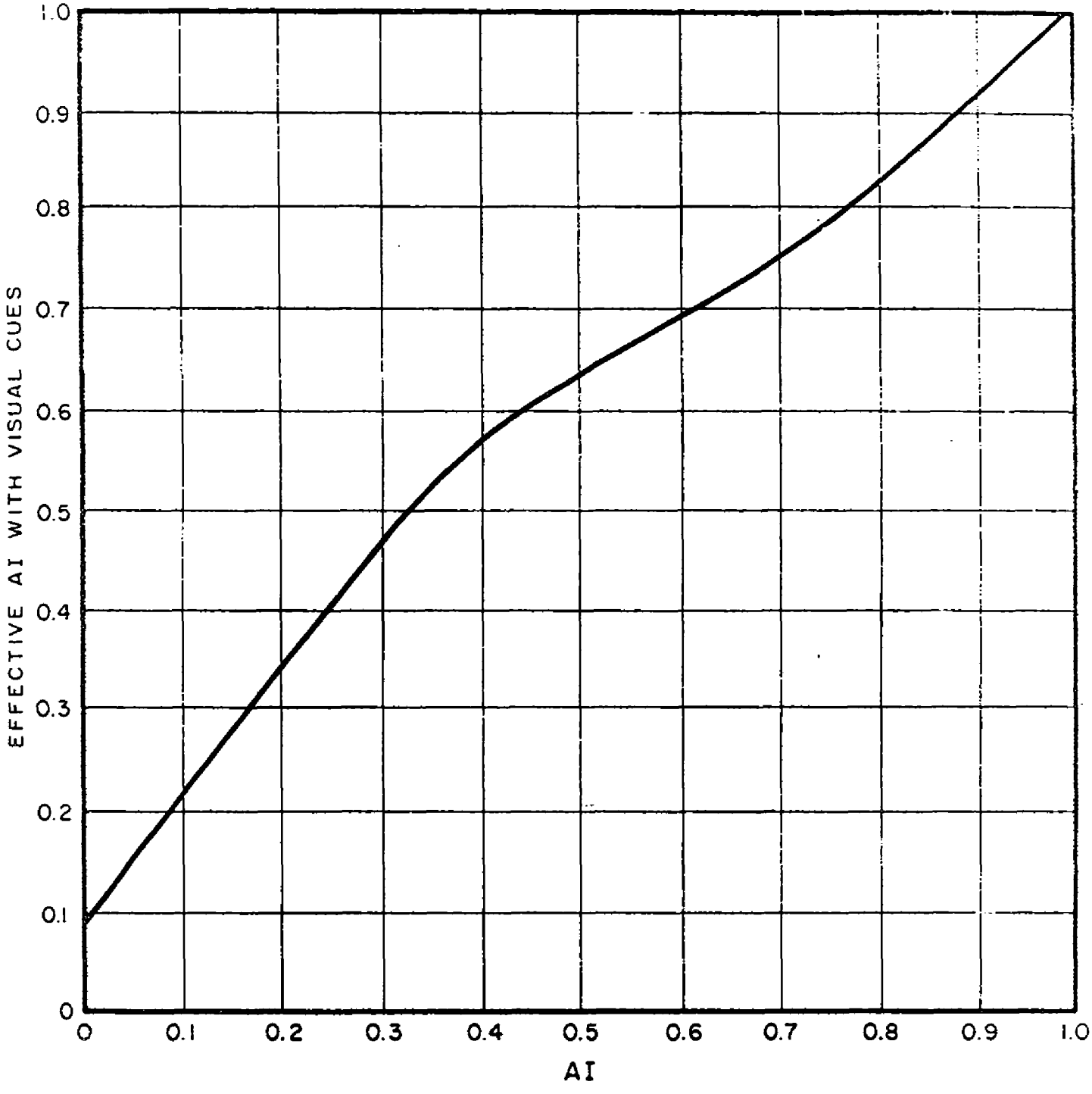
EFFECTIVE AI WITH VISUAL CUES
1.0
0.9
0.8
0.7
0.6
0.5
0.4
0.3
0.2
0.1
0
0
0.1
0.2
0.3
0.4
0.5
0.6
0.7
0.8
0.9
1.0
AI

FIGURE 19

IV. EFFECTS OF NOISE ON STRUCTURES

1. Introduction

The high noise levels produced by jet and rocket engines has led to fatigue failure of structural parts and to excessive vibration resulting in malfunction of equipment. Great effort has been made by many people to analyze and find solutions in various phases of the problem. In spite of the vast literature on the subject there is still no reliable, widely used method for specifying the allowable noise levels for a given aircraft or conversely to define a structure to withstand a given noise level.

Very considerable progress has been made in various areas but the problem is so complex that much remains to be done. There is a need for a more accurate method for calculating the noise pressure levels in the near field of a jet. The space correlations of the pressures which are important in determining the coupling between the pressure and the structure require more study. Although methods for calculating the resonant frequencies of many types of structures have been used with some success, the computation of the response and the stress or strain in practical structures is quite difficult and unreliable. The damping is of paramount importance in determining the response at resonance and is usually measured or estimated rather than calculated. The mechanism of fatigue of structures is not well understood and there is considerable scatter in fatigue data and even some contradictory results.

Fatigue tests on complete structures using jet noise sources are quite expensive and time consuming. Therefore, no large amounts of data have been made available by such means. Instead, most fatigue tests are conducted on small structures, test panels or even small beams with loud

speakers and sirens or mechanical load cycling machines are used to apply the stress loads. The data must be correlated with prototype data under real service conditions. Fitch and his associates have reported (Ref. 39) what appears to be a very promising approach to the problem. They combine engineering analysis with accelerated life testing of a few key structures to determine whether the structures have adequate design margins. This method outlined below will be discussed more fully in later paragraphs.

The analysis of the problem includes the following steps:

(a) Determine the acoustic environment under various operating conditions. Measured data of course are preferred but, if necessary, predictions can be made from engine parameters.

(b) Analyze the service usage and missions of the aircraft to determine the proportion of the design life that the aircraft is exposed to each of the important acoustic loads.

(c) Build a test specimen to simulate each critical structure and test to failure using sinusoidal excitation.

(d) Determine the relation between statistical response to random excitation and sinusoidal excitation for simple structures.

(e) Using the data from the test specimen and a random S-N curve, find the allowable equivalent random sound pressure level which would give the required design life for the critical operations determined in the service usage analysis of step (b).

(f) Compare the allowable sound pressure level with the actual sound pressure to see if adequate margins exist.

Belcher (Ref. 40) and McGowan (Ref. 41) have reported the development of design charts suitable for use by the average structural design engineer. The charts in effect are nomograms relating sound pressure, fatigue life,

resonant frequency and the dimensions of several common panel constructions.

2. Determination of Sound Levels

The most severe acoustic environment for the aircraft structures probably occurs at maximum power during static ground operation. As the vehicle gains speed and altitude the engine noise decreases. Although boundary layer noise increases with speed it is seldom as important as the maximum engine noise.

Measurements of the overall sound pressure and octave band frequency analyses near the aircraft are the preferred method of describing the acoustic environment but it can be estimated using the methods given by Fitch (Ref. 39).

The procedure is a straight forward step by step calculation using standard reference contours and correction factors based on empirical data. The corrections are functions of the exit diameter and expanded exhaust velocity.

The steps in the calculation are outlined below and illustrated at Military Rated Thrust (MRT) and Maximum Afterburner (Max A/B) with data from Table XVI (Ref. 13, Appendix D).

1. Calculate the effective exhaust velocity of the engine.

$$V_e = \frac{tg}{w}$$

t = Thrust/engine, pounds
g = 32.2 ft./sec.^{2}
w = weight flow rate, pounds/sec.

MRT: $V_e = \frac{8310 \times 32.2}{143} = 1871$ ft./sec.

Max A/B: $V_e = \frac{12630 \times 32.2}{143} = 2745$ ft./sec.

TABLE XVI

J79-2 Engine Operating Data
Installed in A3J-1 Aircraft, No Compressor Bleed
(From Appendix D, Reference 13)

	Idle	M.R.T.	Max A/B
Thrust per Engine, lb.	250	8310	12630
Weight Flow, lb./sec.	47.5	143	143
Nozzle Area, $in.^2$	585	350	604
Nozzle Diameter, ft.	2.275	1.760	2.310
Nozzle Pressure Ratio	1.043	2.170	1.935
Nozzle Total Temp., ^oR	959	1580	3500
Nozzle Static Temp., ^oR	950	1360	3040
Nozzle Gas Velocity, ft./sec.	170	1871	2745
Ratio of Specific Heats	1.40	1.33	1.25

2. Calculate and add the change in sound pressure level to each reference contour, utilizing the effective velocity and the velocity exponent, n, for each contour, Fig. 20.

$$\Delta SPL = 10\ n \log \frac{V_e}{1850}$$

MRT: $\Delta SPL = 10\ n \log \frac{1871}{1850} = 0.02\ n$ (negligible)

Max A/B: $\Delta SPL = 10\ n \log \frac{2745}{1850} = 1.718\ n$

n	ΔSPL
4	7
5	9
6	10
7	12

These corrections are added to Fig. 20.

3. Multiply the dimensionless parameters x/d and y/d in Fig. 20 by the exhaust exit diameter to adjust sound pressure level contours to the air vehicle's dimensions.

   For both MRT and Max A/B the exit diameter is 1.76 ft. hence $x = 1.76 \left(\frac{x}{d}\right)$ and $y = 1.76 \left(\frac{y}{d}\right)$.

4. Shift the contours in Item 3 downstream a distance Δx when extrapolating to supersonic exhaust velocities.

$$\Delta x = 6.5\, D_e\, (M_e - 1)^2$$

   M_e is very nearly 1.0 for both MRT and Max A/B and the correction is negligible.

5. Rotate the contours in Item 4 through the angle $\Delta\phi$ which is determined from Fig. 21 about the point on the jet axis Δx downstream.

   MRT: At $V_e = 1871$, $\Delta\phi = 0$

   Max A/B: At $V_e = 2745$, $\Delta\phi = 14^\circ$

6. Calculate the frequency spectra for any position in the near sound field, from Fig. 22, from knowledge of the over-all free-field sound pressure level in Item 5 and the jet velocity and exit diameter.

The first five steps were carried out as outlined above for the A3J at MRT and Max A/B. The sound pressure levels are free-field values for one engine operating above a ground plane. Since the A3J has two engines 3db was added to all the contours. Another 3db was added where the contours were superposed on the aircraft outline to account for reflections from the aircraft. The resulting contours of over-all sound pressure level have been plotted in Figs. 23 and 24. Also shown are the corresponding

measured sound pressure levels given in Ref. 13. There is good agreement at MRT but the calculated values at Max A/B are about 5db higher than the measured values. A measured octave band frequency analysis was available from Ref. 13 for a location 50 ft. from the nozzles at 40° from the center line. This and the corresponding calculated values have been plotted for comparison in Fig. 25.

The 5db discrepancy at Max A/B has not yet been fully explained. Since Fitch's method is a modification of an earlier method by Franken (Ref. 42) a calculation was made by Franken's method. Without afterburner the only difference is that Franken in effect uses a value of 8 for n in Item 2. Since this adder was negligible regardless of the value of n the two methods gave identical results at MRT. At Max A/B Franken uses the same velocity correction as that for MRT, still negligible. The correction for the addition of the afterburner is a function of the thrust of the turbojet at 100% rpm. This adder is obtained from a curve and is applied to all the contours. In this case the adder was 8db instead of the values ranging from 7db to 12db for the different contours in Item 2. The angular rotation is the same as in Fitch's method. The results are plotted in Fig. 26. The calculation is still approximately 5db higher than the measurements at most locations. However, concurrent with this study, research into noise generation by high temperature jets has been carried out under the Phase I program of this contract. Results indicate that for high temperature (afterburning) jets estimates of the noise generated cannot be immediately extrapolated from lower temperature jet noise data by means of a simple velocity or thrust relationship. It appears that further investigation into the generation of noise by high temperature jets is warranted, and that subsequent improvement of noise prediction techniques is required.

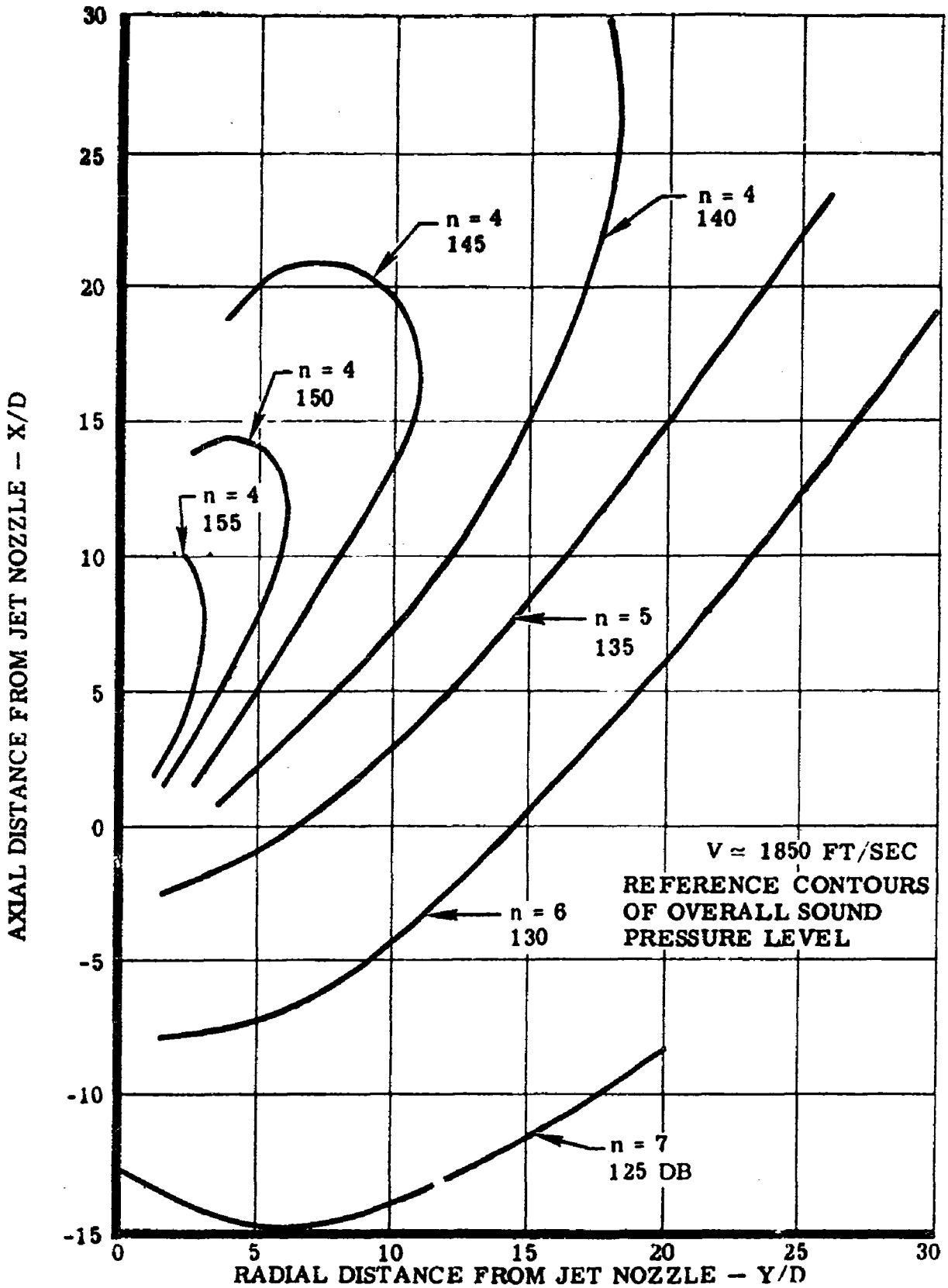

Figure 20. Near Sound Field of a Turbojet (Ref. 39)

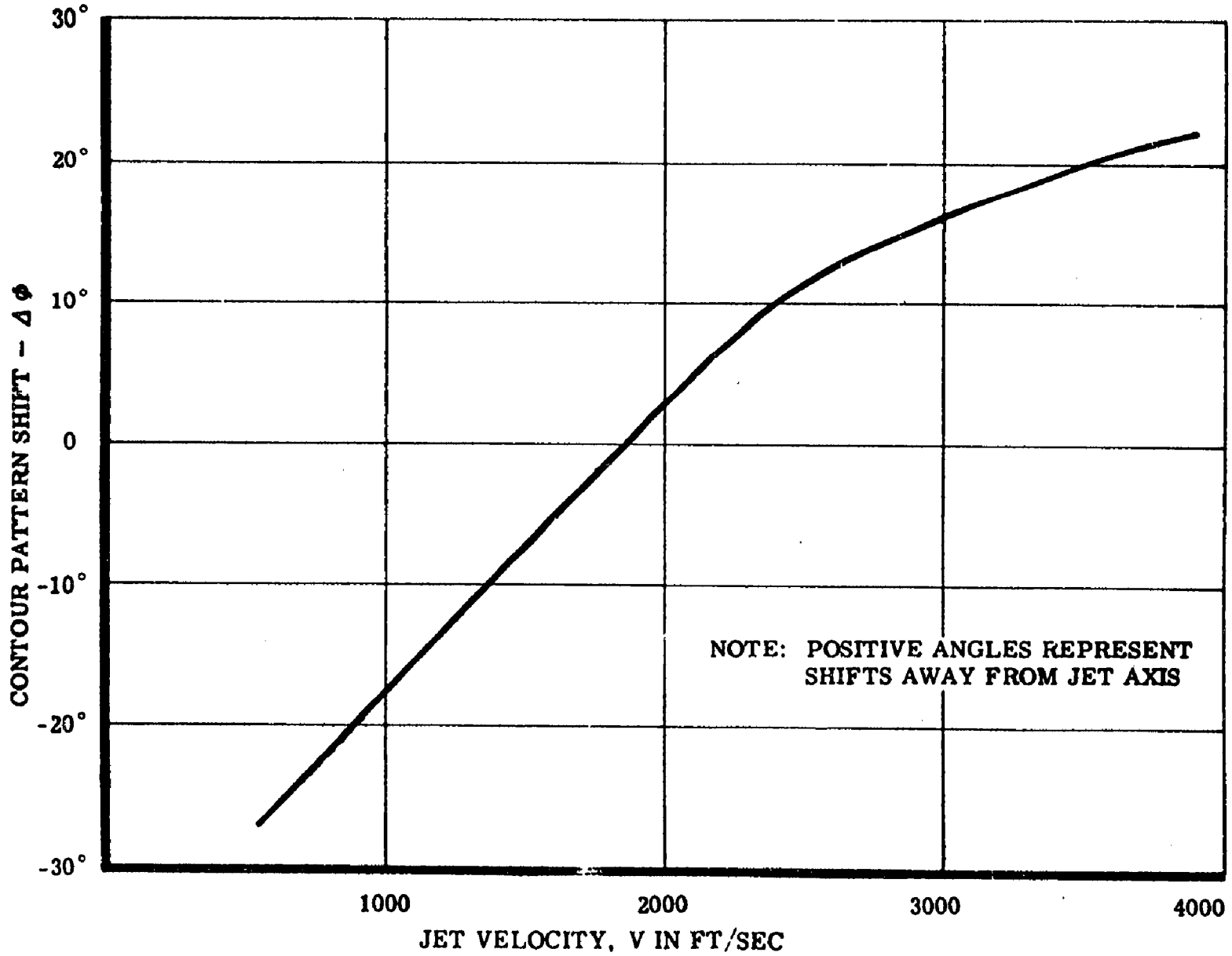

Figure 21 Velocity Dependence of Over-all SPL Contour Pattern (Ref. 39)

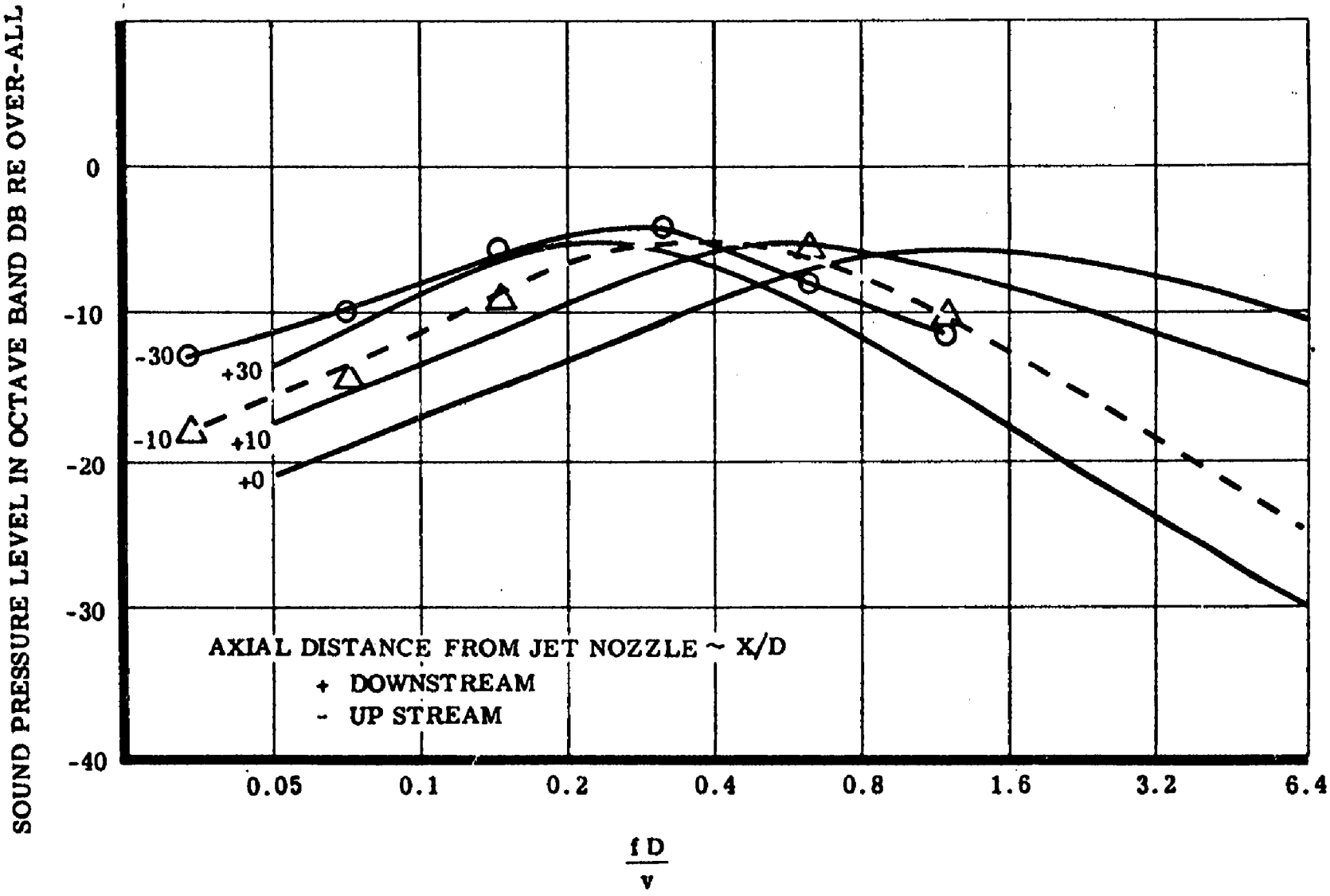

Figure 22. Spectrum of Jet Noise Near Field (Ref. 39)

Fig. 23

Contours of overall SPL for A3J at MRT
— Measured, Ref. 13
... Calculated by Method of Ref. 39

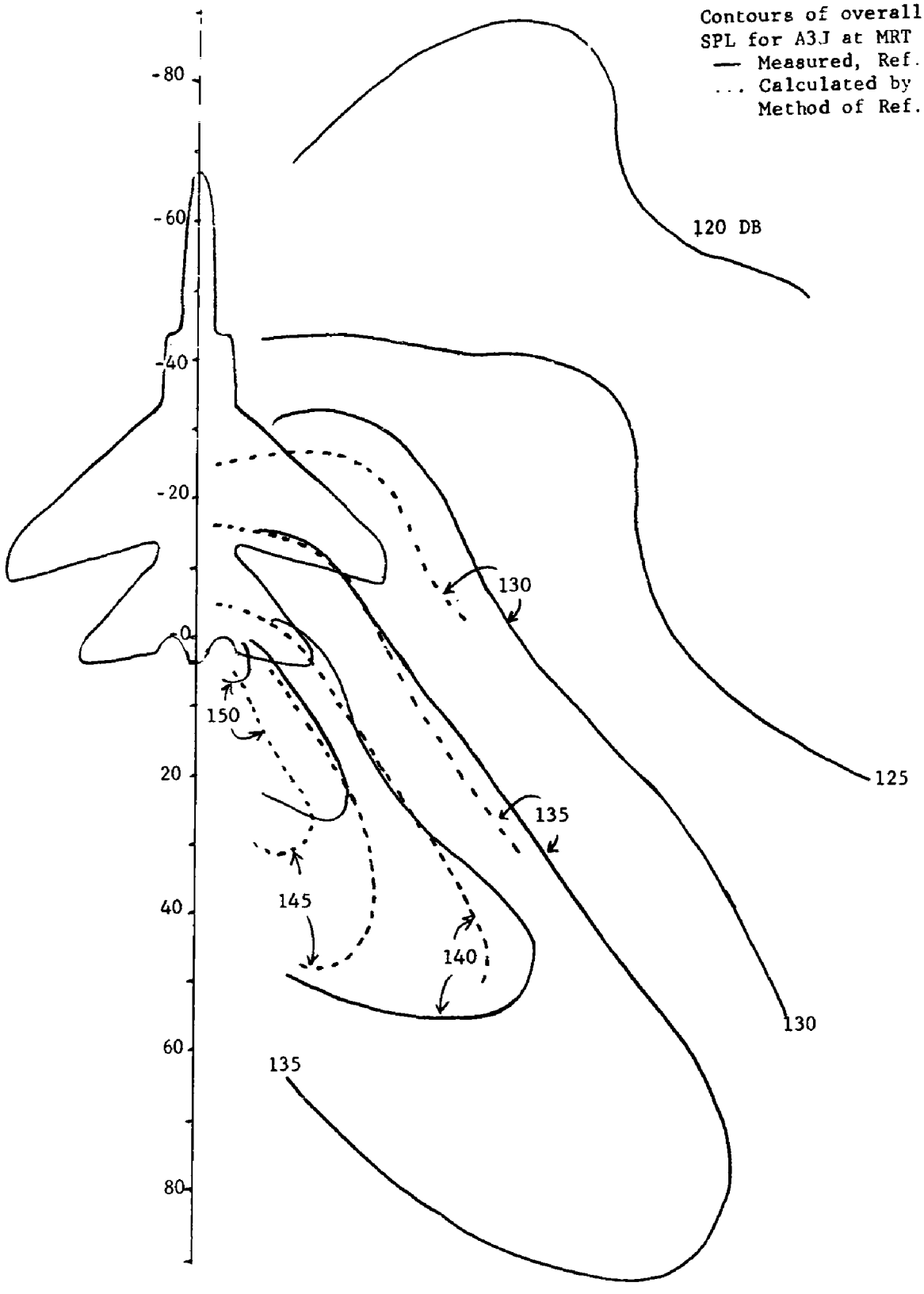

Fig. 24

Contours of Overall SPL for A3J with Max A/B

— Measured, Ref. 13

... Calculated by Method of Ref. 39

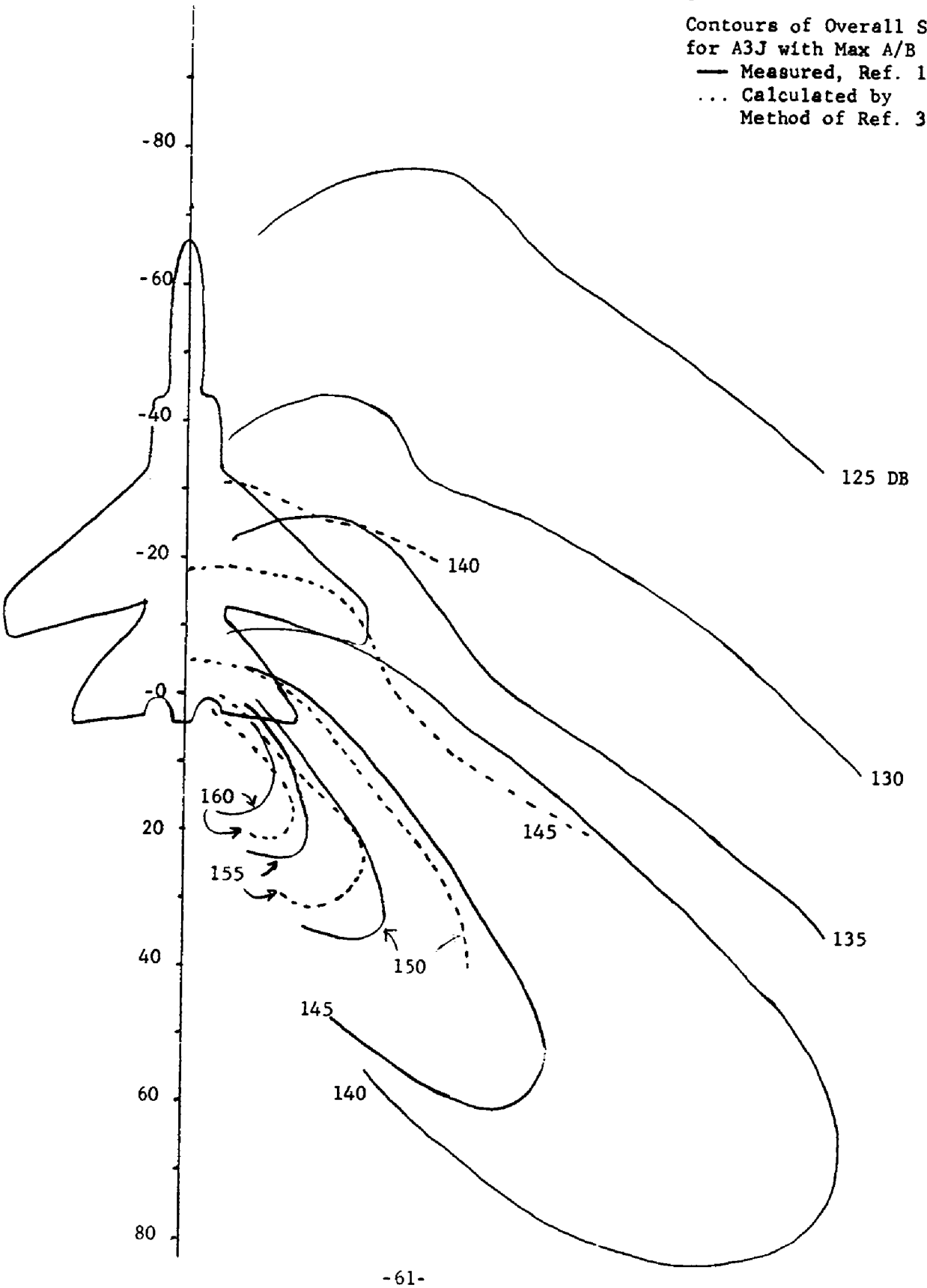

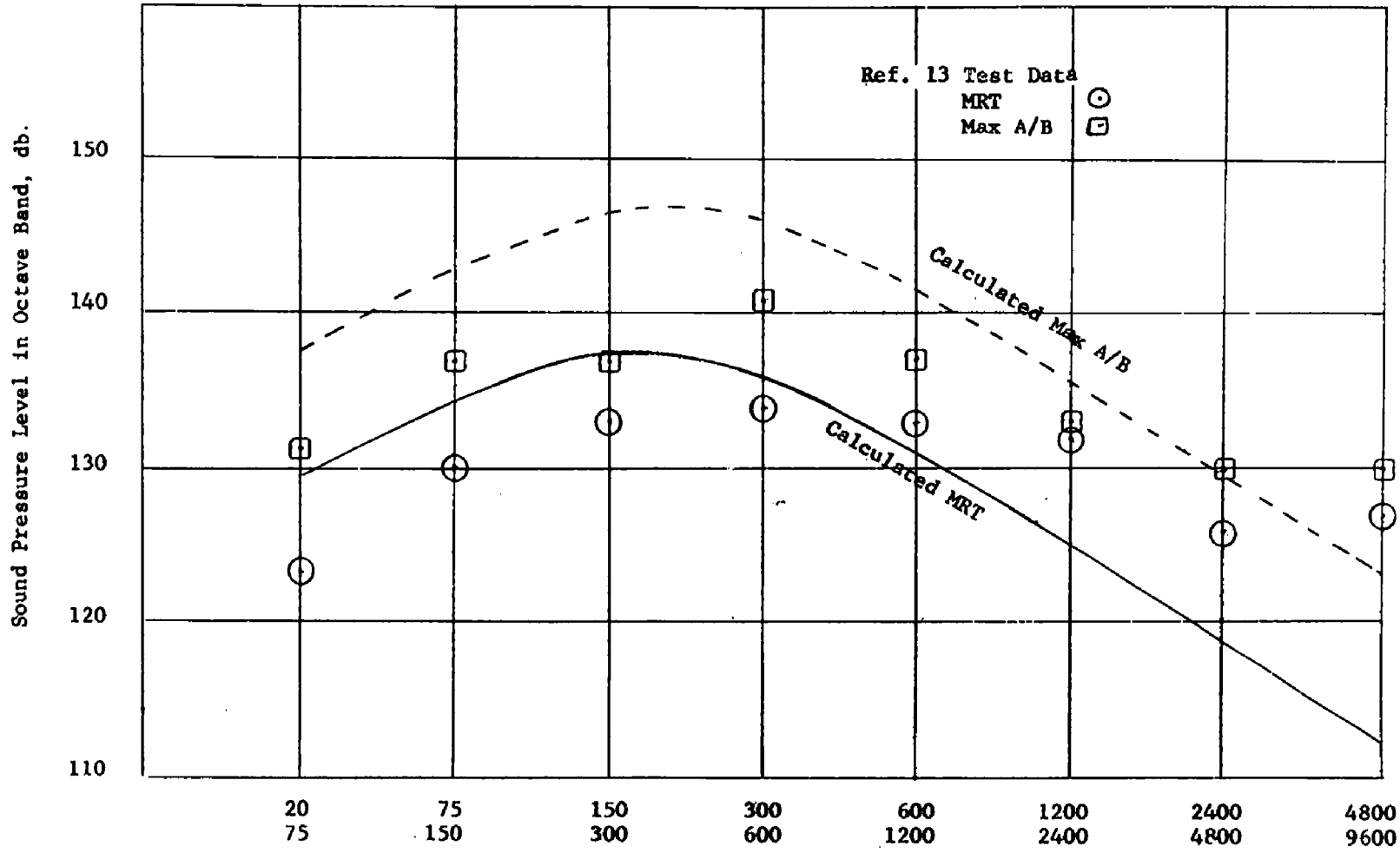

Fig. 25 Measured and Calculated Spectrum of Jet Noise Near Field

Fig. 26

Contours of Overall SPL for A3J with Max A/B

— Measured, Ref. 13
... Calculated by Method of Ref. 42

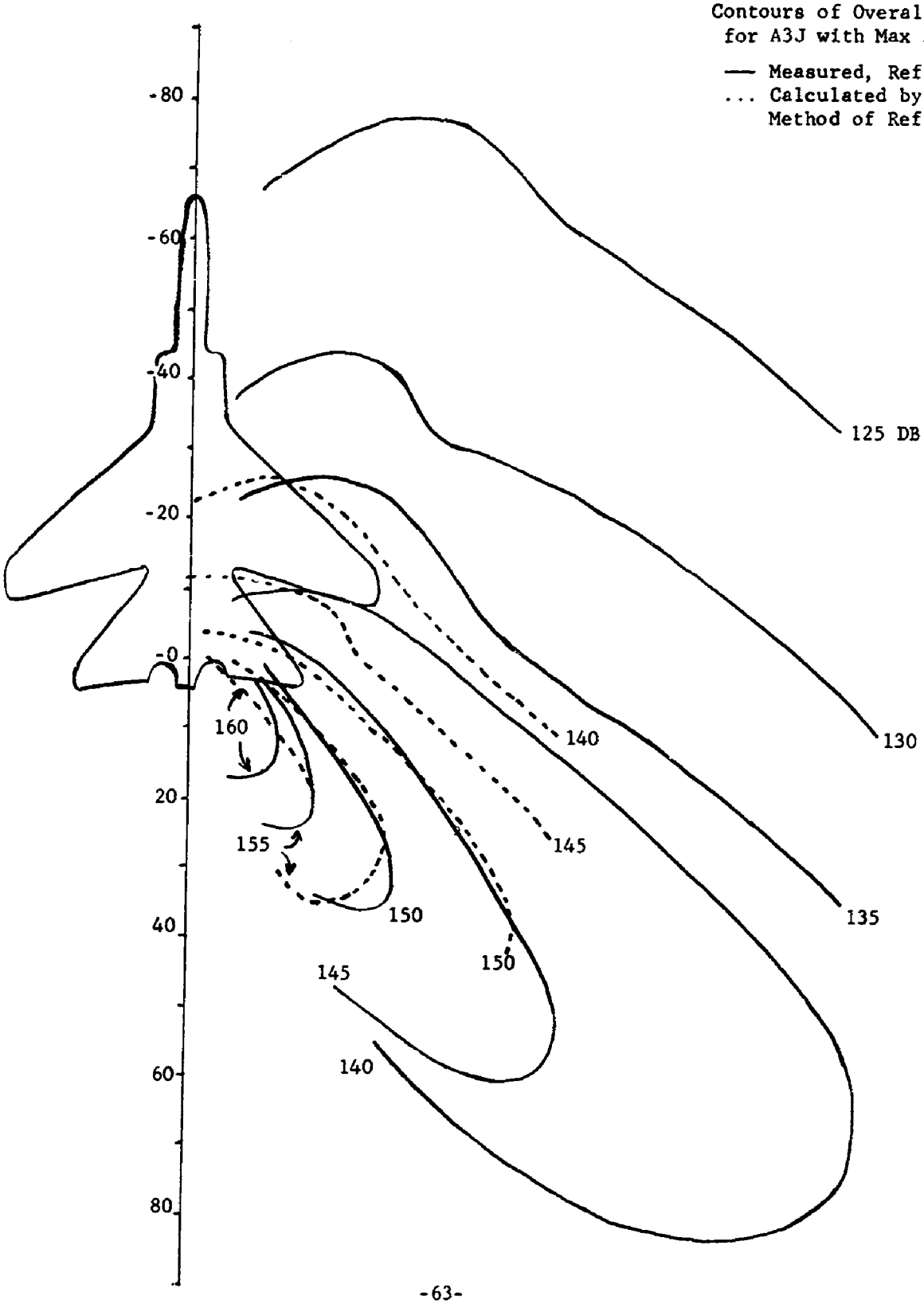

3. Random Noise and Vibration

A random variable, such as jet noise, is varying in time such that its instantaneous values at prescribed times are not predictable and there are no periodicities. Fig. 27 shows samples of a single random variable observed at different time intervals. Presumably one could continue to sample this function indefinitely and obtain different curves. There are, however, statistical parameters of such a random function which are constant under certain frequently encountered conditions.

Let us consider a specific interval x to $x+\Delta x$ of the random variable and find the total time that the variable lies in this interval for all the available samples. We then define the amplitude probability

$$P\ (x,\ x+\Delta x) = \frac{\Sigma \Delta t_i}{T} \qquad (6)$$

where

Δt_i = time during which x_i is in interval between x and $x+\Delta x$

T = total time over which phenomenon is studied

The amplitude probability density is

$$p(x) = \lim_{\Delta x \to 0} P(x,\ x+\Delta x) \qquad (7)$$

Assume that we have a large assembly or ensemble of random time records. Let N be the number of members of the ensemble. At any given time such as $t = t_1$ in Fig. 27 the $x(t_1)$ will be different in the various records but we can count the fraction of records n/N for which $x(t_1)$ is equal to or less than a specified x. This fraction is plotted versus x and tends toward a fixed curve as N approaches ∞. This curve, shown below, is called the

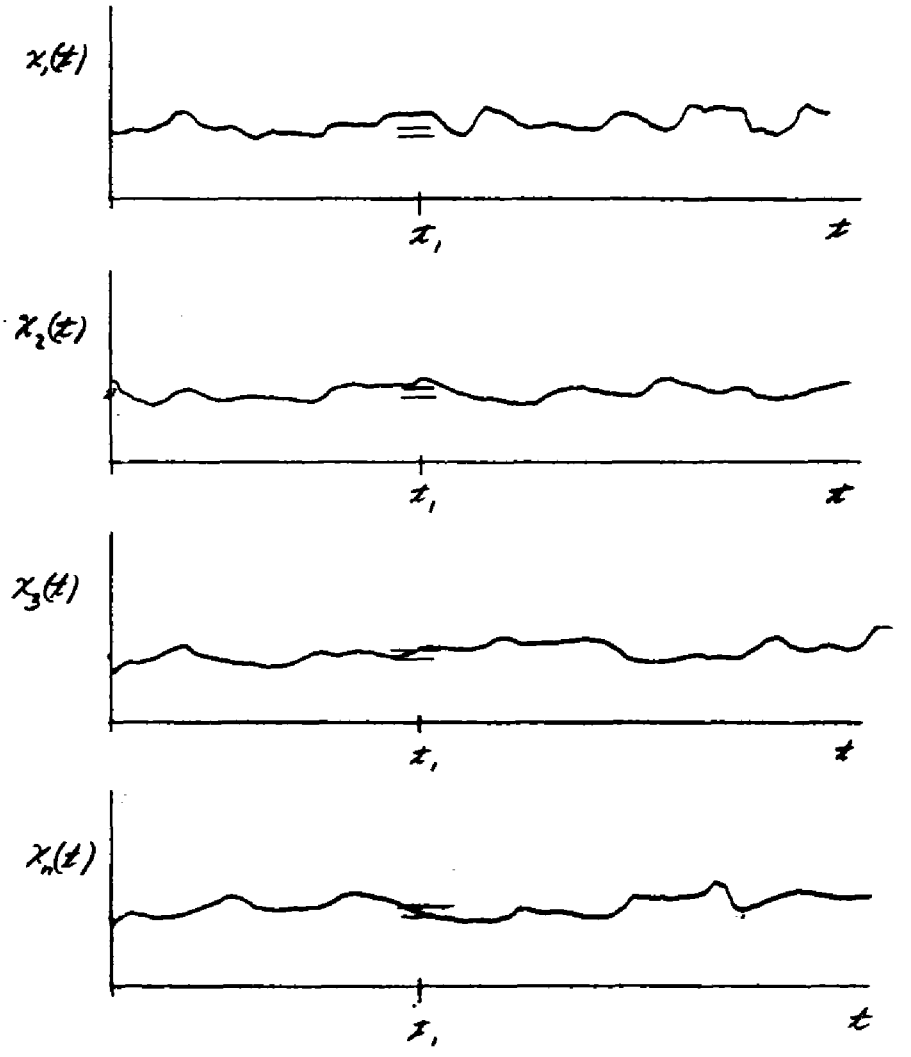

Fig. 27

Ensemble of Random Time Functions

probability distribution $P(x, t_1)$ of the random function at time t_1.

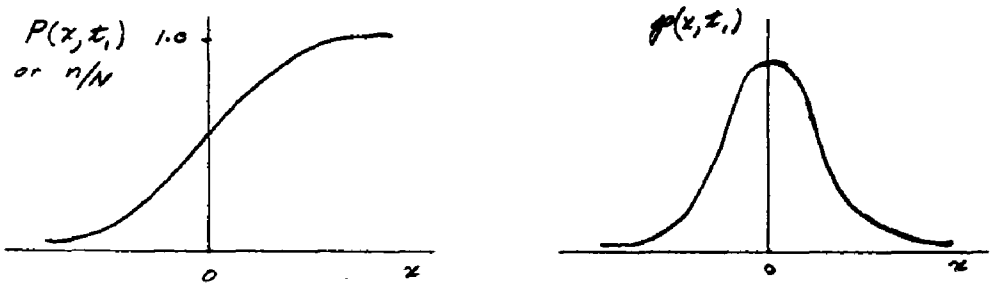

If the derivative exists, we define the probability density function as

$$p(x, t_1) = \frac{d}{dx} P(x, t_1) \tag{8}$$

so that the probability of $x(t_1)$ having a value in the interval between x and $x+dx$ is

$$dP(x,t_1) = p(x,t_1)dx = P(x+dx,t_1) - P(x,t_1) \tag{9}$$

Also

$$P(x,t_1) = \int_{-\infty}^{x} p(x,t_1)dx \tag{10}$$

A random process is <u>stationary</u>; if any translation of the time origin leaves the statistical properties unaffected. It is <u>ergodic</u> if each sample is representative of the process. In particular, if the statistical properties are not changing as a function of time, the probability functions at any other time should be the same as that found at $t = t_1$. Also we should get the same result by counting or averaging over a time interval of sufficient length as by counting or averaging over the ensemble of functions.

The most commonly encountered random process has a Gaussian or "normal"

probability density distribution.

$$p(x,t_1) = \frac{1}{\sigma\sqrt{2\pi}} \epsilon^{-\frac{(x-\bar{x})^2}{2\sigma^2}} \tag{11}$$

First and Second Moments

The first moment of a random function is its average value defined by

$$\bar{x} = \int_{-\infty}^{\infty} x \; p(x,t_1)dx \tag{12}$$

The second moment is defined by

$$\overline{x^2} = \int_{-\infty}^{\infty} x^2 \; p(x,t_1)dx \tag{13}$$

The square of the standard deviation, or variance is defined by

$$\sigma^2 = \int_{-\infty}^{\infty} (x - \bar{x})^2 \; p(x,t_1)dx \tag{14}$$

Note that $\bar{x}$ is a constant and that $\int_{-\infty}^{\infty} p(x,t_1)\, dx = 1$ since $p(x,t_1)$ is a probability density function.

Then

$$\sigma^2 = \overline{x^2} - (\bar{x})^2 \tag{15}$$

If the process has zero mean as is often the case the variance is equal to the mean square value.

For a stationary and ergodic random process the moments are independent of time and time averages can be used instead of the ensemble averages. Thus the average value of x is

$$\langle x \rangle = \lim_{T\to\infty} \frac{1}{2T} \int_{T}^{T} x(t)\, dt \tag{16}$$

and

$$\langle x^2 \rangle = \lim_{T\to\infty} \frac{1}{2T} \int_{-T}^{T} x^2(t)\, dt \tag{17}$$

Power Spectral Density

Random vibration may be considered as the sum of a large number (tending to infinity) of harmonic vibrations of appropriate amplitude and phase.

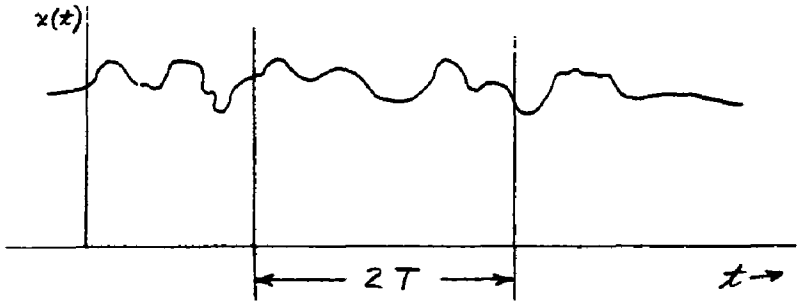

Consider a random function in the time interval 2T. It can be represented by the real part of the Fourier series,

$$x(t) = \mathcal{R}e \sum_{n=-\infty}^{\infty} C_n \epsilon^{jn\omega_o t} = C_o + 2\sum_{n=1}^{\infty} |C_n| \cos(n\omega_o t - \theta_n) \tag{18}$$

where $$\omega_o = \frac{\pi}{T} \tag{19}$$

$$C_n = \frac{1}{2T} \int_{-T}^{T} x(\tau)\, \epsilon^{-jn\omega_o \tau}\, d\tau \tag{20}$$

The mean square value of x(t) is

$$\langle x^2 \rangle = \lim_{T\to\infty} \frac{1}{2T} \int_{-T}^{T} x^2(t)\, dt = \lim_{T\to\infty} \left[C_o^2 + 2\sum_{n=1}^{\infty} |C_n|^2 \right] \tag{21}$$

The contribution to the mean-square value in any frequency interval is the summation of all the components within that frequency band.

If now the interval 2T is doubled, ω_o is one-half its former value and the number of spectrum lines in any frequency interval is twice the former number. The coefficients $|C_n|^2$ must be reduced to one-half their former

values because the mean square of the entire spectrum is a constant for an assumed ergodic process. It follows that for any given frequency interval the sum of the $|C_n|^2$ in that interval is a constant, $\Delta\langle x^2\rangle$. The ratio of $\Delta\langle x^2\rangle$ divided by the frequency interval is called the power spectral density in that frequency interval

$$W(\omega) = \frac{\Delta\langle x^2\rangle}{\Delta\omega}$$

As T approaches ∞, ω_o approaches 0 and the spectrum becomes continuous and the power spectrum density is given by

$$W(\omega) = \lim_{\Delta\omega \to 0} \frac{\Delta\langle x^2\rangle}{\Delta\omega} = \frac{d\langle x^2\rangle}{d\omega} \tag{22}$$

From Eq. 22 we obtain the mean square value

$$\langle x^2\rangle = \int_0^{\infty} W(\omega)\, d\omega \tag{23}$$

The dimensions of the power spectral density are the square of x per radian per second.

Input-Output Relationship

If the input to a linear system is x(t) then the output is

$$y(t) = \int_{-\infty}^{t} x(\tau)h(t-\tau)d\tau = \int_0^{\infty} x(t-\xi)h(\xi)d\xi \tag{24}$$

where h(t) is the response of the system to a unit impulse $\delta(t)$. Assume that the input was 0 for $t<0$ and change the lower limit to 0 in both integrals. Let $x(t) = \epsilon^{j\omega t}$ then Eq. 24 gives

$$y(t) = \int_0^{\infty} \epsilon^{j\omega(t-\tau)} h(\tau) d\tau = \epsilon^{j\omega t} \int_0^{\infty} \epsilon^{-j\omega\tau} h(\tau) d\tau = \epsilon^{j\omega t} A(j\omega) \qquad (25)$$

where
$$A(j\omega) = \int_0^{\infty} \epsilon^{-j\omega\tau} h(\tau)\, d\tau \qquad (26)$$

is defined as response function of the system. $y(t)$ of course is the response to a harmonic excitation. Since a sinusoidal input is given by either the real or imaginary part of $\epsilon^{j\omega t}$ the response to a sinusoidal input is given by the real or imaginary part of $y(t)$. Since $h(\tau)$ is zero for $t < 0$ the lower limit in Eq. 26 can be changed to $-\infty$ without altering the result and $A(j\omega)$ is then the Fourier transform of the impulsive response function $h(\tau)$. If the response to an impulse is known, Eq. 26 can be used to obtain the response function $A(j\omega)$. Often, however, it may be more convenient to calculate the response to a harmonic excitation directly.

Consider now the input function given by Eq. 18 which is a random function over a finite time. Substituting in Eq. 24 we obtain

$$\begin{aligned} y(t) &= \mathcal{R}e \int_0^{\infty} h(\tau) \sum_{n=-\infty}^{\infty} C_n \epsilon^{jn\omega_0(t-\tau)} d\tau \\ &= \mathcal{R}e \sum_{n=-\infty}^{\infty} \left\{ C_n \epsilon^{jn\omega_0 t} \int_0^{\infty} h(\tau) \epsilon^{-jn\omega_0\tau} d\tau \right\} \\ &= \mathcal{R}e \sum_{n=-\infty}^{\infty} C_n \epsilon^{jn\omega_0 t} A(jn\omega_0) \end{aligned}$$

Note that here we have a summation of terms like the one given in Eq. 25 and 26 for a single harmonic. Taking the real part we have

$$y(t) = C_o A(o) + 2 \sum_{n=1}^{\infty} |C_n| \, |A(jn\omega_o)| \cos(n\omega_o t + \alpha_n) \qquad (27)$$

From Eq. 16 the mean-square value of the response is

$$\langle y^2 \rangle = \lim_{T\to\infty} \frac{1}{2T} \int_{-T}^{T} y^2(t)\, dt = C_o^2 A^2(0) + 2\sum_{n=1}^{\infty} \left| C_n \right|^2 \left| A(jn\omega_o) \right|^2 \qquad (28)$$

We find the limit by the same method used in connection with Eq. 21. The power spectral density of the response is

$$W_r(\omega) = W_s(\omega) \left| A(j\omega) \right|^2 \qquad (29)$$

and the mean-square output is

$$\langle y^2 \rangle = \int_0^{\infty} W_r(\omega)\, d\omega = \int_0^{\infty} W_s(\omega) \left| A(j\omega) \right|^2 d\omega \qquad (30)$$

Response of Single Degree of Freedom System

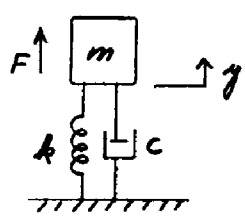

The differential equation for the steady state displacement of the mass in the simple mechanical oscillator shown is

$$m\ddot{y} + c\dot{y} + k y = F\, \epsilon^{j\omega t} \qquad (31)$$

Let

$$\omega_n^2 = \frac{k}{m}$$

$$\delta = \frac{C}{2\sqrt{km}}$$

$$y_o = \frac{F_o}{k} \text{ at } \omega = 0$$

Then Eq. 31 may be written in the dimensionless form

$$\frac{\ddot{y}}{\omega_n^2 y_o} + 2\delta \frac{\dot{y}}{\omega_n y_o} + \frac{y}{y_o} = \frac{F\epsilon^{j\omega t}}{F_o} \tag{32}$$

The displacement response function for unit applied force is

$$A(j\omega) = \frac{\frac{y_o}{F_o}}{1 - \left(\frac{\omega}{\omega_n}\right)^2 + j2\delta \frac{\omega}{\omega_n}} \tag{33}$$

and

$$\left|A(j\omega)\right|^2 = A(j\omega) \cdot A(-j\omega) = \frac{(y_o/F_o)^2}{\left[1 - \left(\frac{\omega}{\omega_n}\right)^2\right]^2 + \left(2\delta \frac{\omega}{\omega_n}\right)^2} \tag{34}$$

Eq. 33 and 34 give the response and the square of the response to a unit sinusoidal excitation force.

When the damping is small the bandwidth, $2\delta\omega_n$, of the response of the mechanical oscillator is small. If the power spectral density of the input function is essentially constant in the neighborhood of the resonant frequency, ω_n, the power spectral density of the response is approximately

$$W_r(\omega) = W_s(\omega_n) \left|A(j\omega)\right|^2 \tag{35}$$

where $W_s(\omega)$ has the constant value $W_s(\omega_n)$, its value at $\omega = \omega_n$. The curve of the response power spectral density versus ω will be very similar to the curve of the square of response to sinusoidal excitation. Under the same conditions, the mean square response is

$$\langle y^2 \rangle = \int_0^\infty W_s(\omega_n) \left|A(j\omega)\right|^2 d\omega$$

$$\langle y^2 \rangle = W_s(\omega_n) \left(\frac{y_o}{F_o}\right)^2 \int_0^\infty \frac{d\omega}{\left[1 - \left(\frac{\omega}{\omega_n}\right)^2\right]^2 + \left(2\delta \frac{\omega}{\omega_n}\right)^2}$$

This integral may be evaluated by convolution in the complex plane to give

$$\langle y^2 \rangle = W_s(\omega_n) \left(\frac{y_o}{F_o}\right)^2 \frac{\pi \omega_n}{4\delta} \tag{36}$$

The response of a lightly damped ($\delta < 0.1$) mechanical oscillator to random excitation has the characteristics of a sinusoidal wave with slowly varying amplitude and phase. Miles (Ref. 43) explained this qualitatively by noting that such a system acts as a narrow band filter passing only those frequencies in the vicinity of ω_n. Then by analogy with the phenomenon of "beats" the sum of two harmonic waves of approximately the same frequency is replaced by a wave having a frequency equal to the average of the two waves and an amplitude envelope that fluctuates at a rate equal to the difference frequency. Thus it can be inferred that the sum of all the frequencies in the pass band is a sinusoidal wave with frequency ω_n and an amplitude that exhibits a random fluctuation at a rate equal to the bandwidth, $2\delta\omega_n$, or less.

It has been stated by many writers that the probability distribution of the envelope is a Rayleigh probability density function. Davenport and Root (Ref. 44), for example, write the response function of a narrow-band Gaussian process as

$$y(t) = V(t) \cos \left[\omega_n t + \phi(t)\right] \tag{37}$$

where the variations of $V(t)$ and $\phi(t)$ are slow compared to those of $\cos \omega_n t$. The function can be expressed as a Fourier series over the interval $0 \leq t \leq T$.

$$y(t) = \sum_{n=1}^{\infty} (y_{cn} \cos n\omega_o t + y_{sn} \sin n\omega_o t) \tag{38}$$

where $\omega_o = \frac{2\pi}{T}$

$$y_{cn} = \frac{2}{T} \int_0^T y(t) \cos n\omega_o t \, dt \tag{39a}$$

$$y_{sn} = \frac{2}{T} \int_0^T y(t) \sin n\omega_o t \, dt \tag{39b}$$

These coefficients are Gaussian random variables which become uncorrelated as $T \to \infty$.

The mean frequency of the resonant response is introduced by writing $n\omega_o$ in Eq. 38 as $(n\omega_o - \omega_n) + \omega_n$, where $\omega_n = 2\pi f_n$, and expanding the sine and cosine factors. The result is

$$y(t) = y_c(t) \cos \omega_n t - y_s(t) \sin \omega_n t \tag{40}$$

with

$$y_c(t) = \sum_{n=1}^{\infty} \left[y_{cn} \cos (n\omega_o - \omega_n)t + y_{sn} \sin (n\omega_o - \omega_n)t \right] \tag{41a}$$

$$y_s(t) = \sum_{n=1}^{\infty} \left[y_{cn} \sin (n\omega_o - \omega_n)t - y_{sn} \cos (n\omega_o - \omega_n)t \right] \tag{41b}$$

Then, expanding Eq. 37 and comparing with Eq. 40, we see that

$$y_c(t) = V(t) \cos \phi(t) \tag{42a}$$

$$y_s(t) = V(t) \sin \phi(t) \tag{42b}$$

It follows that

$$V(t) = \sqrt{y_c^2(t) + y_s^2(t)} \tag{43a}$$

$$\phi(t) = \tan^{-1}\left[\frac{y_s(t)}{y_c(t)}\right] \tag{43b}$$

The only non-vanishing terms in the sums of Eq. 41 are the ones for which the values of $n\omega_o$ fall in the response band near ω_n. Therefore $y_c(t)$ and $y_s(t)$ have frequency components only in a narrow band centered on zero frequency. The envelope and phase likewise have components in the neighborhood of zero frequency.

Let y_{ct} and y_{st} refer to the possible values of $y_c(t)$ and $y_s(t)$ respectively. They are the sums of independent Gaussian random variables having zero means

$$E(y_{ct}) = E(y_{st}) = 0 \tag{44}$$

Here E ( ) stands for the expected value in a statistical sense. The mean square of y_{ct} is obtained from Eq. 41a.

$$E(y_{ct}^2) = \sum_{n=1}^{\infty}\sum_{m=1}^{\infty}\left[\begin{array}{l} E(y_{cn}\, y_{cm})\cos(n\omega_o-\omega_n)t\cos(m\omega_o-\omega_n)t \\ + E(y_{cn}\, y_{sm})\cos(n\omega_o-\omega_n)t\sin(m\omega_o-\omega_n)t \\ + E(y_{sn}\, y_{cm})\sin(n\omega_o-\omega_n)t\cos(m\omega_o-\omega_n)t \\ + E(y_{sn}\, y_{sm})\sin(n\omega_o-\omega_n)t\sin(m\omega_o-\omega_n)t \end{array}\right]$$

Since the coefficients are independent

$$E(y_{cn}\, y_{cm}) = 0 \qquad \text{for } m \neq n$$

$$E(y_{sn}\, y_{sm}) = 0 \qquad \text{for } m \neq n$$

$$E(y_{cn}\, y_{sm}) = 0 \qquad \text{for all m and n}$$

$$E(y_{cn}\, y_{cm}) = E(y_{sn}\, y_{sm}) = E(y_{cn}^2) \text{ for } m = n$$

and

$$E(y_{ct}^2) = \sum_{n=1}^{\infty} E(y_{cn}^2) \left[\cos^2(n\omega_o - \omega)t + \sin^2(n\omega_o - \omega)t\right] = E(y_t^2) \tag{45}$$

Similarly it may be shown that

$$E(y_{st}^2) = E(y_t^2) \tag{46}$$

The variance of the coefficients is

$$\sigma^2(y_{ct}) = E(y_{ct}^2) - E(y_{ct})$$

$$\sigma^2(y_{st}) = E(y_{st}^2) - E(y_{st})$$

Substituting from Eqs. 44, 45, and 46, we obtain

$$\sigma^2(y_{ct}) = \sigma^2(y_{st}) = E(y_t^2)$$

Let $\sigma_y = \sigma(y_t)$. The covariance of y_{ct} and y_{st} is obtained from Eqs. 41a and 41b.

$$E(y_{ct}\, y_{st}) = \sum_{n=1}^{\infty} \sum_{m=1}^{\infty} \begin{bmatrix} E(y_{cn}\, y_{cm}) \cos (n\omega_o - \omega_n)t \sin (n\omega_o - \omega_n)t \\ - E(y_{cn}\, y_{sm}) \cos (n\omega_o - \omega_n)t \cos (n\omega_o - \omega_n)t \\ + E(y_{sn}\, y_{cm}) \sin (n\omega_o - \omega_n)t \sin (n\omega_o - \omega_n)t \\ - E(y_{sn}\, y_{sm}) \sin (n\omega_o - \omega_n)t \cos (n\omega_o - \omega_n)t \end{bmatrix}$$

This reduces to

$$E(y_{ct}\, y_{st}) = \sum_{n=1}^{\infty} E(y_{cn}^2) \begin{bmatrix} \cos(n\omega_o - \omega_n)t \sin(n\omega_o - \omega_n)t \\ -\sin(n\omega_o - \omega_n)t \cos(n\omega_o - \omega_n)t \end{bmatrix} = 0$$

The random variables y_{ct} and y_{st} have been shown to be independent with zero means and variances σ_y^2. Their probability density then is

$$p(y_{ct}) = \frac{1}{\sqrt{2\pi}\,\sigma_y} \exp\left(\frac{-y_{ct}^2}{2\sigma_y}\right)$$

$$p(y_{st}) = \frac{1}{\sqrt{2\pi}\,\sigma_y} \exp\left(\frac{-y_{st}^2}{2\sigma_y}\right)$$

and their joint probability density is

$$p(y_{ct}, y_{st}) = p(y_{ct}) \cdot p(y_{st}) = \frac{1}{2\pi\,\sigma_y^2} \exp -\left(\frac{y_{ct}^2 + y_{st}^2}{2\sigma_y^2}\right) \qquad (47)$$

The joint probability density function of the envelope and phase variables V_t and ϕ_t can be found from Eq. 47 by a simple transformation of variables.

$$p(V_t, \phi_t) = p(y_{ct}, y_{st}) \left|J\right|$$

The Jacobian of the transformation equations, Eqs. 42a and 42b, is given by

$$\left|J\right| = \begin{vmatrix} \frac{\partial y_{ct}}{\partial V_t} & \frac{\partial y_{st}}{\partial V_t} \\ \frac{\partial y_{ct}}{\partial \phi_t} & \frac{\partial y_{st}}{\partial \phi_t} \end{vmatrix} = \begin{vmatrix} \cos \phi_t & \sin \phi_t \\ -V_t \sin \phi_t & V_t \cos \phi_t \end{vmatrix} = V_t$$

Then with V_t from Eq. 43a

$$p(V_t, \phi_t) = \frac{V_t}{2\pi \sigma_y^2} \exp\left(-\frac{V_t^2}{2\sigma_y^2}\right) \tag{48}$$

Since Eqs. 42a and 42b define a transformation only for $V_t \geq 0$ and $0 \leq \phi_t \leq 2\pi$ the joint probability of Eq. 48 applies only over these intervals and is zero elsewhere.

The probability density function of the envelope alone is obtained by integrating Eq. 48 with respect to ϕ_t over the range 0 to 2π.

$$p(V_t) = \frac{V_t}{\sigma_y^2} \exp\left(\frac{-V_t^2}{2\sigma_y^2}\right) \quad \text{for } V_t \geq 0 \tag{49}$$

This is the Rayleigh probability density function.

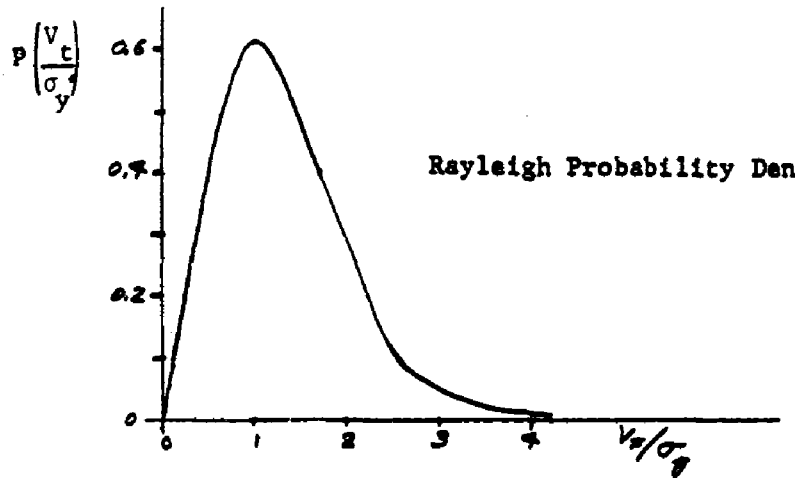

Rayleigh Probability Density Function

Its integral over the defined interval must equal unity.

$$\int_0^\infty p(V_t)\, d\, V_t = \int_0^\infty \frac{V_t}{\sigma_y^2} \exp\left(-\frac{V_t^2}{2\sigma_y^2}\right) dV_t = 1$$

Let $x = \frac{V_t}{\sigma_y}$ then

$$\int_0^\infty x\, e^{-(x^2/2)}\, dx = \int_0^\infty p(x)\, dx = 1$$

or $$p(x) = p\left(\frac{V_t}{\sigma_y}\right) = x\, e^{-(x^2/2)} = \frac{V_t}{\sigma_y} \exp\left(-\frac{V_t^2}{2\sigma_y^2}\right) \qquad (50)$$

4. Fatigue

Fatigue of metals is caused by repeated plastic deformation during cyclic loading. Cracks are initiated at stress concentrations which may be either geometric, for example, at points of attaching a panel to a rib or near a hole, or they may be dynamic, a function of the mode of vibration. The stress life curve developed for constant amplitude cycling of the load has for many years provided the basic data for designing structures to prevent fatigue failure. This curve is referred to as the S-N curve, S for stress and N for cycles of life. In acoustic fatigue a problem arises because of the high rate at which cycles of load are applied rather than a high magnitude of stress. Even so the design of a given structure may be limited by the acoustic load and it is desirable to use the highest possible stress to increase the payload.

The pressure loads produced by jet noise or boundary layer noise are random functions of time. The amplitude distributions are approximated quite well by the "normal" or Gaussian distribution function. With this distribution the major part of the damage to a structure is caused by a relatively few cycles at the higher stress levels. Collection of fatigue life data with random excitation is therefore relatively inefficient and time consuming. Although some life data are available for random excitation, a much greater amount has been taken for S-N curves at constant amplitude sinusoidal excitation. It is desirable therefore to utilize this vast experience if possible by finding a relationship between cumulative fatigue damage under random loading and available S-N data.

Much work is being done on life testing of both samples and structures utilizing random noise sources as well as programmed sinusoidal testing to duplicate the essential effects of random noise.

4A. Linear Accumulation of Damage

Probably the most widely used method for analyzing fatigue damage and predicting structural life is Miner's Rule. It is relatively simple to apply and gives reasonable results. Numerous other methods have been proposed which are aimed at improving the accuracy by including the effects of stress interaction and non-linearitics. Some of these methods will be discussed in later paragraphs.

Miner's method has the advantage that it makes use of the available S-N data and provides for the linear accumulation of damage without regard to time history of loading. The order in which variable amplitudes of stress or rest periods are applied are not included. It is assumed that the stress cycles are fully reversed. This is approximately true for a lightly damped structure vibrating in a single predominant mode with zero mean stress even though the excitation is Gaussian.

Miner's Rule is based on an S-N curve such as Fig. 28. Let the load be cycled for n_1 cycles at stress amplitude S_1.

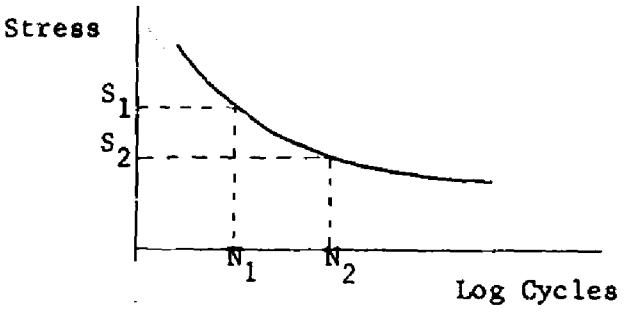

Fig. 28

Since the total life at this stress is N_1 cycles it is postulated that there has been damage equivalent to an $\frac{n_1}{N_1}$ proportion of the expected life. It is clear that failure should occur when this proportion equals 1. If the load is also cycled at S_2 for n_2 cycles the total damage is

$$\frac{n_1}{N_1} + \frac{n_2}{N_2}$$

Thus for any number of stress levels the condition for failure is

$$\frac{n_1}{N_1} + \frac{n_2}{N_2} + \ldots + \frac{n_i}{N_i} = 1$$

Let the total number of cycles at the various loads be given by

$$N = \Sigma n_i$$

Then the condition for failure can be written

$$\frac{n_1}{N N_1} + \frac{n_2}{N N_2} + \ldots + \frac{n_i}{N N_i} = \frac{1}{N}$$

For a random load the probability of occurrence of a given stress amplitude is

$$p_i = \frac{n_i}{N}$$

Hence $$\frac{p_1}{N_1} + \frac{p_2}{N_2} + \ldots + \frac{p_i}{N_i} = \frac{1}{N}$$

or the total life, in terms of cycles to failure, is given by

$$N = \frac{1}{\sum \frac{p_i}{N_i}} \tag{51}$$

For a Gaussian distribution of stress the distribution of the peak amplitudes in the response of a single degree of freedom vibrating system is given by the well-known Rayleigh distribution function. (See Eq. 49)

$$p(s) = \frac{s}{\sigma^2} e^{-\left(s^2/2\sigma^2\right)} \tag{52}$$

where s is the magnitude of peak stress and σ is the root mean square stress for the case of zero average stress. Since this is a continuous function of s the summation in Eq. 51 can be replaced by an integral.

Then the number of random cycles is

$$N_R = \frac{1}{\int_o^\infty \frac{p(\vec{s})ds}{N(s)}} \tag{53}$$

where N(s) is expressed by the equation for the constant amplitude S-N curve.

Miles (Ref. 43) used the function

$$N(s) = \left(\frac{s_1}{s}\right)^\alpha$$

where s_1 is the stress for which the equation would predict failure at one cycle although the equation should not be extrapolated this far. α is the reciprocal of the slope of a log S vs. log N curve. Miles derived an expression for the equivalent stress, or "reduced stress", which would produce the same fatigue damage as the random load after the same total number of cycles of loading.

$$S_e = \left(\frac{\sum s_i^{\alpha} n_i}{\sum n_i}\right)^{1/\alpha}$$

Shanley (Ref. 45) has suggested that α should be replaced by 2α in this equation. Belcher, et al (Ref. 40) have shown that the log S - log N curve may lead to highly conservative results. They have instead obtained graphical or numerical solutions of Eq. 53 using data from actual S-N curves for various materials. The procedure as explained below is based on an example including a table and curves from Ref. 39.

From Eqs. 52 and 53 we obtain

$$\frac{1}{N_R} = \int_o^\infty \frac{(s/\sigma^2)\ e^{-\left(s^2/2\sigma^2\right)}}{N(s)} ds$$

or for numerical calculation

$$\frac{1}{N_R} = \sum \left[\frac{\frac{s}{\sigma} e^{-\frac{1}{2}(s/\sigma)^2} \Delta\left(\frac{s}{\sigma}\right)}{N(s)} \right] = \sum \frac{p\left(\frac{s}{\sigma}\right) \Delta\left(\frac{s}{\sigma}\right)}{N(s)} \qquad (54)$$

Having an S-N curve for the material, Fig. 29, and the Rayleigh probability distribution curve Fig. 30, we can solve Eq. 54 for N_R for any selected value of the random rms stress, σ. By repeating the calculations for other values of σ we obtain the points for plotting a random S-N curve.

The calculation for each σ is facilitated by a table such as Table XVII. First, a value for the rms stress, σ, is assumed, then values of the relative stress $\frac{s}{\sigma}$ are chosen at discrete intervals. For each relative stress, $\frac{s}{\sigma}$, the relative number of cycles, $p\left(\frac{s}{\sigma}\right)$, is read from the Rayleigh distribution curve, Fig. 30. Multiplying each relative stress by σ gives the corresponding stress, s, which can be used to enter the S-N curve, Fig. 29, to obtain N(s), the number of allowable cycles at that stress. The ratio $\frac{p\left(\frac{s}{\sigma}\right)}{N(s)}$ is the relative damage or damage density and is plotted versus $\frac{s}{\sigma}$ in Fig. 31. At the maximum damage density we can read the relative stress and obtain the peak damage stress, s_{pd}. The area under this curve represents the summation indicated in Eq. 54 and can be computed by multiplying the sum of $\frac{p\left(\frac{s}{\sigma}\right)}{N(s)}$ as given in the last column in Table XVII by the relative stress interval $\Delta\left(\frac{s}{\sigma}\right)$. The result is the reciprocal of the predicted life cycles at the assumed rms level of the random stress. The same process was repeated for other values of σ and the results plotted in Fig. 29 as a random S-N curve. The peak damage stress, s_{pd}, is also plotted. It is seen that s_{pd} is 3 to 4 times the rms stress. Referring to the Rayleigh distribution curve we see that it is only one per cent or so of the stress cycles which cause most of the damage. In a siren test the stress is

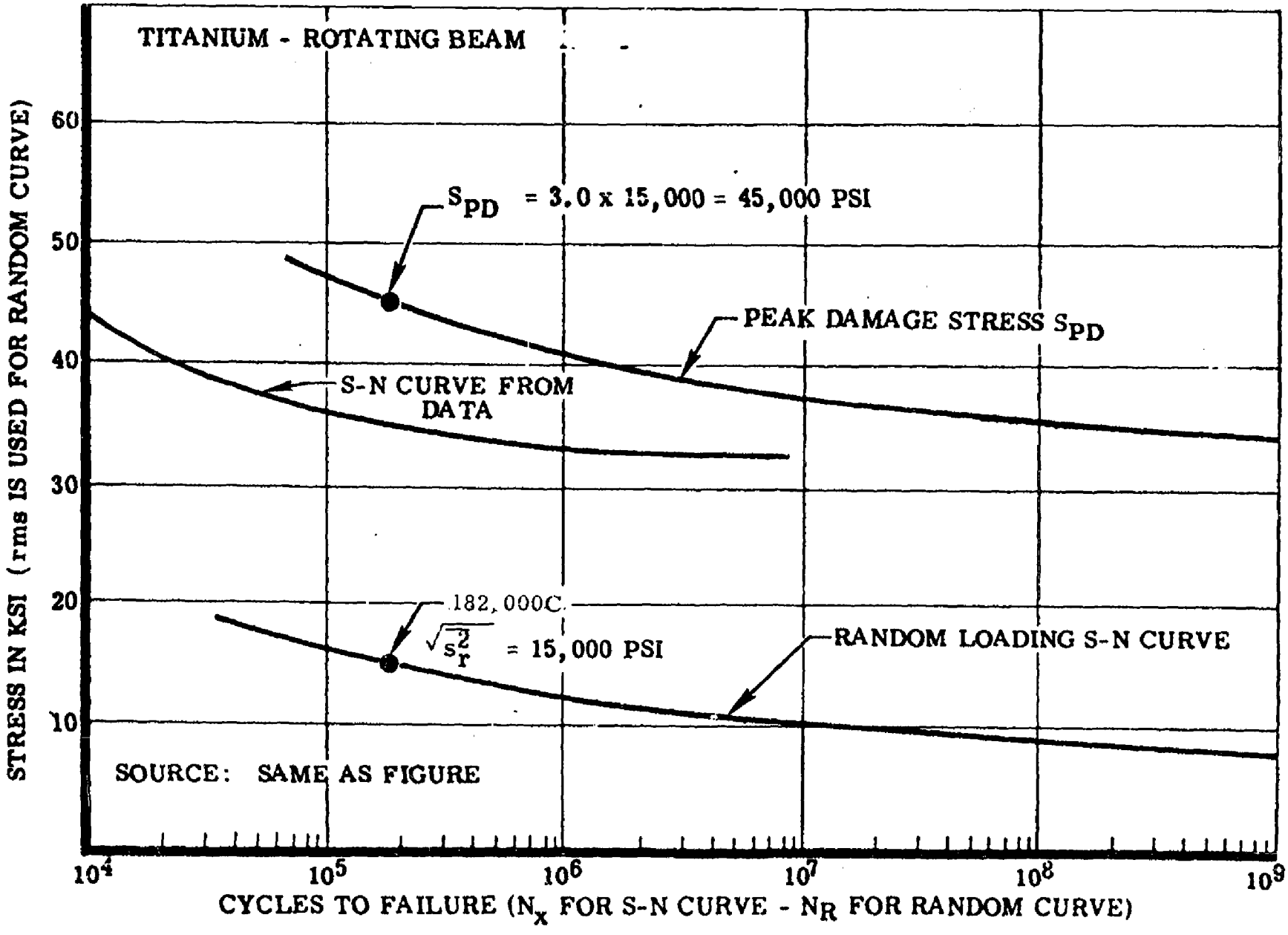

Figure 29. Comparison Between Actual and Predicted Spectrum Life (Ref. 39)

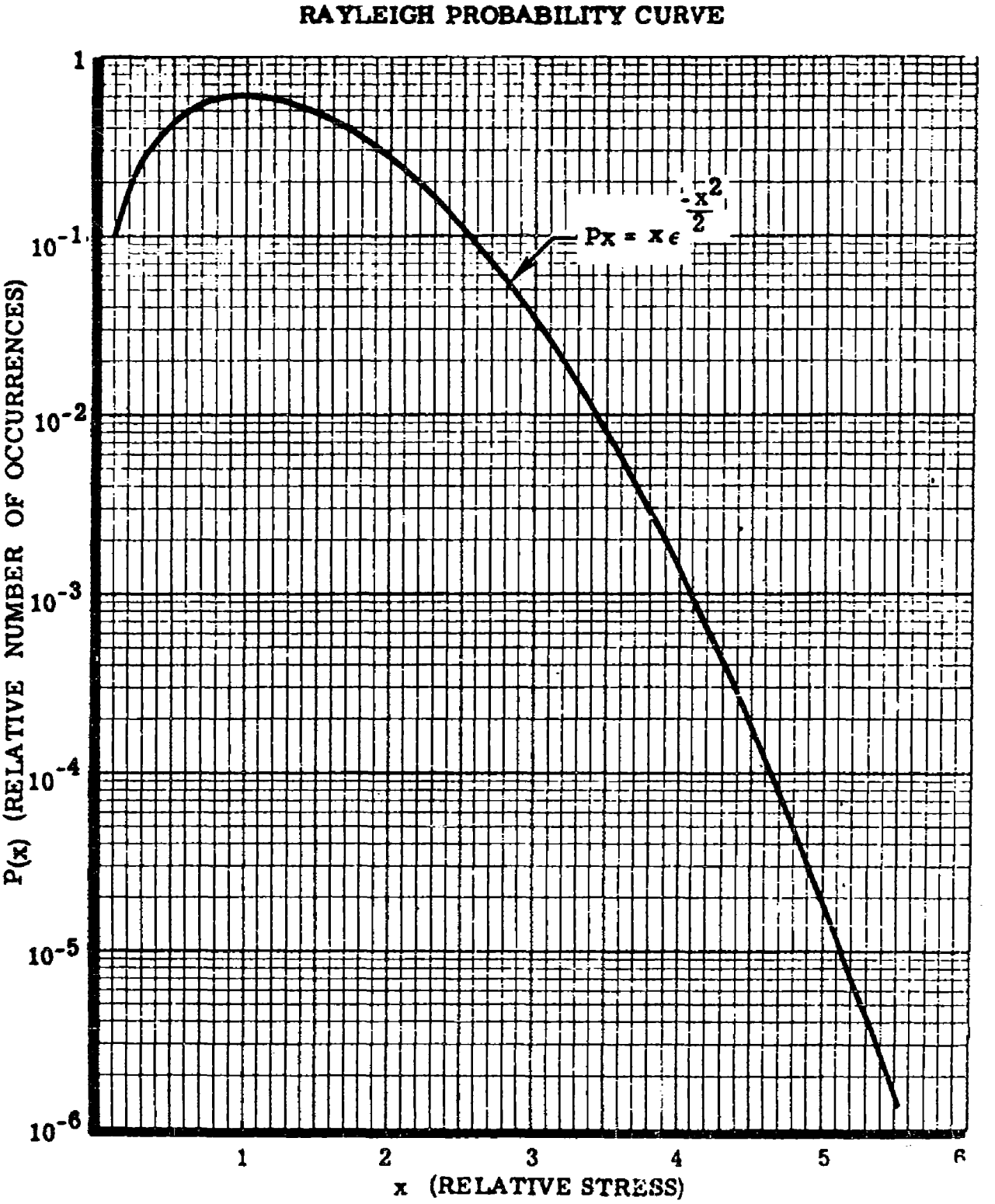

Figure 30 Rayleigh Probability Curves (Ref 35)

CUMULATIVE DAMAGE TABLE FOR ANNEALED TITANIUM

σ=15,000 PSI (ASSUMED)

$\frac{s}{\sigma}$	$p(\frac{s}{\sigma})$	N(s)	$p(\frac{s}{\sigma})/N(s)$
2.2	$(1.95)\ (10^{-1})$	$(4)\ (10^{6})$	$(0.05)\ (10^{-6})$
2.4	$(1.34)\ (10^{-1})$	$(9.5)\ (10^{4})$	$(1.41)\ (10^{-6})$
2.6	$(8.8)\ (10^{-2})$	$(2.9)\ (10^{4})$	$(3.04)\ (10^{-6})$
2.8	$(5.6)\ (10^{-2})$	$(1.5)\ (10^{4})$	$(3.73)\ (10^{-6})$
3.0	$(3.5)\ (10^{-2})$	$(8.5)\ (10^{3})$	$(4.12)\ (10^{-6})$
3.2	$(2.0)\ (10^{-2})$	$(5.6)\ (10^{3})$	$(3.57)\ (10^{-6})$
3.4	$(1.05)\ (10^{-2})$	$(3.3)\ (10^{3})$	$(3.18)\ (10^{-6})$
3.6	$(5.5)\ (10^{-3})$	$(2.2)\ (10^{3})$	$(2.5)\ (10^{-6})$
3.8	$(2.8)\ (10^{-3})$	$(1.4)\ (10^{3})$	$(2.0)\ (10^{-6})$
4.0	$(1.5)\ (10^{-3})$	$(9.5)\ (10^{2})$	$(1.58)\ (10^{-6})$
4.2	$(6.2)\ (10^{-4})$	$(6.4)\ (10^{2})$	$(0.97)\ (10^{-6})$
4.4	$(2.7)\ (10^{-4})$	$(4.3)\ (10^{2})$	$(0.63)\ (10^{-6})$
4.6	$(1.2)\ (10^{-4})$	$(3)\ (10^{2})$	$(0.4)\ (10^{-6})$
4.8	$(4.8)\ (10^{-5})$	$(2.2)\ (10^{2})$	$(0.22)\ (10^{-6})$
Σ			$(27.4)\ (10^{-6})$

$$\frac{\Delta s}{\sigma} = 0.2$$

$$\sum \frac{p(\frac{s}{\sigma})}{N(s)} = 0.2 \times 27.4 \times 10^{-6} = 5.49 \times 10^{-6}$$

$$N_R = \frac{1}{5.49 \times 10^{-6}} = 182{,}000$$

TABLE 17. CUMULATIVE DAMAGE TABLE

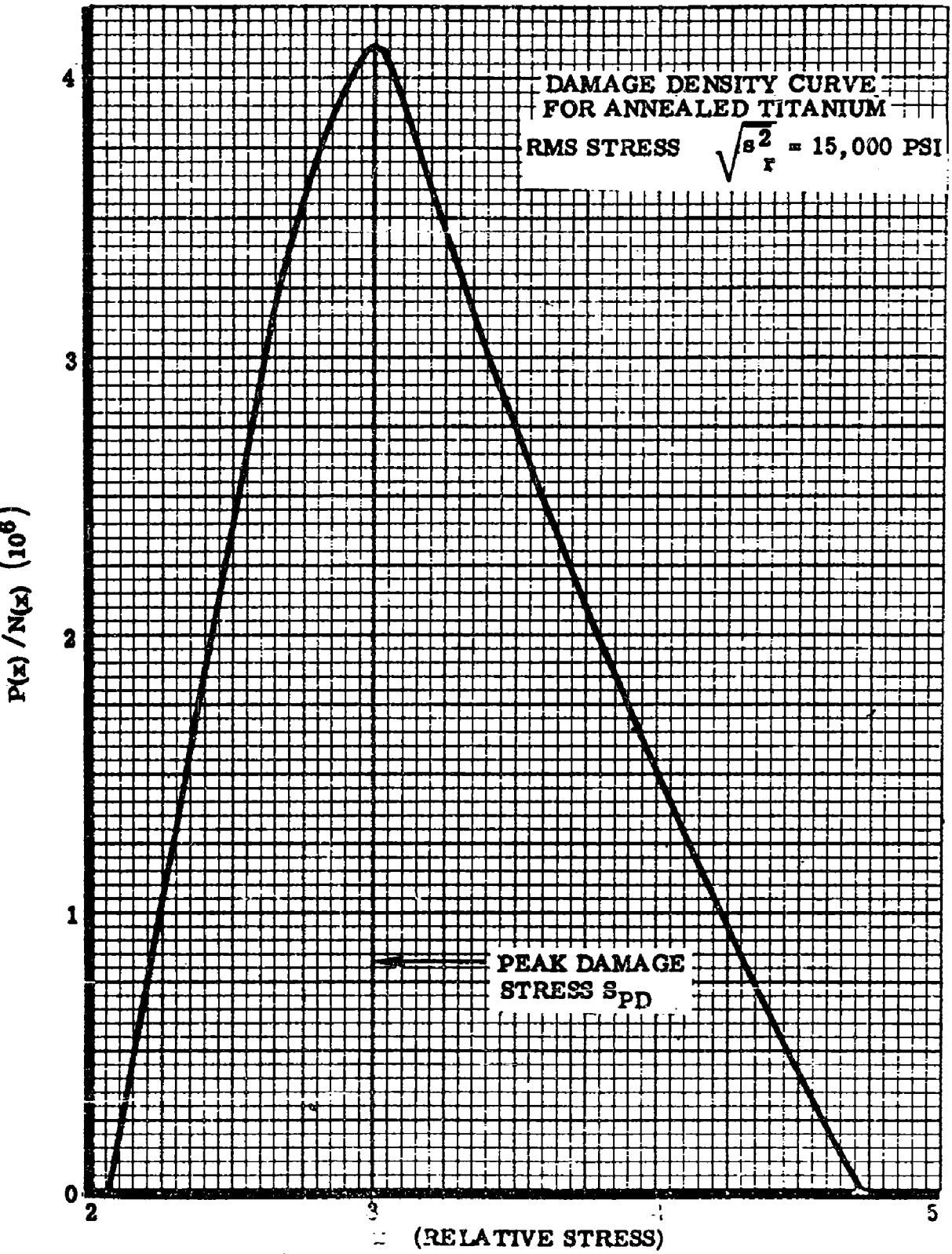

Figure 31. Damage Density Curve (Ref. 39)

usually pretty close to s_{pd}. Thus the siren can apply enough cycles to fail the sample in a few minutes whereas the equivalent random source of noise would require hours.

Random S-N curves for several materials as well as honeycomb structures have been computed and are given in Ref. 39.

There has been criticism that Miner's rule ignores factors which are known to influence fatigue life. For example, the time sequence of variable loads is neglected. In two level block testing on mild steel samples Kommers (Ref. 46) found that improved fatigue strength could be obtained by applying the low loads first. The opposite effect was found in aluminum, (Ref. 47). When many blocks of stresses alternating between low and high are used the sequence effect becomes less important as the number of blocks is increased but it apparently does not completely disappear.

Miner's rule makes no allowance for rest periods and there is no way to include the effects of static loading. Residual tensile stress is detrimental but compressive stress may be beneficial.

Schjelderup (Ref. 48) has analyzed the strain gage response of sheet rib structures to excitation by a jet engine on an aircraft and in a test cell. He found that the Rayleigh distribution accurately described the distribution of peaks in both cases. Thus for a lightly damped single degree of freedom system the response is a sinusoid with varying amplitude. But with many modes the response is a complex wave form. According to Schjelderup some distribution other than the Rayleigh must be used for multimode response but he did not offer a substitute. As we shall see later Belcher (Ref. 40) applies a multimode correction factor in his method.

Many writers have reported that $\sum \frac{n_i}{N}$ can often be larger or smaller

than unity at failure. For example Fralich (Ref. 49) has reported that the fatigue life was over estimated for some notched SAE 4130 steel beam samples. Ref. 47 cites the report by Hooke and Head that Miner's rule over estimated the life of notched samples by as much as 3-1/2 times at low stresses and somewhat less at higher stresses. The same reference also cites the work of R. W. Fralich on notched test pieces of 7075 AL alloy which were subjected to reverse bending within the range of their natural frequency. Contrary to the results of Hooke and Head he found that Miner's rule under estimated the life at high stresses and predicted it accurately at low stresses. Ref. 47 mentioned that a program of research was undertaken at the University of Southampton to investigate the contradictions in the results reported in random loading studies. A preliminary report by M. T. Lowcock and T. R. G. Williams concluded that "1) an accurate estimate of the fatigue life under variable loading conditions can be obtained from the rms of the stress and the S/N curve of the material. 2) There is a discontinuity in the S/N curve of L.73 alloy at a stress level of 16 tons/in.^{2}, and the shape of the variable loading fatigue graph is modified by the discontinuity."

4B. Freudenthal Method

The discontinuity in the S-N curve has been investigated by Freudenthal. (Ref. 50). Based on tests on small plain samples there appear to be two distinct mechanisms of fatigue. The first is called high level fatigue. It occurs at either high stress or low frequencies such that the deformation is akin to that in unidirectional "static" deformation. Failure is related to a critical amount of total plastic deformation or of strain hardening due to distortion and breakdown of the grain structure. It corresponds to the short-life portion of the S-N curve which has a high slope.

Rapid cycling stresses of small amplitudes produce less strain hardening and no significant distortion. Instead a multitude of fine slip bands are concentrated in striations so that individual dislocations cannot be resolved. This corresponds to the longer-life portion of the S-N curve with smaller slope.

The two mechanisms differ in the way energy is released as heat as well as the way cracks are initiated. The transition between the two mechanisms should be sharp but its location depends on the frequency of cyclic stressing, the initial condition of the grain structure, the blocking of the primary slip system by dislocations and the intensity of the mean stress.

With varying stress amplitudes there is an interaction between the two mechanisms. In particular the high level mechanism has the effect of accelerating damage by the low level mechanism. Thus a relatively few cycles at the high level will shorten the fatigue life under the low level stress amplitudes far beyond any damage immediately associated with the high level cycles. Freudenthal considered using an interaction factor to predict this effect. He concluded however that it would be better to create a ficticious S-N curve for variable loading. He defined the S-N curve in two segments as follows:

$$\left(N_i/\bar{N}\right) = \left(S_i/\bar{S}\right)^{-\nu} \qquad N_i \leqq \bar{N}$$

$$\left(N_i/\bar{N}\right) = \left(S_i/\bar{S}\right)^{-\rho} \qquad N_i \geqq \bar{N}$$

where $(\bar{N}, \bar{S})$ is the point on the S-N curve at the boundary between high level and low level fatigue and (N_i, S_i) is any other point on the ficticious S-N curve. The stress interaction is introduced by changing the

exponent from ν to ρ. For materials such as 2024 and 7075 aluminum and 4340 steel $8<\nu<16$ and $4<\rho<8$.

Freudenthal states that the effect may be different for larger or more complex samples. Thus a certain amount of testing would be needed to establish the parameters.

4C. Smith's Cumulative Damage Method

Ref. 39 outlines a method proposed by C. R. Smith which would modify the S-N curve so that Miner's method could be used. He argues that the principal errors in fatigue life prediction are due to the residual stresses at concentrations. Thus the few cycles of high stresses in random loading alter the S-N curve. The S-N curve can be corrected by applying a preload that is equivalent to the highest probable load that can be expected in the first ten per cent of service life. Although Miner's method can be used with the modified S-N curves new data must be acquired for each material and load spectrum. The available S-N data cannot be used with this method.

4D. Other Methods of Fatigue Analysis

Fuller (Ref. 51) has developed a method for predicting the life of a structure exposed to narrow band random stress as well as broad band random stress. It is also applicable to variable-cycle loading provided the stress patterns or blocks of stresses are repeated enough times to make the order of loading unimportant.

The order in which stresses are applied affects the total cycles to failure. For two levels of stress cycles with S_1 greater then S_2 the accumulated cycle ratio $\sum \frac{n}{N}$ is less than 1.0 at failure, while with $S_1 < S_2$ the cycle ratio is greater than 1.0. If an S-N curve is determined using samples which have all been cycled at a constant maximum stress for an equal number of cycles, the new S-N curve will cross the original S-N curve

at the value of the pre-stress. The number of cycles at pre-stress are included in the new plot.

Samples stressed below the pre-stress will fail earlier than predicted by the original S-N curve because the pre-stress cycles are more damaging than an equal number of cycles at the test stress. Furthermore Freudenthal has shown that there is a stress interaction which may cause more rapid accumulation of damage at the test stress after a higher pre-stress. If the test stress is larger than the pre-stress the total life is generally longer than would be indicated by the original S-N curve at the test stress. It is thought that understressing tends to relieve the peak residual stresses in the sample and increase the life. The new S-N curve for the pre-stressed samples would thus tend to rotate about the pre-stress point on the original S-N curve. The amount of rotation is approximately proportional to the accumulated cycle ratio $R=\sum \frac{n}{N}$ of the pre-stress. For no pre-stress R=0 and there is no rotation and all points lie on the original S-N curve. For R=1.0 the sample must fail before any test cycles are applied.

Fig. 32 illustrates the rotation of the S-N curve. First s_1 is applied for n_1 cycles and curve 1-1 is rotated into 2-2. Then s_2 is applied for n_2 cycles. The curve is further rotated about the point at the intersection of the curve 2-2 with the stress level s_2. This results in curve 3-3. It can be seen that the fatigue life will not be less than that given by the original S-N curve for the maximum stress, nor will it be longer than that given by the original S-N curve for the minimum stress. The actual fatigue life for variable cycle loading would fall in this interval with its actual location a function of the load distribution. As a practical matter the upper limit of the interval is established by extrapolating the highest slope tangent to the original S-N curve down to the minimum stress. A computed factor, β, locates the predicted fatigue life as the fraction of

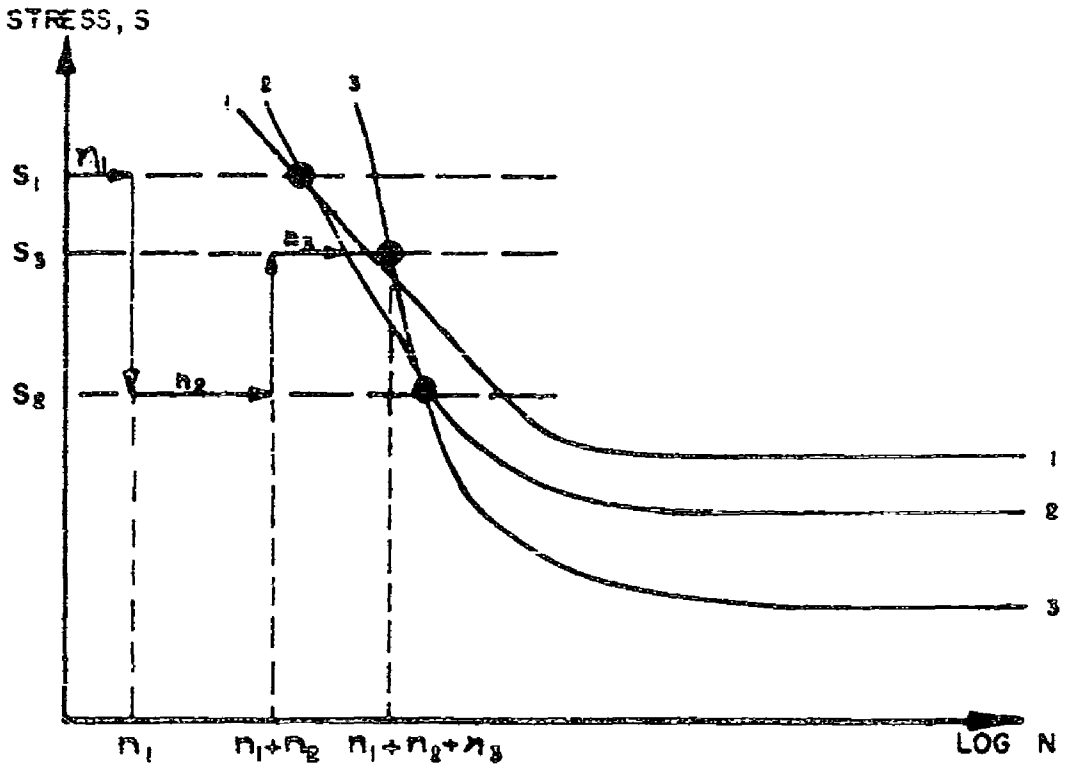

CURVE 1-1 BASIC S-N CURVE
CURVE 2-2 CURVE INDICATING TOTAL CYCLES TO FAILURE INCLUDING n_1 CYCLES AT S_1
CURVE 3-3 CURVE INDICATING TOTAL CYCLES TO FAILURE INCLUDING n_1 CYCLES AT S_1 AND n_2 CYCLES AT S_2

FIGURE 32. EFFECT OF PRESTRESS CYCLES ON TOTAL CYCLES TO FAILURE (Ref. 51)

the interval from the upper life limit. Thus if β is near zero most of the stress cycles were at the lowest stress and the fatigue life would be at the upper limit of the interval. If β=1.0 all of the stress cycles would be at the maximum stress and failure would occur at the lower limit of the life interval or at the life shown on the original S-N curve.

For variable stress cycles with a continuous distribution between a minimum, S_a, and maximum S_A', Fuller gives the following equation for β:

$$\beta = \frac{1}{q\left|S_A' - S_a\right|} \int_{S_a}^{S_A'} \left[\log\ P(S-S_a) + q\right]\ ds$$

If the lowest stress is zero this reduces to

$$\beta = \frac{1}{q\ S_A'} \int_{0}^{S_A'} \left[\log\ P(S) + q\right]\ ds$$

q is a stress sensitivity factor which must be selected by the user of this method based either on experience or on two-level block testing. P(S-Sa) is the cumulative probabilty distribution of the stress loading. For a Rayleigh distribution of peaks about zero mean, β is simply a constant, $\frac{2}{3}$.

Fuller has analyzed Trotter's narrow band random data (Ref. 52) using the β method and obtained very good results, see Fig. 33. β is equal to A/I. He also analyzed the results of extensive tests on samples loaded with three different broad band random stress spectra. With suitable choice of the stress sensitivity factor, q, the results looked very promising.

4E. Strain Life Method

In their analysis of sonic fatigue life determined by siren testing,

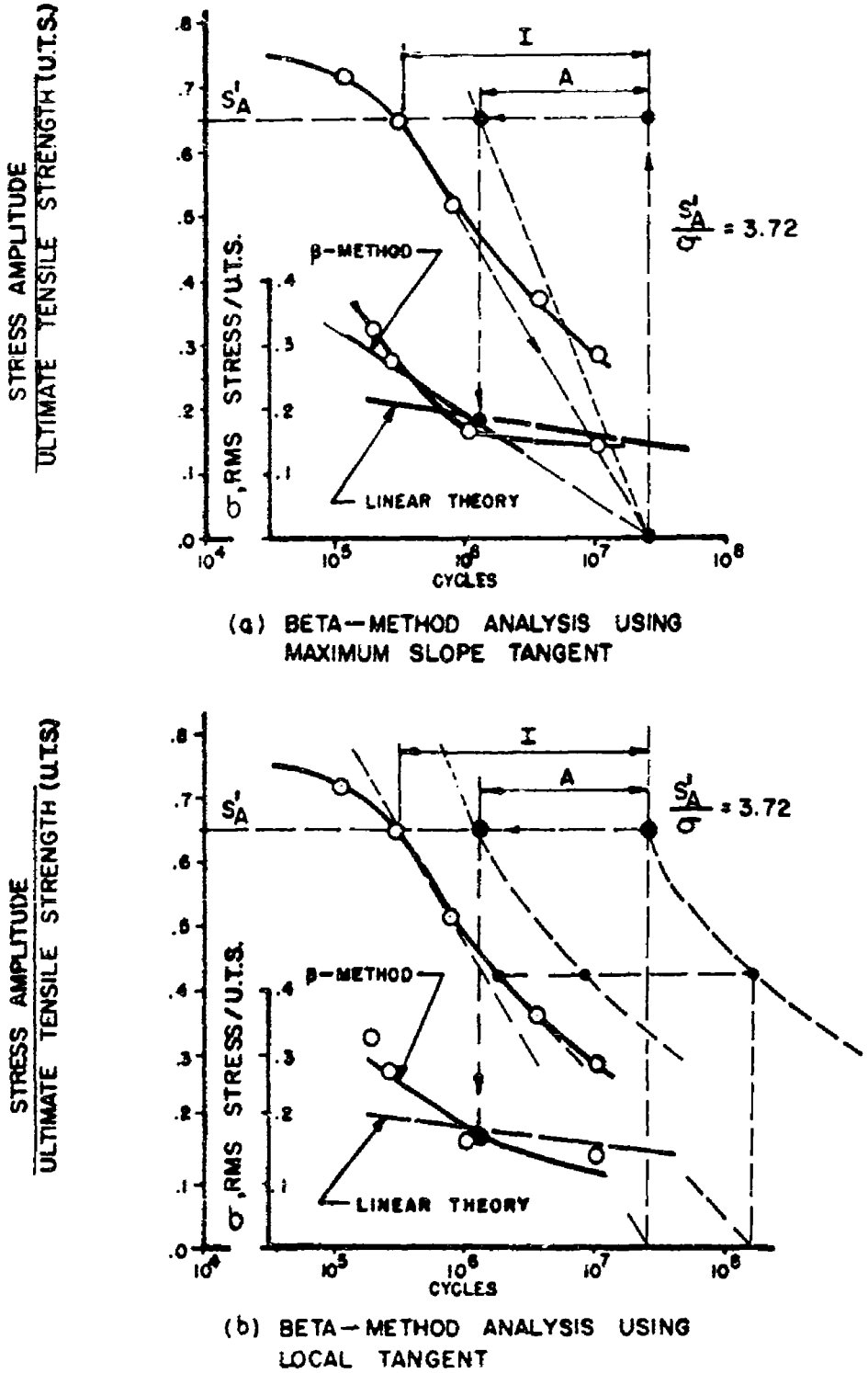

FIGURE 33 **COMPARISON OF ANALYSIS AND TEST RESULTS, TROTTER'S NARROW BAND RANDOM TESTS** (Ref. 51)

P. W. Smith and C. I. Malme (Ref. 53) have used Miner's rule to determine the fatigue life under random excitation from siren tests in much the same manner as Belcher (Ref. 40). They argue however that better results are obtained if strain-life curves from constant amplitude testing are used instead of the more widely used S-N curves. There is no difference of course at low stresses below the yield point where strain is proportional to stress. Above the yield point the peak stress and peak strain are nonlinearly related. The question arises whether either the local stress or local strain can be considered linearly related to the overall structural response. The peak strains usually are concentrated in localized areas such as in the vicinity of a hole or weld or other point of attachment. The fatigue damage thus will occur mostly in these small localized regions. It is assumed that plastic yielding in these small areas will not affect the surrounding material and hence will not alter the response of the structure. Therefore it is assumed that the local strains in the fatiguing area are linearly related to the structural response.

The use of strain instead of stress is important only at short lifetimes when a significant portion of the damage is due to strains above the local yield point. A constant stress lifetime curve tends to a lower slope in this region while the corresponding strain-life curve continues to rise smoothly toward the strain which will cause failure in a "static" tensile test.

Below the yield point the constant stress S-N curve is easily converted to a constant strain lifetime curve. The ultimate strain for failure in one cycle in a static test gives the extreme end of the curve. Until test data is accumulated the points in between must be estimated by extrapolation.

For high rms stresses in a random test we find that the Rayleigh

distribution may predict a small probability of occurrence of large peak stresses exceeding the ultimate strength of the material. Presumably failure should occur by fracture of the material much sooner than actually occurs by fatigue during the test. Some workers have avoided this dilema by arbitrarily truncating the stress distribution. An example is given in Ref. 53 which shows that the use of strain instead of stress gives a more reasonable result. For a structure of 2024 aluminum without stress concentrations an rms strain of $1.9(10)^{-3}$ corresponds to rms stress of 20,000 psi. A lifetime of $1.6(10)^{5}$ cycles is computed if the rare, very high strains are ignored. The ultimate strength of the material, 64,000 psi., is only 3.2 times the rms stress. The Rayleigh distribution predicts that this stress will be exceeded about 6 times in every 1000 cycles. Consequently the fracture of the material would be expected to be more likely than the accumulation of significant fatigue damage. If strain is used rather than stress the problem of failure by rare exceedances disappears. The ultimate strain for 2024 aluminum is about 0.19. This is so much greater than the rms strain of $1.9(10)^{-3}$ that the Rayleigh distribution predicts it will be exceeded only one in 10^{2171}, or practically not at all.

4F. Scatter of Fatigue Data

It is evident that there is not yet a clear understanding of fatigue and that there are deficiencies in the methods for predicting fatigue life under variable loading conditions. The prediction of fatigue life is largely empirical and good judgement and experience are essential to proper evaluation of all the many variables which enter.

The scatter in fatigue data cannot be avoided. The formation of a fatigue crack depends on residual stresses in the material which arise

from the forming, heat treating, machining or even handling of the material. The metallurgical structure including the shape, size and orientation of the grains will affect the fatigue. Variations are also caused by a lack of randomness in the loading, unknown stress concentrations, stress interactions, time history of the load, nonlinearity, pre-loads as well as errors in measurement. It follows from the shape of the S-N curve that a change of about 5 per cent in the stress will lead to about 100 per cent change in the fatigue life in the long life region. A somewhat more comforting view of the situation is to ask what design margin in stress or acoustic load is required to meet a given design life. Eventually it may be possible to apply a statistical confidence interval to S-N data. Fig. 34 from Ref. 39 shows how the upper and lower envelopes of the S-N data for a much tested material convert to random S-N curves. The conversion follows the Rayleigh distribution of peaks and Miner's rule for damage accumulation.

For the development of engineering design data it appears quite reasonable to use Miner's rule to take advantage of its simplicity and the possibility of using the large amounts of available S-N data. With appropriate design margins it can give good results. (Ref. 53 and 54).

5. Stress Response to Acoustic Loads

The acoustic pressures in the near field of a jet engine produce random vibration and stresses in the aircraft structure. In particular the exposed cover panels are subjected to intense pressures which may cause fatigue failure although the effect on stiffening ribs or frames may also be important. Miles (Ref. 43) analyzed the response of a single

MATERIAL 2024-T3 BARE F_{tu} = 68,000 PSI TYPE OF LOADING (REVERSED AXIAL)
TYPE OF CONCENTRATION (K_t = 1)

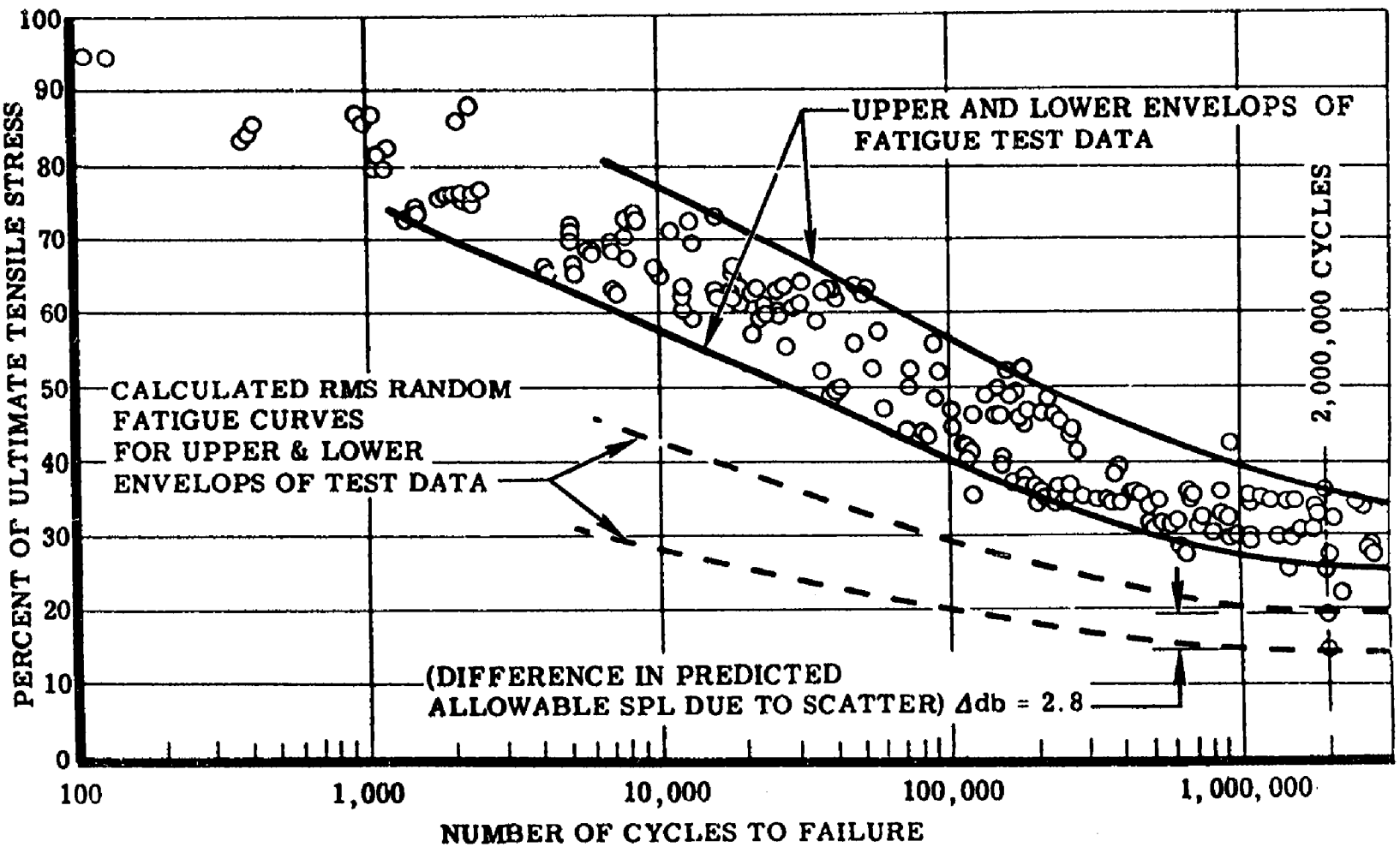

Figure 34. Effect of Fatigue Data Scatter on Allowable Sound Pressure Level (Ref. 39)

degree of freedom system to a random excitation. Powell developed a more powerful approach which included several modes of vibration and the space correlation of the applied pressure field. (Ref. 55). Unfortunately this requires more information than is usually available in the design stage. A knowledge of the mechanical impedance of the structure is needed which depends on the mode shapes, the natural frequencies and the structural and acoustic damping of each normal mode. Also the power spectral density and the narrow band spatial correlation of the pressure field are required.

5A. Sine-Random Stress Equivalence

Belcher, Van Dyck and Eshleman (Ref. 40) extended Mile's work to develop the equivalence relation between random and sinusoidal stress response so that siren tests could be related to random noise response. The same method is used by Fitch (Ref. 39). The equivalence relation can be derived as shown below. Eq. 34 gives the square of the displacement response of a single degree of freedom system to a unit applied force. If the static displacement per unit force yo/Fo is replaced by the static stress per unit pressure, $^{s}_{o}$, and the result multiplied by the square of the rms pressure, p_s^2, Eq. 34 gives the square of the rms stress response, S_s.

$$S_s^2 = \frac{S_o^2 p_s^2}{\left[1-\left(\frac{\omega}{\omega_n}\right)^2\right]^2 + \left(2\zeta\frac{\omega}{\omega_n}\right)^2}$$

Here the subscript, s, denotes sinusoidal test conditions. At resonance

$$S_s^2 = \frac{S_o^2 p_s^2}{4\sigma_s^2} \qquad (55)$$

Eq. 36 gives the mean square displacement response of the single degree of freedom system to a force spectral density. We shall use the subscript, r, to denote random instead of the subscript, s, which previously stood for source. Eq. 36 then is

$$\langle y_r^2 \rangle = W_r(\omega_n) \left(\frac{yo}{Fo}\right)^2 \frac{\pi \omega_n}{4\delta}$$

If we define the applied power spectrum per 1 cps band width instead of per radian per second we have

$$W_r(\omega_n) = \frac{1}{2\pi} W_r(f_n)$$

and

$$\langle y_r^2 \rangle = W_r(f_n) \left(\frac{yo}{Fo}\right)^2 \frac{\pi f_n}{4\delta}$$

If we replace yo/Fo by the static stress per unit pressure, S_o, and change the applied spectral density to the square of the rms sound pressure in a one cycleband width we obtain the square of the rms stress response.

$$\langle s_r^2 \rangle = \frac{p_r^2 S_o^2 \pi f_n}{4\delta_r} \tag{56}$$

The ratio of random to sinusoidal stress is

$$\frac{S_r^2}{S_s^2} = \pi f_n \frac{\delta_s^2 p_r^2}{\delta_r p_s^2} \tag{57}$$

If the damping in the two environments is the same

$$\frac{S_r^2}{S_s^2} = \pi f_n \delta \frac{p_r^2}{p_s^2} \tag{58}$$

Smith and Malme (Ref. 53) point out that the acoustic damping in the

siren test duct may not be the same as that for a structure in the open. In fact they preferred to use the actual measured response to random pressure rather than relying on a calculation such as Eq. 56 which includes the damping.

5B. Correction for Non-Linearity

Aircraft panels exhibit nonlinear stress response. Conventional skin stringer construction is nonlinear because of the membrane stresses which become important at relatively low loads. Honeycomb structures on the other hand have almost linear response.

The correction for non-linearity would not be necessary if the siren test were conducted at the peak damage stress S_{pd}. The actual test is run at several pressure levels so that a plot of stress versus pressure level can be made. The correction for non-linearity to be applied to Eq. 58 is simply to multiply Eq. 58 by

$$\lambda = \left[\frac{S_{pd}/P_{pd}}{S_t/P_t} \right]^2 \tag{59}$$

where the subscripts, pd and t, denote peak damage and test values at failure. Ordinarily the actual stresses at the location of the failure will not be measured but the test should give a curve of relative stresses versus pressure.

Thus

$$\frac{S'_{pd}}{S_{pd}} = \frac{S'_t}{S_t} \tag{60}$$

where the primes indicate relative stresses. λ then can be written

$$\lambda = \left[\frac{S'_{pd}/P_{pd}}{S'_t/P_t} \right]^2 \tag{61}$$

The test pressure, p_t, is known so that the relative test stress, S_t', can be obtained from the load curve. S_{pd} is obtained from the peak damage curve for the desired life and S_t is obtained from the original S-N curve at the test life. Then Eq. 60 is used to calculate S_{pd}'. Finally p_{pd} can be read from the load curve at S_{pd}' and Eq. 59 used to calculate λ.

5C. Correction for Multimode Response

Although it has been pointed out that only a few of the many possible modes of a structure will be important there is the problem of deciding how many and which of the modes are significant. Ideally there should be enough strain gages properly located to indicate the maximum stress in each mode. The modes producing the highest stresses are the most important.

Belcher (Ref. 40) stated that probably the greatest errors in the sine - random equivalence computation were encountered in the interpretation of multiple-mode data. In multi-mode response the stress response cycles are not fully reversed as they are if a single mode response is predominant. The suggested multimode correction factor to be applied to Eq. 58 is the ratio of the total rms stress to the rms stress in a particular mode. A separate correction is required for each mode.

$$\gamma_i = \frac{\Sigma S_{r_j}^2}{S_{ri}^2}$$

The basic information required is the stress versus frequency curve with constant pressure, p_s, applied. The damping ratio, δ, and the relative stress for each mode can be obtained from it. Substituting for S_r^2 from Eq. 58 we obtain for constant p_s,

$$\gamma_i = \frac{\sum_j f_{nj}\, \delta_j\, p_{rj}^2\, S_{sj}^2}{f_{ni}\, \delta_i\, p_{ri}^2\, S_{si}^2} \qquad (62)$$

5D. Corrected Sine - Random Stress Equivalence

The corrections for nonlinearity and multi-mode response as given by Eqs. 61 and 62 applied to Eq. 58 yield

$$\frac{S_r^2}{S_s^2} = \pi f_n \delta \frac{p_r^2}{p_s^2} \lambda \gamma \qquad (63)$$

It should be recalled that this condition applies at the resonant frequency, f_n. The other quantities are:

S_r = rms stress response to random pressure

S_s = rms stress response to sinusoidal pressure

p_r = random rms pressure spectral density (rms pressure in a one cycle per second band)

p_s = rms sinusoidal pressure

δ = damping ratio

λ = nonlinearity correction, Eq. 61

γ = multimode correction, Eq. 62

6. Siren Testing

The siren testing of the critical structure is the heart of the method proposed by Belcher (Ref. 40) and Fitch (Ref. 39). It provides information on the resonant frequencies and shapes of the important modes. The sample structure is tested to failure. The life, used with a random S-N curve, in effect provides the correction for the unknown stress concentrations and coupling factors.

The samples to be tested must be selected so that they are representative of the critical parts of the aircraft. This depends on both the distribution of the sound pressure field and estimates of the acoustic strength of the various parts of the structure; the parts with the highest ratios of pressure to strength should be selected for study.

It is of course the objective to simulate the structure and its boundary conditions and attachment to other parts of the aircraft. This means that the method of fastening the panel should be the same as in the prototype. Although some preliminary work may be confined to testing of panels only, the final tests should include other parts attached to the panels which might influence the response or the resonant frequencies. The electrical, hydraulic and other hardware must be included. For multiple span panels the center spans are more likely to have representative boundary conditions. Therefore it is reasonable to strengthen the edge spans slightly by decreasing their width. This will increase the probability that the failure will occur in the more representative spans.

The sample should be adequately strain gaged. Preliminary frequency scans using a low pressure source outside the siren test chamber are useful for determining the resonant frequencies and observing the mode shapes. Experience with such tests will help assure that strain gages have been properly placed to measure the maximum stresses. In addition such a test will provide the data on damping in the various modes. The frequencies and modes that produce the highest relative stresses are chosen for the siren test. If more than one mode is considered important, tests must be run at each such reasonant frequency. If the stress versus frequency curve shows nonlinearities, such as unsymmetrical resonance peaks, the damping must be determined from decay curves with appropriate filters

used to separate the modes.

The actual fatigue test is conducted in a siren test facility. Here grazing incidence is used because it usually simulates more accurately the service environment. Also there is better coupling to higher order modes of the structure and the system is not plagued by variations of the pressure due to shifts in standing ware patterns.

Stress versus pressure data are needed to provide corrections for nonlinear response. This can be obtained by the technique of step testing. Starting at some relatively low sound pressure level the sample is exposed for some nominal period of time, say 15 minutes, to each of the selected test frequencies. Then the sound pressure is increased a small step and the tests at each frequency are repeated. Fitch (Ref. 39) used 3 db steps and Smith and Malme (Ref. 53) used 2 db steps. The entire process is repeated until failure occurs. The test results give the cycles applied at each frequency at each pressure level as well as maximum relative stress at each frequency and pressure level. This technique minimizes the number of sample which must be tested.

Fitch (Ref. 39) gives the following discussion summarizing the accuracy of the method and the sources of error.

"Comparison of test results under random and sinusoidal loading has been made for a number of specimens. The variation between measured and computed stress ratios was found to be on the order of $\pm$ 3 db. Some of the more obvious sources of error in computations for stress, and for fatigue life, not necessarily the order of importance, are:

1. An error of one db in sound pressure measurement represents approximately 12 per cent error in load.

2. If the siren excitation frequency is off resonance, a large non-conservative error in damage accumulation can occur.

3. Damping factors depend on how they are measured.

4. The propagation direction of the sound relative to the panel in a siren test and in an air frame application is not, in general, the same.

5. Harmonics of the siren fundamental pressure wave may excite higher modes of the structure.

6. The nonlinearity of the structure depends not only on the design but also on the quality of fabrication, which is variable among specimens, e.g. skins which are tightly stretched begin to diaphram at lower pressures than do loose skins. This can have a large effect on λ.

7. If there is more than one significant mode, additional effects which contribute to errors exist.

(a) It is not necessary to know the actual values of stress for each mode, but the relative stress amplitudes must be known if the computed value of γ is to be meaningful.

(b) The possibility of obtaining misleading strain gage readings because of a non-zero geometric angle between the principal stresses must be considered.

(c) There is no certainty that the structural area which is critical when all modes are excited simultaneously (as by random noise) is the location of failure in the discrete frequency test.

(d) Coupling between modes, especially when there is little difference between the resonance frequencies, causes difficulties in measuring the damping factors and results

and results in questionable interpretation of their physical meaning.

8. For a specified life, allowable stress varies as much as ± 15 per cent for a plain smooth specimen, and an additional variation of ± 15 per cent occurs for a notched specimen."

7. Example Test and Evaluation

Fitch (Ref. 39) gives an analysis of a hypothetical problem to illustrate the methods he had proposed. His analysis will be summarized here for the same reason.

The vehicle is assumed to be a Mach 3 intercept fighter having two engines, in the 30,000-pound thrust class, with after burners. The sound field was calculated but since the methods were illustrated in Section IV-2 for the A3J aircraft the details of the calculation will not be repeated here. We assume that we have the overall sound pattern shown in Fig. 35. The specimen to be simulated and fatigue tested was selected in the vertical stabilizer as shown in Fig. 35. The octave band frequency analysis of the sound pressure level at the test specimen was found to be:

Octave Band, cps	20 / 75	75 / 150	150 / 300	300 / 600	600 / 1200	1200 / 2400	2400 / 4800	4800 / 9600
Sound Pressure Level, db.	134	138	142	146	150	150	149	147

Detailed analyses of the various possible missions of the aircraft were made to estimate the relative amounts of time to be spent at the various power settings of the engines for the many operations performed. Detailed operating logs for various types of aircraft and missions are needed to accomplish this. The key information derived from the analyses for our present purpose was that there would be an estimated 22 hours of operation at Max A/B power at sea level for a 3000 hours flight life of

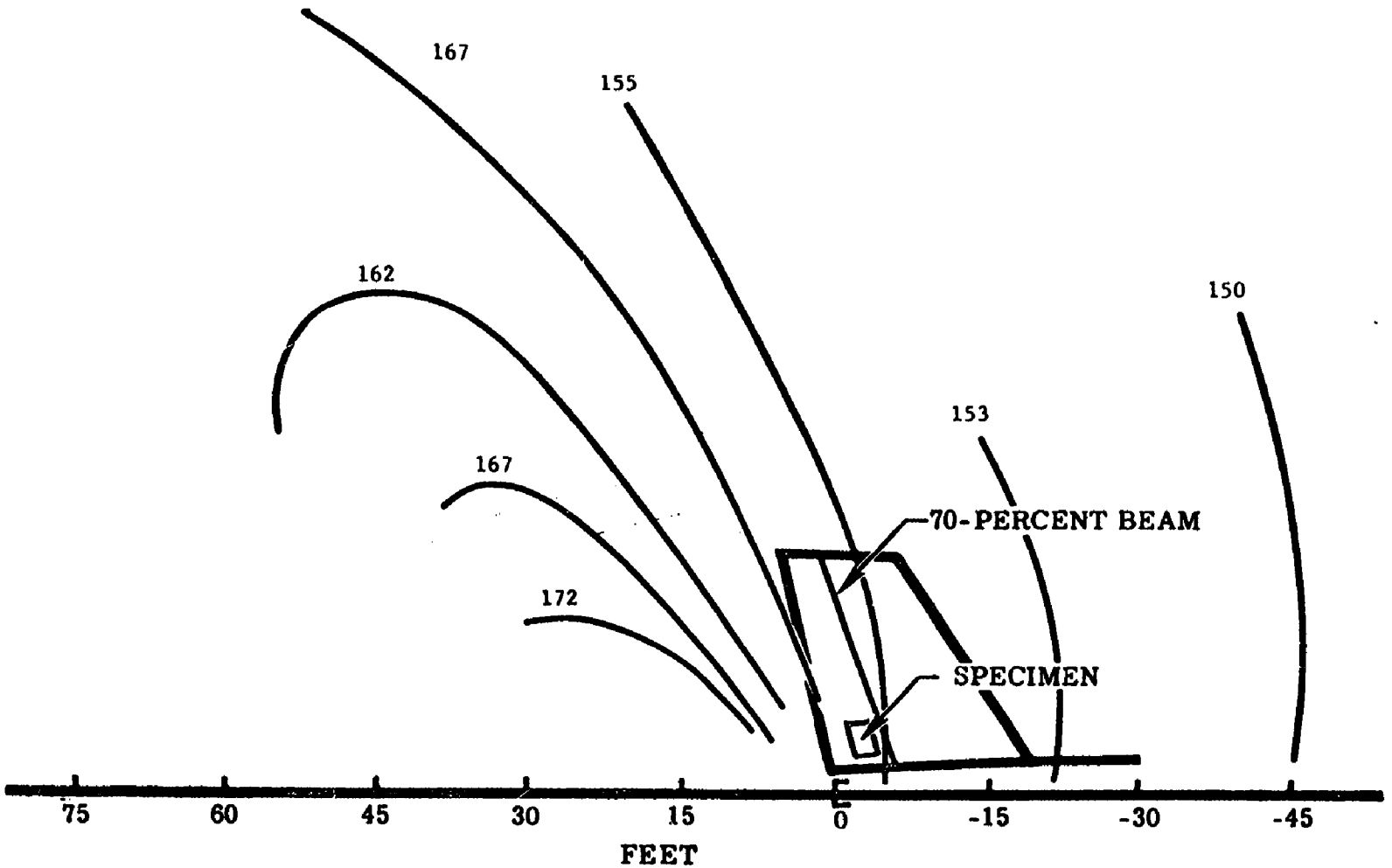

FIGURE 35. **Over-all Near Field** (Ref. 39)

the aircraft. This includes take-off and maintainance operations. It will be recalled that the engine sound pressure level decreases rapidly as the aircraft gains speed and altitude.

The random S-N curve for the 6Al-4V Ti material of which the specimen was constructed is shown in Fig. 36. The results of a representative frequency scan at 145 db is shown in Fig. 37. It is seen that two resonant frequencies, 652 cps and 695 cps, appear to be important. The specimen was siren tested for 15 minute intervals at each of the two resonant frequencies, then the sound pressure level was raised 3 db and the process repeated until failure occurred. The stress levels were recorded at all gages during the runs. The test results for the gage nearest the failure and oriented at right angles to the line of failure were given as follows:

Time Minutes	Sound Pressure db	Frequency cps	Relative Stress psi
15	148	652	13,200
15	148	695	6,500
15	151	652	15,300
15	151	695	9,200
3	154	652	21,700

The plot of the stress load curve from the above data is shown in Fig. 38. For the principal mode at 652 cps there were $n_{151} = 5.9(10)^5$ cycles at 151 db and $n_{154} = 1.2(10)^5$ cycles at 154 db. The condition for failure is

$$(n_{151}/N_{151}) + (n_{154}/N_{154}) = 1$$

Assume for the moment that all the damage accumulated at 154 db so that $N_{154} = n_{154} = 1.2(10)^5$. From the S-N curve, Fig. 36, the corresponding stress is $S_{154} = 87,500$ psi. For the 652 cps mode the stress load curve, Fig. 38, gives

$$S_{151} = \frac{S'_{151}}{S'_{154}} \times S_{154} = \frac{16,700}{21,710} \times S_{154} = 0.77 \quad S_{154}$$

Then $S_{151} = 67,300$ psi. The S-N curve shows that $N_{151} = \infty$. This means

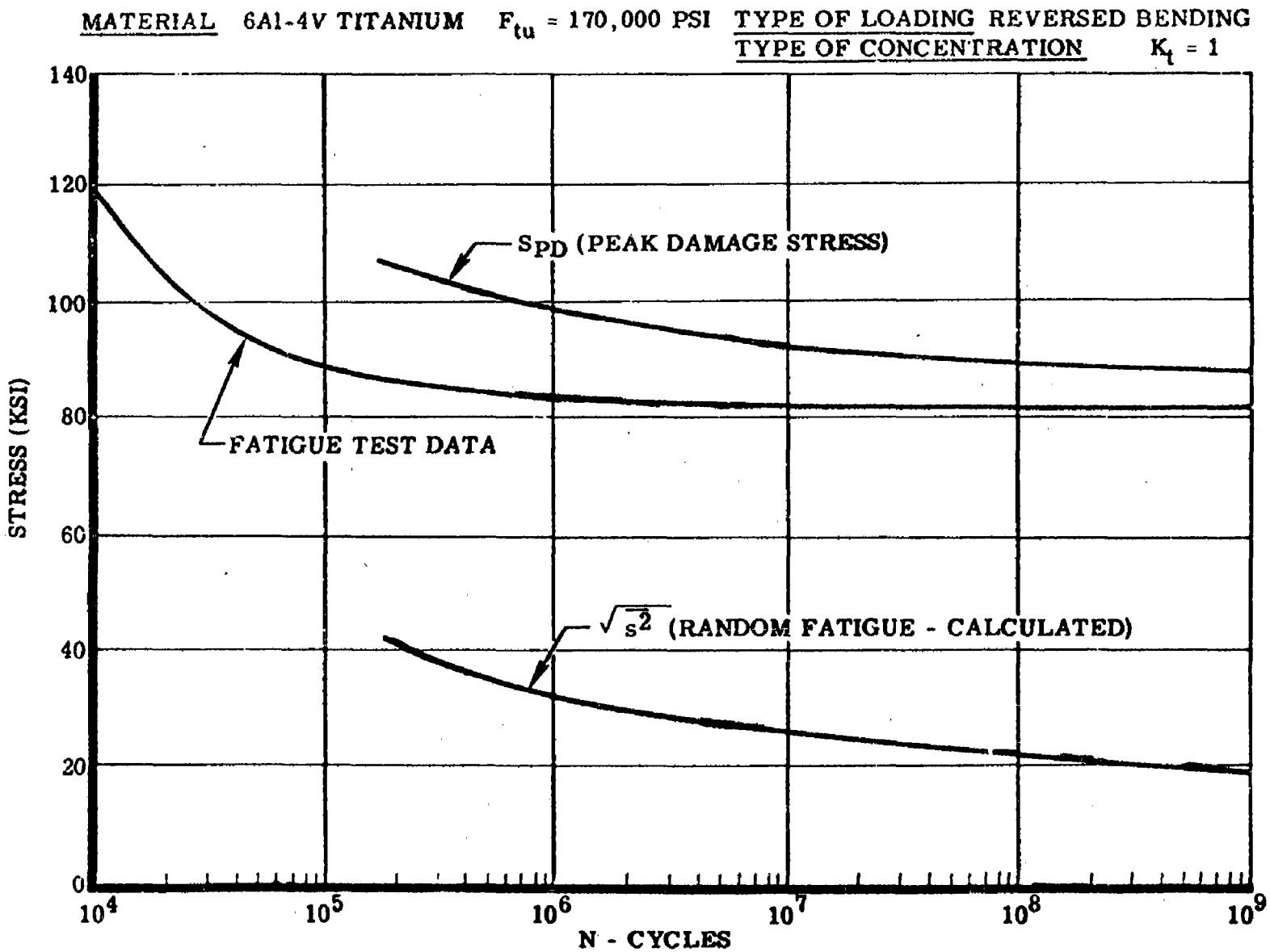

Figure 36. Calculated Random Fatigue and Peak Damage Curves (Ref. 39)

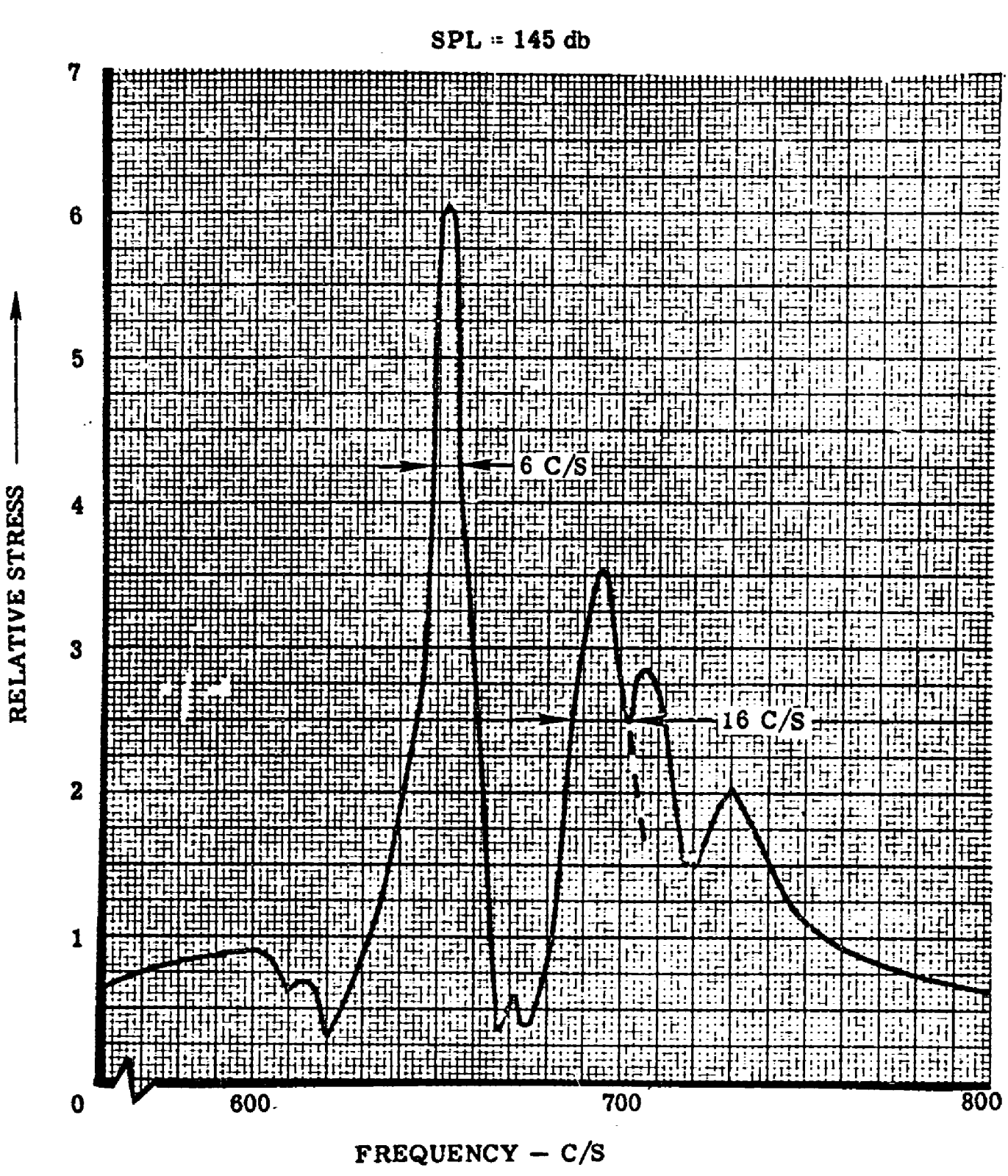

Figure 37. Stress - Frequency Curve (For Example Problem) (Ref. 39)

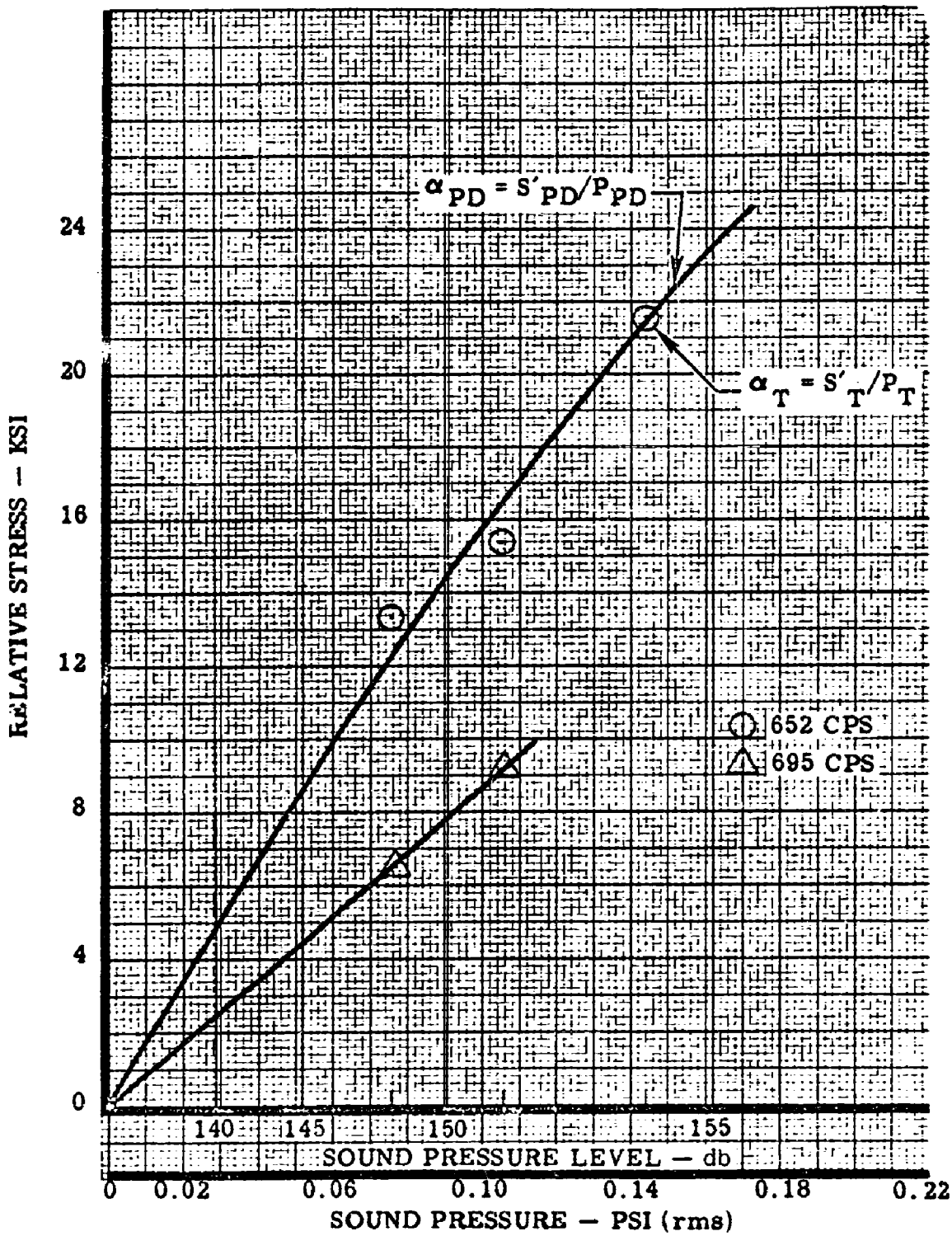

Figure 38. Stress - Load Curves (For Example Problem) (Ref. 39)

that there was no damage accumulated at 151 db. If N_{151} had not been infinite it would have been necessary to solve for N_{151} and N_{154} by trial and error.

The correction for multimode response is Eq. 62.

$$\gamma_i = \left(\sum_j \delta_j f_{nj} p_{rj}^2 S_{sj}^2 \right) \Big/ \delta_i f_{ni} p_{ri}^2 S_{si}^2$$

The frequency scan curve, Fig. 37, gives the following data:

f_{ni}	Δf_i	$\delta_i = \frac{\Delta f_i}{2f_{ni}}$	Relative S_{si}	S_{si}^2	$\delta_i S_{si}^2 f_{ni}$
652	6	0.0046	6	36	108
695	16	0.0015	3.5	12.3	12.8

Assuming that the random pressure will be the same at the two frequencies

$\gamma = \frac{120.8}{108} = 1.12.$

The nonlinearity correction factor from Eq. 59 is:

$$\lambda = \left[\frac{S_{pd}}{S_t} \quad \frac{p_t}{p_{pd}} \right]^2$$

The desired life of the structure was found from the mission analysis to be 22 hours or $5.2(10)^7$ cycles at 652 cps for Max A/B operation at sea level. At $5.2(10)^7$ cycles the peak damage curve in Fig. 36 gives $S_{pd} = 90{,}000$ psi. At the test life, $n_{154} = 1.2(10)^5$ cycles, the original S-N curve in Fig. 36 gives $S_t = 87{,}500$ psi.

From Eq. 60 we find:

$$S'_{pd} = \frac{S_{pd}}{S_t} \; S'_t = \frac{90{,}000}{87{,}500} \times 21{,}710 = 22{,}330 \text{ psi}$$

At $S'_{pd} = 22{,}330$ psi the stress load curve gives $p_{pd} = 0.151$ psi for the 652 cps mode. The test sound pressure level is equal to 0.144 psi.

$$\lambda = \left[\frac{90{,}000}{87{,}500} \times \frac{0.144}{0.151} \right]^2 = 0.963$$

From the siren random equivalence relation, Eq. 63, we obtain

$$\frac{p_r}{p_s} = \left(\frac{1}{\pi\delta f_n}\right)^{\frac{1}{2}} \left(\frac{S_r}{S_s}\right) \left(\frac{1}{\gamma\lambda}\right)^{\frac{1}{2}}$$

Here $S_s = S_t = 87{,}500$ psi or 61,800 psi (rms). The random stress $S_r =$ 23,000 psi (rms) is found from the random S-N curve, Fig. 36, at the desired life of $5.2(10)^7$ cycles. Then with $\delta = 0.0046$, $f_n = 652$ cps, $\gamma = 1.12$, $\lambda = 0.963$ we obtain

$$\frac{p_r}{p_s} = 0.117$$

$$db_r = db_s + 20 \log_{10} \; 0.117$$

$$db_r = 154 - 19 = 135$$

This is the allowable random spectrum level at 652 cps for the desired life. With a flat spectrum the 600/1200 cps allowable octave band level would be

$$db_{600/1200} = 135 + 10 \log_{10} (\text{Octave Band width} = 600 \text{ cps})$$

$$= 135 + 28 = 163 \text{ db.}$$

The acoustic environment at the location simulated by the test specimen was given previously with 150 db in the 600/1200 cps band. Thus there is a 13 db margin which should be adequate.

A similar calculation for the 695 cps mode indicated a design margin of 8 db with the assumption that failure had occured in this mode at the end of the 151 db test period. This did not happen so we know the design margin must be greater than 8 db. In order to find out more accurately what it is a step test must be run on another specimen in this mode only.

8. Design Charts

Belcher (Ref. 40) and more recently McGowan (Ref. 41) have described the development of design charts or nomograms which relate fatigue life, sound pressure level and the dimensional parameters of several of the simpler structures.

With a J-71 jet engine as the source of random noise Belcher and his associates obtained a limited number of fatigue failures of skin-rib constructions. They used the data as the basis in developing a design chart.

For a long panel the stress in the skin is proportional to the pressure and the square of the ratio of width to thickness (rib spacing to thickness)

$$\sigma \propto \frac{p\ S^2}{t_s^2}$$

Where σ = rms stress, p = rms pressure, S = rib spacing, t_s = skin thickness. Using this for the ratio of stress to pressure $S_o = \frac{S^2}{t_s^2}$ in Eq. 56 we see that

$$S_r^2 = \frac{S^4}{t_s^4}\ p_r^2\ \frac{\pi f_n}{4\delta}$$

Assuming that the ratio f_n/δ is constant for panels of various widths and thicknesses it is possible to draw a nomogram relating the stress, pressure, rib spacing and rib thickness. Belcher introduced the fatigue life data from the above tests in the same design chart. Although he did not show that f_n/δ is constant the data appeared to fit within the normal scatter for S-N data. Siren fatigue data were converted by the sine-random equivalence procedure discussed earlier and also entered on the design chart with about the same accuracy as the random test data.

McGowan evidently carried the work further using the same techniques. He reported that the ribs were critical in the bend radius of the flange. Since the same parameters are involved for the ribs as for the skin, the

rib data can be superimposed on the same design chart, Fig. 39. For a long panel the resonance in the fundamental mode is a function of the skin thickness and rib spacing. This too is shown on the design charts.

The design chart can be used to find a skin thickness, t_s, rib thickness, t_r, and rib spacing, S, to withstand a given sound pressure level, db_R, for a given life, N_R. Conversely, given the panel configuration one can find the life for a given sound pressure level or the allowable sound pressure level for a desired life. Here db_R is the spectrum level, db per one cycle per second band width.

Normally the life is given in hours so that a frequency must be estimated to obtain the corresponding cycles of life. The sound pressure level for the frequency is obtained from a plot of the sound level spectrum and a safety margin added to give db_R. The design chart can then be used to obtain several combinations of rib spacing and rib and skin thicknesses to meet the required life. After a practical combination has been selected, the resonant frequency is read from the chart and a new cycles of life computed. A new db_R is then read from the chart and compared with the sound pressure level at the resonant frequency. If the design margin is inadequate, some other combination must be tried.

McGowan gave design charts for the following structures:

a. Conventional skin and rib construction.

b. Skin and rib with scalloped doublers at the ribs.

c. Attachments.

d. Rib with lightening hole.

e. Beaded panels.

f. Honeycomb panels.

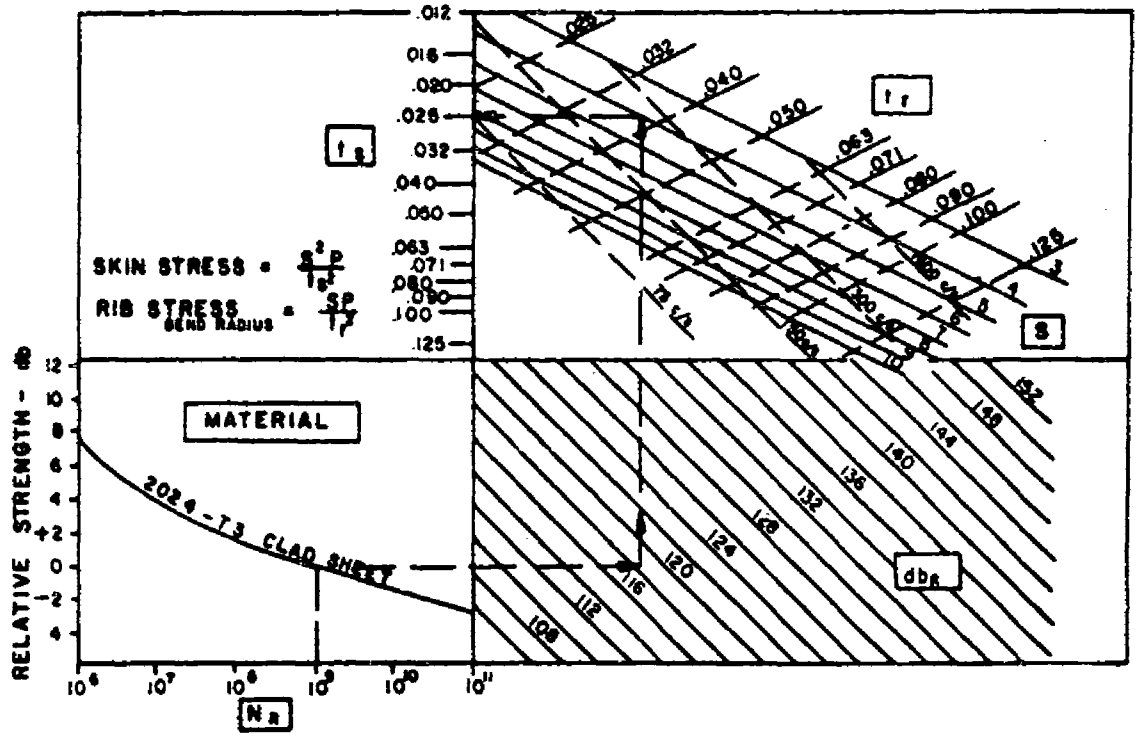

FIGURE 39. DESIGN CHART — SKIN RIB CONSTRUCTION (Ref. 41)

The design chart for the skin and rib with scalloped doublers at the ribs is given in Fig. 40. The doublers improve the fatigue characteristics of the panels. For a life of 10^9 cycles an 0.032 inch skin with rib spacings of 4 inches will withstand 123 db without doublers but will withstand 131 db with doublers. The skin thickness would have to be increased from 0.032 to 0.050 inches to accomplish the same improvement without doublers. Of course the rib thickness and the resonant frequency would also be changed.

The design charts thus facilitate the evaluation of the design alternatives for panels. This is very helpful because most of the failures are panel failures near or aft of the engine exit nozzle. Although the charts have been adjusted for the unknowns such as stress concentrations and boundary conditions by the use of test data there still remain questions of accuracy of simulation and the errors produced by multiple mode response. McGowan concluded that the charts provide the means to meet the preliminary design acoustic requirements. However, if the charts indicate acoustic fatigue is the primary design criterion or if there is a design margin less than 6 db, McGowan recommends that a proof test be conducted in a simulated service environment.

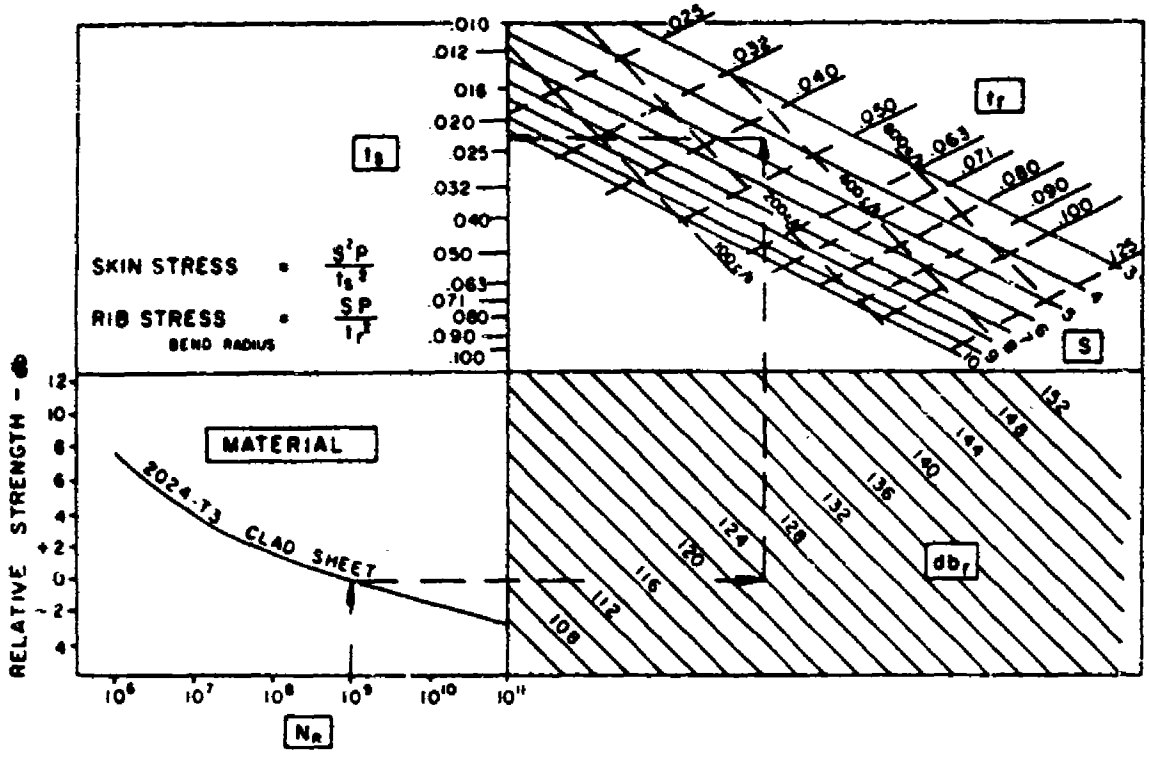

FIGURE 40. DESIGN CHART — SKIN WITH BONDED DOUBLER AND RIB CONSTRUCTION (Ref. 41)

REFERENCES

1. K. M. Eldred et al, "Criteria for Short Time Exposure of Personnel to High Intensity Jet Aircraft Noise", WADC TN 55-355, 1955.

2. Air Force Regulation AFR 160-3, "Medical Service, Hazardous Noise Exposure", Oct. 1956.

3. W. D. Ward et al, "Dependence of Temporary Threshold Shift at 4 KC on Intensity and Time", JASA Vol. 30, p. 944, Oct. 1958.

4. W. D. Ward et al, "Temporary Threshold Shift from Octave-Band Noise: Applications to Damage Risk Criteria", JASA Vol. 31, p. 522, April 1959.

5. W. D. Ward et al, "Relation Between Recovery from Temporary Threshold Shift and Duration of Exposure", JASA Vol. 31, p. 600, May 1959.

6. W. D. Ward et al, "Temporary Threshold Shift Produced by Intermittent Exposure to Noise", JASA Vol. 31, p. 791, June 1959.

7. J. C. Nixon & A. Glorig, "Noise Induced Permanent Threshold Shift at 2000 cps and 4000 cps", JASA Vol. 33, p. 904, July 1961.

8. K. D. Kryter, "Damage-Risk Criterion for Steady State Noise", JASA, Vol. 35, pp. 1515-1525, Oct. 1963.

9. H. Davis, "Auditory and Non-Auditory Effects of High Intensity Noise", Research Project NM 130199 Subtask 1, Report No. 7, 1958.

10. W. D. Ward, "Hearing of Naval Aircraft Maintenance Personnel", JASA Vol. 29, pp. 1289-1301, Dec. 1957.

11. A. C. Pietrasanta "Jet Noise Problem in Aircraft Carrier Islands", JASA Vol. 28, p. 427, May 1956.

12. Mercy & Bernstein, "Report of Investigation of Jet Aircraft Noise for XF37-1 and F7U-3 Aircraft on Board USS Coral Sea", Material Laboratory Project 5280-9 Final Report, N. Y. Naval Shipyard, Dec. 1953.

13. G. A. Failey, "Acoustic Survey of A3J-1 Aircraft", North American Aviation, Inc. Report NA61H-463, Nov. 1961.

14. Cox, J. R., "The Noise Cumulator", Noise Control, Vol. 4, p. 54, (1955).

15. Ades, H. W. et al, "Feasibility Studies for Hearing Conservation Program Aboard CVA-Type Aircraft Carriers", Research Project MR005.13-2005 Subtask 1, Report 8, U.S. Naval School of Aviation Medicine (1960).

16. L. L. Beranek, "Noise Control in Office and Factory Spaces", Trans. Chem. Engr. Conferences, Industrial Hygiene Foundation of America, Nov. 15, 1950.

17. L. L. Beranek, "Acoustics", McGraw-Hill, 1954.

18. M. Strasberg, "Criteria for Setting Airborne Noise Level Limits in Shipboard Spaces", Rep. No. 371-N-12, Dept. of Navy, Bureau of Ships, 1952.

19. R. G. Klump & J. C. Webster, "Physical Measurements of Equally Speech-Interferring Navy Noises", JASA Vol. 35, pp. 1328-1338, Sept., 1963.

20. N. R. French & J. C. Steinberg, "Factors Governing the Intelligibility of Speech Sounds, JASA, Vol. 19, pp. 90-119, 1947.

21. K. D. Kryter, "On Predicting the Intelligibility of Speech from Acoustical Measures", Jour. of Speech & Hearing Disorders, pp. 208-217, June, 1956.

22. K. D. Kryter, "Human Engineering Principles for the Design of Speech Communication Systems", AFCCDD TR 60-27, U.S. Dept. of Commerce, Office of Technical Services, Washington, D. C.

23. K. D. Kryter, "Validation of the Articulation Index", JASA Vol. 34, pp. 1698-1702, Nov., 1962.

24. K. D. Kryter et al, "A Test of the 20-Band and Octave-Band Methods of Computing the Articulation Index", EST-TDR-62-4, U.S. Dept. of Commerce, Office of Technical Services, Washington, D. C.

25. J. C. Webster & R. G. Klump, "Articulation Index and Average Curve-Fitting Methods of Predicting Speech Interference", JASA, Vol. 35, pp. 1339-1344, Sept., 1963.

26. C. M. Ashley, "Simplifying Room Sound Power Calculations", ASHRAE Journal, pp. 51-59, July, 1963.

27. K. D. Kryter, "Methods for the Calculation and the Use of the Articulation Index", JASA, Vol. 34, pp. 1689-1697, Nov., 1962.

28. G. A. Miller, "The Masking of Speech", Psychol. Bull. 44, pp. 105-129, 1947.

29. H. K. Dunn & S. D. White, "Statistical Measurements on Conversational Speech", JASA Vol. 11, pp. 278-288, 1940.

30. K. D. Kryter, "Effects of Ear Protective Devices on the Intelligibility of Speech in Noise", JASA Vol. 18, pp. 443-447, 1946.

31. W. Wathen-Dunn & D. W. Lipke, "On the Power Gained by Clipping Speech", JASA Vol. 30, pp. 36-40, Jan., 1958.

32. J. M. Pickett, "Effect of Vocal Force on the Intelligibility of Speech", JASA, Vol. 28, pp. 902-905, 1956.

33. J. M. Pickett & I. Pollack, "Prediction of Speech Intelligibility at High Noise Levels", JASA, Vol. 30, pp. 955-963, 1958.

34. R. C. Bilger & I. J. Hirsh, "Masking of Tones by Bands of Noise", JASA, Vol. 28, pp. 623-630, 1956.

35. N. L. Carter & K. O. Kryter, "Masking of Pure Tones and Speech", J. Auditory Research, Vol. 2, pp. 66-98, 1962.

36. G. A. Miller & J.C.R. Licklider, "The Intelligibility of Interrupted Speech", JASA, Vol. 22, pp. 167-173, 1950.

37. V. O. Knudsen & C. M. Harris, "Acoustical Designing in Architecture", Wiley & Sons, 1950, Chap. 9.

38. W. H. Sumby & I. Pollack, "Visual Contribution to Speech Intelligibility in Noise", JASA, Vol. 26, pp. 212-215, 1954.

39. G. E. Fitch, et al, "Establishment of the Approach to, and Development of, Interim Design Criteria for Sonic Fatigue", Report No. ASD-TDR-62-26, Wright-Patterson Air Force Base, June 1962.

40. P. M. Belcher, J. D. VanDyke, Jr., A. L. Eshleman, Jr., "Development of Aircraft Structure to Withstand Acoustical Loads", Aero/Space Engineering, Vol. 18, 1959.

41. P. R. McGowan, "Designing Structures for Acoustic Fatigue", Engineering Paper 1482, Douglas Aircraft Co., Long Beach, California.

42. P. A. Franken, et al, "Methods of Flight Vehicle Noise Prediction", WADC Technical Report No. 58-343, Wright Patterson Air Force Base.

43. John W. Miles, "On Structural Fatigue Under Random Loading", Jour. of Aeronautical Sciences, Vol. 21, 1954.

44. W. B. Davenport, Jr., and W. L. Root, Random Signals and Noise (book), McGraw-Hill Book Co., Inc., 1958.

45. F. R. Shanley, "A Theory of Fatigue Based on Unbonding During Reversed Slip", RAND Rep. P-350, Santa Monica, California, 1952.

46. J. B. Kommers, Proc. ASTM vol. 45, p. 532, 1945.

47. Department of Aeronautics & Astronautics, University of Southampton, Noise and Acoustic Fatigue in Aeronautics, April 1963, Chapter 21.

48. H. C. Schjelderup, "A New Look at Structural Peak Distributions Under Random Vibration, WADC Tech. Report 59-676.

49. F. R. Fralich, "Experimental Investigation of Effects of Random Loading on the Fatigue Life of Notched Cantilever-beam Specimens of S.A.E. 4130 Normalized Steel", NASA TN D-663.

50. A. M. Freudenthal, "Fatigue of Materials and Structures Under Random Loading", WADC Tech. Report 59-676.

51. J. R. Fuller, "Research on Techniques of Establishing Random Type Fatigue Curves for Broad Band Sonic Loading" Technical Report No. ASD-TDR-62-501, Wright Patterson Air Force Base.

52. W. D. Trotter, "Fatigue of 2024-T3 Aluminum Sheet Under Random Loading", Test Report T2-1601, Boeing Airplane Co., Nov. 1958.

53. P. W. Smith, Jr., and C. I. Malme, Sonic Fatigue Life Determination by Siren Testing, Tech. Report.No. ASD-TR-61-639, Wright Patterson Air Force Base.

54. P. M. Belcher, A. L. Eshleman and J. D. VanDyke, "A Comparison of Stress Response and Fatigue Test Results under Random and Sinusoidal Acoustic Loading", The Journal of the Acoustical Society of America, vol. 31, No. 1, p. 125, January 1959.

55. A. Powell, "On the Fatigue Failure of Structures Due to Vibrations Excited by Random Pressure Fields", The Journal of the Acoustical Society of America, Vol. 30, No. 12, pp. 1130-1134, Dec. 1958.

UNCLASSIFIED